IMPROVEMENT OF THE OBSERVATION METHOD TO PREDICT MEANDER MIGRATION BY USING A PROBABILISTIC ANALYSIS

A Thesis

by

MIFROKHAH HANIFFA

Submitted to the Office of Graduate and Professional Studies of
Texas A&M University
in partial fulfillment of the requirements for the degree of

MASTER OF SCIENCE

Chair of Committee,	Jean-Louis Briaud
Committee Members,	Charles Aubeny
	Mark Everett
Head of Department,	Robin Autenrieth

May 2019

Major Subject: Civil Engineering

Copyright 2019 Mifrokhah Haniffa

ABSTRACT

River meander migration is a product of fluvial activities including erosion and deposition. It may cause problems if it is close to vital infrastructure and its migration rate is noticeable for design life of infrastructure. Different methods to predict meander migration have been proposed. However, most of them do not integrate all general components of meander: geometry, flow, and soil.

The Observation Method for Meander (OMM) is a prediction method which is developed by accommodating those components. River geometry is represented by past river movement from aerial photos or map observation, river flow is represented by discharge data from United States Geological Survey, and soil properties are represented by erosion function parameters obtained from erosion tests. This method results critical velocity in the field and soil parameters to create calibrated and observed migration versus time plot. For future prediction, the previous OMM used deterministic analysis which results in a single precise predicted migration. By including probabilistic method, uncertainty that might exist in the prediction is considered.

Eight meanders in Brazos River near City of Sugar Land were selected for this study. The prediction was conducted for next 30 years. Deterministic prediction was carried out by using the same method of the previous OMM. Probabilistic prediction was carried out by generating 100 equally possible future flows from statistical parameters of the past flow. A code was written in a single MATLAB code to do calibration, deterministic prediction, and probabilistic prediction. The results showed that there was a slight difference between deterministic and probabilistic prediction.

ACKNOWLEDGEMENTS

I would like to thank my committee chair, Dr. Jean-Louis Briaud, and my committee members, Dr. Charles Aubeny and Dr. Mark Everett, for their guidance and support throughout the course of this research. Also, I would like to thank Dr. Ignacio Rodriguez-Iturbe, Dr. Francisco Olivera, and Mabel Chedid, Ph.D. for the discussion.

Thanks also go to my friends from Indonesian Students Association and Fulbright Student Association and colleagues and the department faculty and staff from Zachry Department of Civil Engineering for making my time at Texas A&M University a great experience.

Finally, thanks to my parents, siblings, family, and fiancé for their encouragement, patience, and love.

CONTRIBUTORS AND FUNDING SOURCES

Contributors

This work was supervised by a thesis committee consisting of Dr. Briaud and Dr. Aubeny of the Department of Civil Engineering and Dr. Everett of the Department of Geology and Geophysics.

The experimental data was collected by Huitt-Zollars and Erosion Function Apparatus tests were analyzed by Mabel Chedid, Ph.D. The analyses in Chapter 4 were conducted by improving the work of Axel Manuel Montalvo-Bartolomei of the Department of Civil Engineering which were published in 2014.

All other work conducted for the thesis was completed by the student independently.

Funding Sources

Graduate study was supported by Fulbright Master's Degree Scholarship from the U.S. Department of State's Bureau of Educational and Cultural Affairs and added by generosity of the donors through Troy Marceleno '60 Fellowship in 2017-2018 and Civil Engineering General Fellowships in 2018-2019.

This work was also made possible in part by data from Huitt-Zollars. Its contents are solely the responsibility of the authors and do not necessarily represent the official views of Huitt-Zollars.

TABLE OF CONTENTS

Page

ABSTRACT ii

ACKNOWLEDGEMENTS iii

CONTRIBUTORS AND FUNDING SOURCES iv

TABLE OF CONTENTS v

LIST OF FIGURES vii

LIST OF TABLES xiii

1. INTRODUCTION 1

1.1. Introduction 1
1.2. Research Objectives 1
1.3. General Approach 2

2. LITERATURE REVIEW 4

2.1. Introduction 4
2.2. Meander Migration Concepts 5
2.3. Meander Migration Prediction Methods 7

3. OBSERVATION METHOD FOR MEANDER (OMM) 15

3.1. General Steps 15
3.2. Deterministic Analysis 21
3.3. Probabilistic Analysis 22

4. FIELD APPLICATION STUDY WITH PROBABILITY ANALYSIS 24

4.1. Description of Case Histories 24
4.2. Calibration Step 31
4.3. Deterministic Prediction 51
4.4. Probabilistic Prediction 67
4.5. Comparison of Deterministic Prediction with Probabilistic Prediction 83
4.6. Discussion of Results 83
4.7. Prediction for 65-Year Period 84

5. CRITICAL ANALYSIS OF THE OMM 95

5.1. Optimum Prediction Direction 95
5.2. Future Hydrograph 96
5.3. Probability Density Function (PDF) of Meander Migration 103
5.4. Uncertainties Excluded in OMM 105

6. CONCLUSIONS AND RECOMMENDATIONS 106

6.1. Conclusions 106
6.2. Recommendations 107

REFERENCES 109

APPENDIX 111

LIST OF FIGURES

Page

Figure 1. Map of selected sites at Brazos River. Modified from [Google Earth, 2018]. 2

Figure 2. A. Helicoidal flow at a bend apex; B. model of the flow structure in meandering channels. Black lines indicate surface currents and white lines represent near-bed currents. Reprinted from [Knighton, 1998 in Lagasse et al., 2004]. 4

Figure 3. Parameters of meander geometry. Reprinted from [Briaud et al., 2007] 5

Figure 4. Modified Brice classification of meandering channels. Reprinted from [Lagasse et al., 2004]. 6

Figure 5. Modes of movement. Reprinted from [Lagasse et al., 2004]. 7

Figure 6. Best-fit circle from outer bank delineation and the predicted circles . Reprinted from [Lagasse el al., 2004]. 9

Figure 7. Comparison of data used by Brice (1982) and some rivers in Texas. Reprinted from [Briaud et al., 2001]. 11

Figure 8. Comparison of data from Beatton River and some rivers in Texas. Reprinted from [Briaud et al., 2001]. 12

Figure 9. Output plot of MEANDER program. Reprinted from [Briaud et al., 2007]. 13

Figure 10. Output table of MEANDER program. Reprinted from [Briaud et al., 2007]. 14

Figure 11. Velocity hydrograph of Brazos River from 1953 to 2018. Data retrieved from USGS website. 16

Figure 12. River movement observation at AOI 6 in Brazos River 17

Figure 13. Erosion Function Apparatus (EFA); principle (a) and equipment (b). Reprinted from [Briaud, 2013]. 18

Figure 14. Erosion categories for soil and rocks based on velocity. Reprinted from [Briaud, 2013]. 18

Figure 15. EFA test results from field samples in Brazos River 19

Figure 16. Calibrated and observed migration versus time plot for AOI 6 Direction 1 21

Figure 17. Observed migration versus calibrated migration plot for AOI 6 Direction 1 21

Figure 18. Probability density function (PDF) and cumulative density function (CDF) of original and fitted distribution 23

Figure 19. HEC-RAS discharge vs velocity curve for Brazos River 25

Figure 20. Velocity hydrograph of Brazos River from 1953 to 2018 after being converted from discharge data of USGS Gage 08114000. 26

Figure 21. River movement observation at AOI 3 27

Figure 22. River movement observation at AOI 4 27

Figure 23. River movement observation at AOI 5 28

Figure 24. River movement observation at AOI 6 28

Figure 25. River movement observation at AOI 7 29

Figure 26. River movement observation at AOI 8 29

Figure 27. River movement observation at AOI 9 30

Figure 28. River movement observation at AOI 10 30

Figure 29. EFA test results from field samples in Brazos River 31

Figure 30. Calibrated and observed migration of AOI 3 Direction 1 32

Figure 31. Calibrated and observed migration of AOI 3 Direction 2 33

Figure 32. Calibrated and observed migration of AOI 3 Direction 3 34

Figure 33. Calibrated and observed migration of AOI 4 Direction 1 35

Figure 34. Calibrated and observed migration of AOI 4 Direction 2 36

Figure 35. Calibrated and observed migration of AOI 4 Direction 3 37

Figure 36. Calibrated and observed migration of AOI 5 Direction 1 38

Figure 37. Calibrated and observed migration of AOI 5 Direction 2 39

Figure 38. Calibrated and observed migration of AOI 5 Direction 3 40

Figure 39. Calibrated and observed migration of AOI 6 Direction 1 41

Figure 40. Calibrated and observed migration of AOI 6 Direction 2 42

Figure 41. Calibrated and observed migration of AOI 7 Direction 1 43
Figure 42. Calibrated and observed migration of AOI 7 Direction 2 44
Figure 43. Calibrated and observed migration of AOI 8 Direction 1 45
Figure 44. Calibrated and observed migration of AOI 8 Direction 2 46
Figure 45. Calibrated and observed migration of AOI 9 Direction 1 47
Figure 46. Calibrated and observed migration of AOI 9 Direction 2 48
Figure 47. Calibrated and observed migration of AOI 10 Direction 1 49
Figure 48. Calibrated and observed migration of AOI 10 Direction 2 50
Figure 49. Calibrated and observed migration of AOI 10 Direction 3 51
Figure 50. Deterministic prediction of AOI 3 Direction 1..... 52
Figure 51. Deterministic prediction of AOI 3 Direction 2..... 53
Figure 52. Deterministic prediction of AOI 3 Direction 3..... 53
Figure 53. Deterministic prediction of AOI 4 Direction 1..... 54
Figure 54. Deterministic prediction of AOI 4 Direction 2..... 54
Figure 55. Deterministic prediction of AOI 4 Direction 3..... 55
Figure 56. Deterministic prediction of AOI 5 Direction 1..... 55
Figure 57. Deterministic prediction of AOI 5 Direction 2..... 56
Figure 58. Deterministic prediction of AOI 5 Direction 3..... 56
Figure 59. Deterministic prediction of AOI 6 Direction 1..... 57
Figure 60. Deterministic prediction of AOI 6 Direction 2..... 57
Figure 61. Deterministic prediction of AOI 7 Direction 1..... 58
Figure 62. Deterministic prediction of AOI 7 Direction 2..... 58
Figure 63. Deterministic prediction of AOI 8 Direction 1..... 59
Figure 64. Deterministic prediction of AOI 8 Direction 2..... 59

Figure 65. Deterministic prediction of AOI 9 Direction 1 60
Figure 66. Deterministic prediction of AOI 9 Direction 2 60
Figure 67. Deterministic prediction of AOI 10 Direction 1 61
Figure 68. Deterministic prediction of AOI 10 Direction 2 61
Figure 69. Deterministic prediction of AOI 10 Direction 3 62
Figure 70. River position of AOI 3 in 2048 based on deterministic prediction 63
Figure 71. River position of AOI 4 in 2048 based on deterministic prediction 63
Figure 72. River position of AOI 5 in 2048 based on deterministic prediction 64
Figure 73. River position of AOI 6 in 2048 based on deterministic prediction 64
Figure 74. River position of AOI 7 in 2048 based on deterministic prediction 65
Figure 75. River position of AOI 8 in 2048 based on deterministic prediction 65
Figure 76. River position of AOI 9 in 2048 based on deterministic prediction 66
Figure 77. River position of AOI 10 in 2048 based on deterministic prediction 66
Figure 78. Probability density function (PDF) and cumulative density function (CDF) of original and fitted distribution of the past flow hydrograph 68
Figure 79. CDF of original data and random sample 70
Figure 80. Past and predicted flow hydrograph 70
Figure 81. PDF and CDF of future migration prediction 71
Figure 82. Exceedance curve of future migration 72
Figure 83. Exceedance curve of future migration in AOI 3 74
Figure 84. Exceedance curve of future migration in AOI 4 74
Figure 85. Exceedance curve of future migration in AOI 5 75
Figure 86. Exceedance curve of future migration in AOI 6 76
Figure 87. Exceedance curve of future migration in AOI 7 76
Figure 88. Exceedance curve of future migration in AOI 8 77

Figure 89. Exceedance curve of future migration in AOI 9 77
Figure 90. Exceedance curve of future migration in AOI 10 78
Figure 91. River position of AOI 3 in 2048 based on probabilistic prediction 79
Figure 92. River position of AOI 4 in 2048 based on probabilistic prediction 79
Figure 93. River position of AOI 5 in 2048 based on probabilistic prediction 80
Figure 94. River position of AOI 6 in 2048 based on probabilistic prediction 80
Figure 95. River position of AOI 7 in 2048 based on probabilistic prediction 81
Figure 96. River position of AOI 8 in 2048 based on probabilistic prediction 81
Figure 97. River position of AOI 9 in 2048 based on probabilistic prediction 82
Figure 98. River position of AOI 10 in 2048 based on probabilistic prediction 82
Figure 99. Future position of AOI 3 Direction 1 in 2083 85
Figure 100. Future position of AOI 3 Direction 2 in 2083 85
Figure 101. Future position of AOI 3 Direction 3 in 2083 86
Figure 102. Future position of AOI 4 Direction 1 in 2083 86
Figure 103. Future position of AOI 4 Direction 2 in 2083 87
Figure 104. Future position of AOI 4 Direction 3 in 2083 87
Figure 105. Future position of AOI 5 Direction 1 in 2083 88
Figure 106. Future position of AOI 5 Direction 2 in 2083 88
Figure 107. Future position of AOI 5 Direction 3 in 2083 89
Figure 108. Future position of AOI 6 Direction 1 in 2083 89
Figure 109. Future position of AOI 6 Direction 2 in 2083 90
Figure 110. Future position of OAI 7 Direction 1 in 2083 90
Figure 111. Future position of AOI 7 Direction 2 in 2083 91
Figure 112. Future position of AOI 8 Direction 1 in 2083 91

Figure 113. Future position of AOI 8 Direction 2 in 2083 92

Figure 114. Future position of AOI 9 Direction 1 in 2083 92

Figure 115. Future position of AOI 9 Direction 2 in 2083 93

Figure 116. Future position of AOI 10 Direction 1 in 2083 93

Figure 117. Future position of AOI 10 Direction 2 in 2083 94

Figure 118. Future position of AOI 10 Direction 3 in 2083 94

Figure 119. Future migration from one random sampling of probabilistic prediction 97

Figure 120. Past and predicted flow hydrograph using maximum yearly flow 98

Figure 121. Cumulative density function (CDF) of original and fitted distribution of the past flow hydrograph using maximum yearly flow 98

Figure 122. Comparison of prediction using mean daily flow and maximum yearly flow 103

Figure 123. Future migration of AOI 5 Direction 2 probabilistic prediction for 20-year and 40-year prediction 104

LIST OF TABLES

Page

Table 1. Location of bend apex of each meander 3

Table 2. HEC-RAS interpolation 25

Table 3. Calibration data of AOI 3 Direction 1 32

Table 4. Calibration data of AOI 3 Direction 2 33

Table 5. Calibration data of AOI 3 Direction 3 33

Table 6. Calibration data of AOI 4 Direction 1 34

Table 7. Calibration data of AOI 4 Direction 2 35

Table 8. Calibration data of AOI 4 Direction 3 36

Table 9. Calibration data of AOI 5 Direction 1 37

Table 10. Calibration data of AOI 5 Direction 2 38

Table 11. Calibration data of AOI 5 Direction 3 39

Table 12. Calibration data of AOI 6 Direction 1 40

Table 13. Calibration data of AOI 6 Direction 2 41

Table 14. Calibration data of AOI 7 Direction 1 42

Table 15. Calibration data of AOI 7 Direction 2 43

Table 16. Calibration data of AOI 8 Direction 1 44

Table 17. Calibration data of AOI 8 Direction 2 45

Table 18. Calibration data of AOI 9 Direction 1 46

Table 19. Calibration data of AOI 9 Direction 2 47

Table 20. Calibration data of AOI 10 Direction 1 48

Table 21. Calibration data of AOI 10 Direction 2 49

Table 22. Calibration data of AOI 10 Direction 3 50

Table 23. Future predicted position and migration distance by deterministic prediction..... 52

Table 24. Comparison of statistical parameters of original data and fitted lognormal distribution 68

Table 25. Comparison of random sampling from lognormal distribution and original data 69

Table 26. Future predicted position and migration distance by probabilistic prediction..... 72

Table 27. Future predicted position from deterministic and probabilistic prediction for next 65 years 84

Table 28. Comparison of random sampling from original data dan fitted distribution of maximum yearly flow 98

Table 29. Equivalent time calculation for regression analysis 99

Table 30. Equivalent time calculation for prediction..... 101

1. INTRODUCTION

1.1. Introduction

River meander migration is a product of fluvial activity involving erosion and deposition. It becomes an issue for engineering if the meander is close to vital infrastructure and its migration rate is noticeable for design life of infrastructure. Problems due to river meander migration can be bridge pier and abutment scour, levee failures, and loss of floodplain. Therefore, prediction of river meander migration is important to minimize the impacts.

General components in meander migration are soil, geometry, and river. To understand meander behavior and to predict migration rate, those three aspects must be taken into account. Previous prediction methods have been developed using different approaches. Montalvo-Bartolomei (2014) developed Observation Method of Meander (OMM) which integrated past movement of river, flow history, and soil properties to predict migration based on past meander behavior. Although the method can result high accuracy of predicted migration compared to observed migration, the problem arises if it is used for predicting future migration because data of future flow hydrograph is undiscovered. The main purpose of this study is to solve the problem in order to predict future migration more accurately and reasonable.

1.2. Research Objectives

The objectives of this research are the following:

- Improve the previous method (called Observation Method of Meander/OMM) using probabilistic prediction for river meander migration.

- Apply the previous and the proposed method for river meander migration in Brazos River crossing City of Sugar Land for next 30 years to predict whether the future river will be likely to reach embankment or not.
- Compare the prediction from deterministic and probabilistic analysis.

1.3. General Approach

Improvement of OMM uses similar input data and procedures with the previous study. River selected for this study is Brazos River near City of Sugar Land, Texas and there are eight areas of interest (AOI) starting from AOI 3 to AOI 10 (Figure 1). The precise location of bend apex of each meander is listed in Table 1. Period of time selected for this study is from 1953 to 2018 to obtain erosion parameters required for future prediction from 2018 to 2048.

Figure 1. Map of selected sites at Brazos River. Modified from [Google Earth, 2018].

Table 1. Location of bend apex of each meander

AOI	N	W
AOI 3	29º31’47.29” N	95º36’06.24” W
AOI 4	29º31’33.07” N	95º36’45.98” W
AOI 5	29º33’33.45” N	95º38’40.04” W
AOI 6	29º33’58.26” N	95º40’03.28” W
AOI 7	29º34’33.61” N	95º40’05.60” W
AOI 8	29º35’00.11” N	95º40’53.87” W
AOI 9	29º34’14.88” N	95º41’42.37” W
AOI 10	29º34’13.21” N	95º43’03.23” W

This research only covers analytical study using existing data obtained from the field, laboratory testing, and secondary data. Site investigation and laboratory testing from field samples were not conducted by the writer. Secondary data are flow hydrograph of Brazos River from 1953 to 2018 which is retrieved from USGS website and aerial photos of the river. Analytical study is conducted using previous software code and spreadsheet, but it is improved by probabilistic approach to predict future migration.

2. LITERATURE REVIEW

2.1. Introduction

Erosion and deposition are main components in river meander migration. Erosion happens at the outer bank and deposition happens at the inner bank (Figure 2). These processes is due to helicoidal flow from super-elevated water surface against the outer bank (Lagasse et al., 2004). Erosion is often a combination of steep cliff undercutting because the highest hydraulic stress is at the bottom and sloughing of the overhang into the river. The lowest velocity is at the inner bank and it causes deposition of the eroded soil. Water velocity and radius of meander curvature control hydraulic shear stress and soil erodibility controls resisting shear stress. (Briaud & Montalvo-Bartolomei, 2017). Although these processes naturally happen, they can be affected by vegetation or human activities.

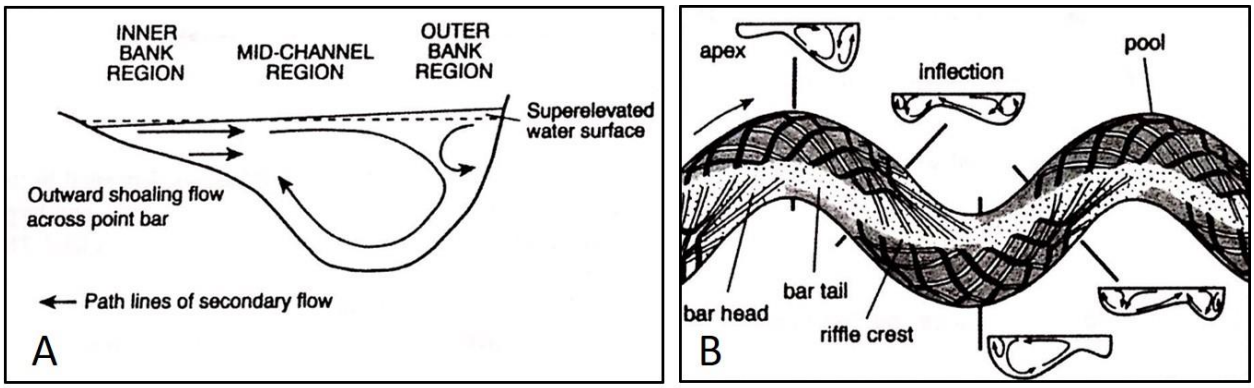

Figure 2. A. Helicoidal flow at a bend apex; B. model of the flow structure in meandering channels. Black lines indicate surface currents and white lines represent near-bed currents. Reprinted from [Knighton, 1998 in Lagasse et al., 2004].

Recognition of river geometry is the key in meander study. A channel bend is assumed as an arch to reduce complexity of its original shape (Briaud et al., 2007). The parameters of meander geometry as illustrated by Figure 3.

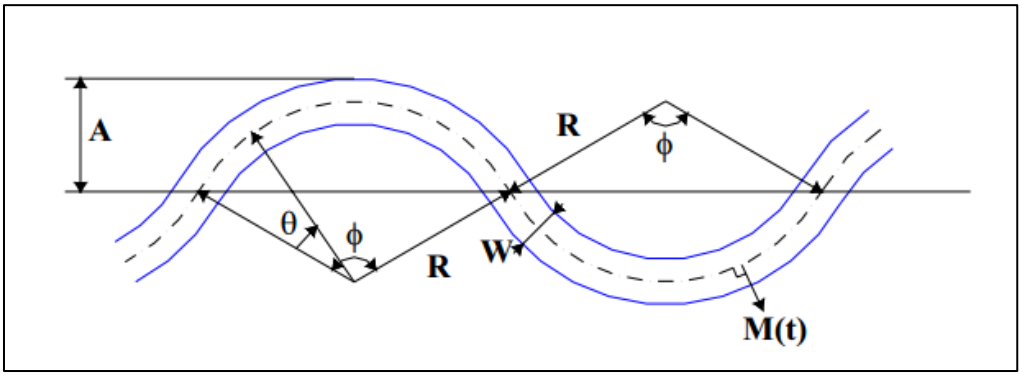

Figure 3. Parameters of meander geometry. Reprinted from [Briaud et al., 2007]

where A is meander amplitude, W is channel width, M is channel migration distance, R is radius of curvature, φ is bend angle, θ is relative angle ($0 \leq \theta \leq \varphi$) within each bend, and t is time.

2.2. Meander Migration Concepts

Before river meander migration prediction can be established, its fundamental concepts must be recognized. Lagasse et al. (2004) classified meandering streams into stable meander and active meander according to migration rate. Stable meander does not have such a noticeable migration rate for design life of infrastructure that will trigger little or no risk. Active meander happens when a river has sufficient energy to deform its river banks through erosion and sedimentation process. Determination of meander stability is a basic screening in migration prediction.

Brice (1982) distinguished meander lateral stability based on degree of river width after comprehensive study from historical documentation and field observation. Highly sinuous and equal-width channels are the most stable, equal-width channels with lower sinuosity is slightly active, and wider-at-bend channels are the most active. Modified Brice classification (Lagasse et al., 2004) helps in screening out channel types which have insignificant lateral migration rate.

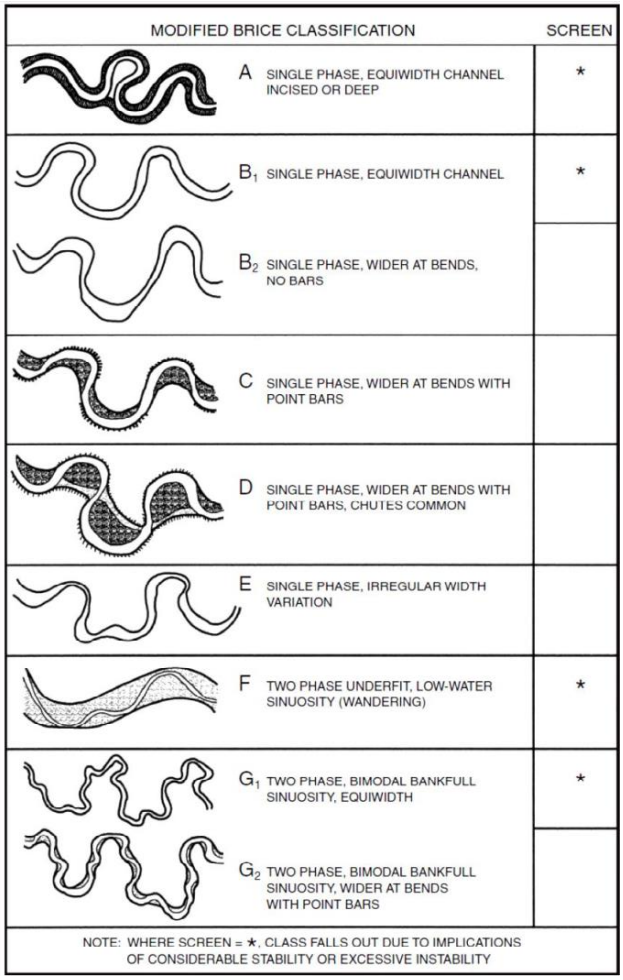

Figure 4. Modified Brice classification of meandering channels. Reprinted from [Lagasse et al., 2004].

Meander bend can be described by four types of movement: extension, translation, expansion and contraction, and rotation (Lagasse et al., 2004). Extension is across-valley movement and can be measured from its centroid. Translation is down-valley movement and also can be measured from its centroid. Expansion is movement by increasing bend radius and contraction is movement by decreasing bend radius. Rotation is movement by changing orientation of meander bend. However, actual meander bend can migrate in several movements and one part of the bend may be deformed faster.

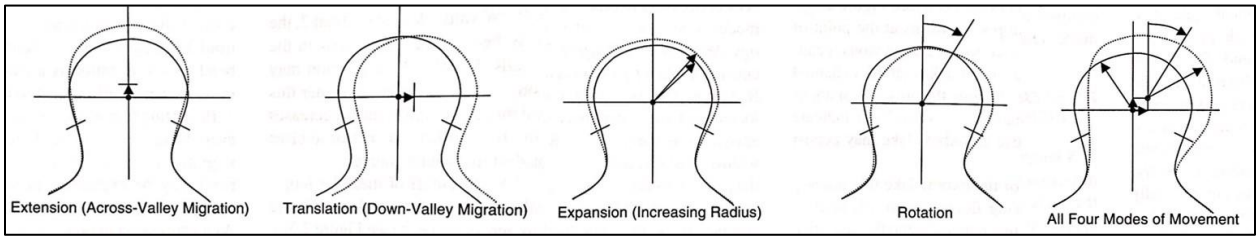

Figure 5. Modes of movement. Reprinted from [Lagasse et al., 2004].

2.3. Meander Migration Prediction Methods

Meander migration has been an issue for hydraulic and geotechnical engineers for many years especially meander in a river crossing any infrastructure or residential and commercial area. Meander migration prediction is challenging due to various influencing factors and each river may have exclusive behaviors. In general, meander migration prediction which has been developed can be divided into (Montalvo-Bartolomei, 2014):

- Time sequences map and extrapolation
- Empirical methods
- Analytical methods

2.3.1. Time Sequences Map and Extrapolation

Brice (1982) used aerial photos and maps from two or more different times to measure lateral stability of a channel. This method was then reprocessed by Lagasse et al. (2004) in two methods: manual and computer-assisted.

Aerial photos or maps which have been obtained must be on same scale. Then, some identifying features which appear in all of the maps or photos, such as highway and specific buildings are marked. Riverbank lines are traced and best-fit circles of each outer bank of meander are drawn. The radius and centroid of each circle are recorded. Annual rate of river movement can be obtained by dividing distance of movement by difference of years as defined by Eq. 1

$$\Delta R_{CA} = (R_{C2} - R_{C1})/Y_A \quad \text{(Eq. 1)}$$

$$\Delta R_{CB} = (R_{C3} - R_{C2})/Y_B$$

where ΔR_{CX} is rate of change in radius of curvature during period X (in ft/yr or m/yr), R_{CX} is radius of curvature in Year X, Y_X is number of years in Period X.

This method assumes that the direction and rate of river movement are constant during the period (Montalvo-Bartolomei, 2014). For Period C (Year 3 to Year 4), the most recent rate will be used instead of long-term average rate to calculate distance of centroid migration (Eq. 2), the predicted radius and angle of migration are obtained by extrapolation (Eq. 3 and 4).

$$D_C = \left(\frac{D_B}{Y_B}\right) Y_C \quad \text{(Eq. 2)}$$

$$R_{C4} = R_{C3} + \frac{R_{C3} - R_{C2}}{Y_B} Y_C \quad \text{(Eq. 3)}$$

$$\theta_C = \theta_B + \frac{\theta_B - \theta_A}{Y_B} Y_C \quad \text{(Eq. 4)}$$

where D_X is distance of centroid migration for Period X (in ft or m), Y_X is number of years in Period X, R_{C4} is predicted radius of curvature in Year 4 (in ft or m), R_{C3} is radius of curvature in

Year 3 (in ft or m), R_{C2} is radius of curvature in Year 2 (in ft or m), θ_C is predicted angle of migration for Period C, θ_A is predicted angle of migration for Period A, and θ_B is predicted angle of migration for Period B.

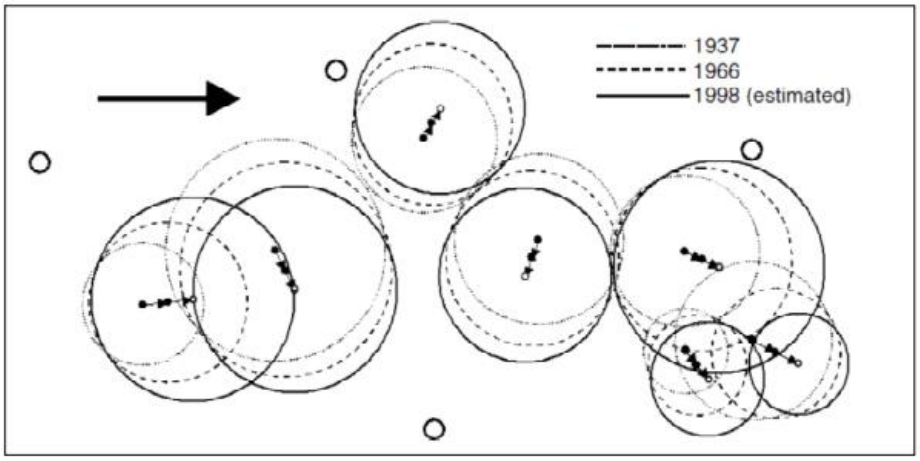

Figure 6. Best-fit circle from outer bank delineation and the predicted circles . Reprinted from [Lagasse el al., 2004].

In computer-assisted method, the entire procedures are conducted using GIS-based software: Data Logger and Channel Migration Predictor. The result of this method is a database containing information such as coordinates of each centroid, radius of each circle, orientation of bend centerline, three channel widths (upstream, apex, and downstream) measurement, wavelength and amplitude of each bend, and riverbank line files.

2.3.2. Empirical Methods

Empirical methods use equations with different variables based on experiment or observation to determine migration rate. Most of the equations contain parameter from river geometry.

Keady and Priest (1977 in Briaud et al., 2007) developed an equation based on observation from rivers in Arkansas, Louisiana, Tennessee, and Alberta, Canada to calculate meander migration.

$$\frac{V}{\sqrt{gA}} = \varphi(s) \qquad \text{(Eq. 5)}$$

where V is migration rate (in ft/yr), g is acceleration of gravity (in ft/s^2), A is meander amplitude (ft), s is surface slope, and $\varphi(s)$ is function of s. Although slope is important, river flow condition is also influenced by rainfall which is not involved in the equation and large migration usually happens during a flood.

Hooke (1980) investigated migration rate on rivers in Devon, England and proposed that migration rate was related to catchment area.

$$Y = 8.67 + 0.114A \quad (r = 0.63) \qquad \text{(Eq. 6)}$$

$$Y = 2.45A^{0.45} \quad (r = 0.73)$$

where Y is migration rate (in m/year) and A is catchment area (in km^2). Briaud et al. (2007) explained that catchment area could represent rainfall and flow rate. However, rivers with the same catchment area might have different precipitation level.

Briaud et al. (2001) summarized and compared their study from some rivers in Texas with data used by Brice (1982) which proposed that migration rate is controlled by channel width and obtained an equation from regression analysis as follows

$$M_r = 0.01b \qquad \text{(Eq. 7)}$$

where M_r is meander migration rate (in m/yr) and b is channel width (in m). However, rivers with wide bend tend to have a higher migration rate than predicted by the equation.

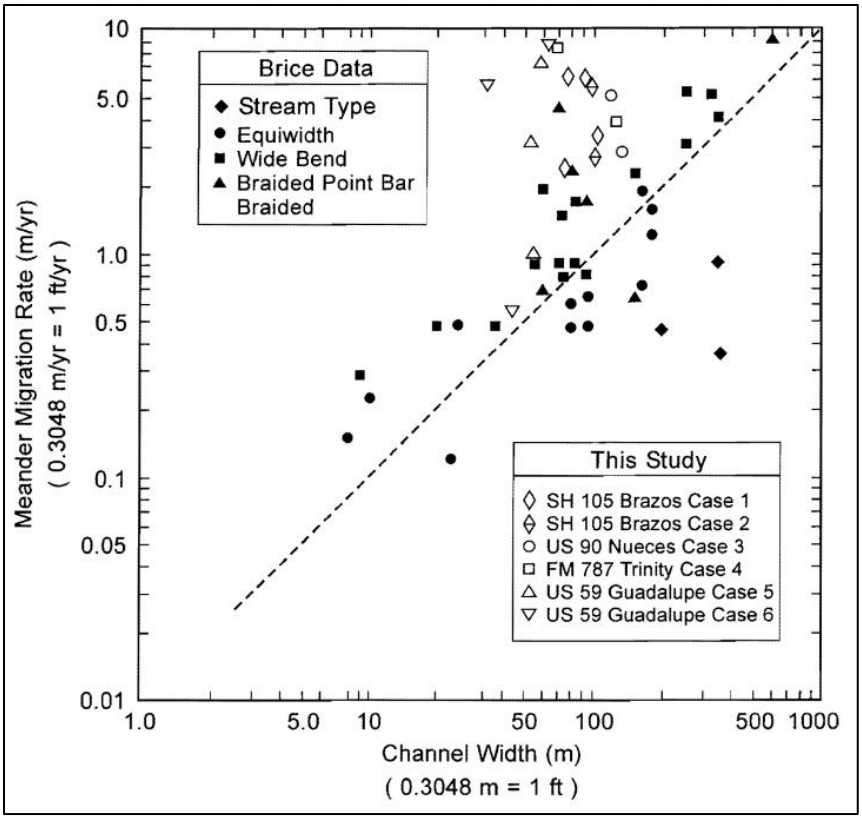

Figure 7. Comparison of data used by Brice (1982) and some rivers in Texas. Reprinted from [Briaud et al., 2001].

Nanson and Hickin (1983) proposed that migration rate is influenced by radius of curvature to channel width ratio (r_c/b). Based on their data from 16 bends in Beatton River, the highest migration rate is when r_c/b is between 2 and 3. Briaud et al. (2001) evaluated this method by comparing data from Beatton River to data from some rivers in Texas (Figure 7). At r_c/b is between 2 and 3, centrifugal force is maximum and forces water to follow the outer bank which can produce maximum migration rate. Although the relationship of migration rate and r_c/b is satisfied, the data are scattered and do not show a clear trendline (Briaud et al., 2007).

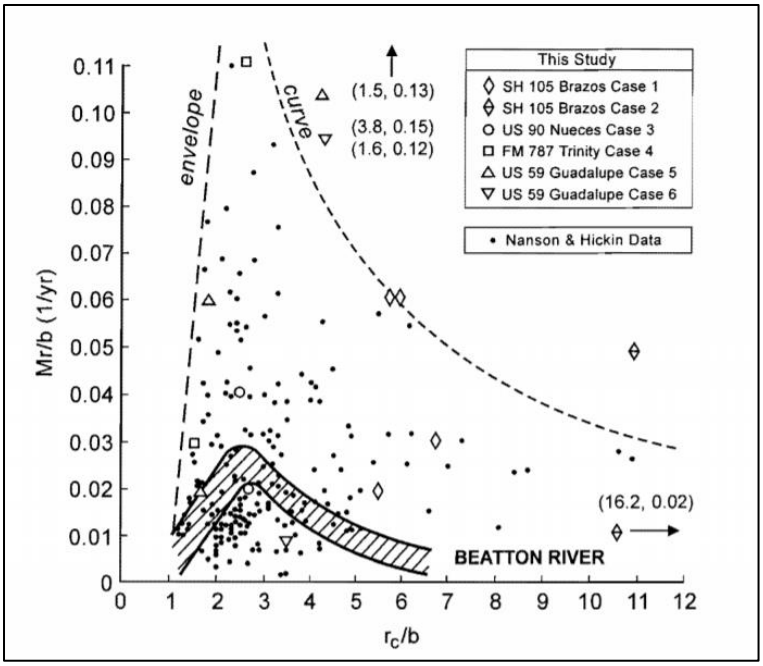

Figure 8. Comparison of data from Beatton River and some rivers in Texas. Reprinted from [Briaud et al., 2001].

Odgaard (1987) developed a new equation by correlating erosion rates with channel characteristics as follows.

$$\frac{\bar{v}}{u} = 2E\frac{b}{r_c}\left(1+\frac{b}{2r_c}\right)^{-1}F \qquad \text{(Eq. 8)}$$

$$E = \frac{e}{8}\left(\frac{3\alpha}{2}\frac{\sqrt{\theta}}{k}\frac{m+1}{m+2}F_{Dc}-1\right),\ F = 1-\exp\left(-B\frac{r_c\varphi}{b}\left(1-\frac{\beta}{\varphi}\right)\right),\ B = \frac{2k^2}{(m+1)^2}\frac{b}{d_c}$$

where $\bar{v}$ is average erosion rate (in m/yr), u is reach-average mean velocity (in m/s), b is bank-full width of channel (in m), r_c is radius of curvature (in m), e is erosion constant, α is 1.27, θ is Shield's parameter (equals 0.06), m is friction parameter, k is Karman's constant (equals 0.4), F_{Dc} is particle Froude number, φ is bend angle, β is angle from cross over to first bank erosion occurrence, d_c is center line flow depth.

2.3.3. Analytical Methods

2.3.3.1. TAMU-MEANDER Program

TAMU-MEANDER is a software developed by Texas Transportation Institute (TTI) in 2005. The program is available online and free of charge. Detail explanation of the software development and guideline can be found in TTI Report 4378-1 which is included with the software. The program integrates data from river geometry, soil properties obtained from erosion tests, and river flow. For river geometry, the user requires to input coordinate file of the river and river width. Critical shear stress, number of points in Erosion Function Apparatus (EFA) tests, shear stress and scour rate of each test points, and soil type (sand or clay) are input data for soil properties. Hydrologic data can be in discharge or velocity. If using discharge, tables of discharge versus velocity and discharge versus water depth are required. If using velocity, table of velocity versus depth is required. All these tables are obtained from HEC-RAS simulation. Three analyses used in prediction are constant flow, hydrograph which can be retrieved from United States Geological Survey (USGS) database, and risk analysis using hydrograph data or a 100-year flood and a 500-year flood. Results of this method are output plot and output table containing initial coordinates, final coordinates, and migration.

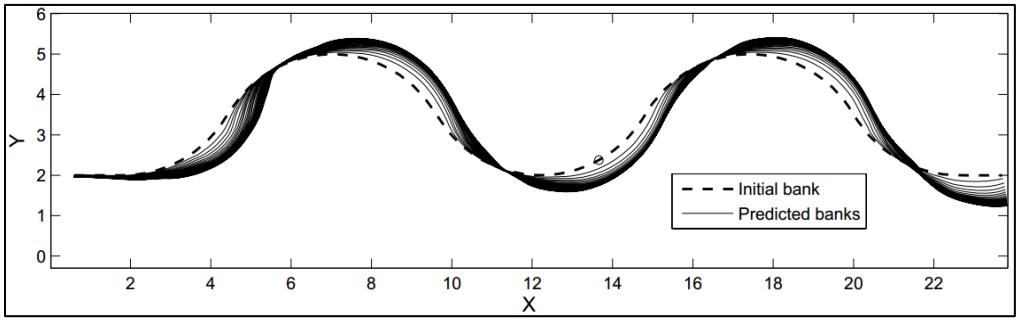

Figure 9. Output plot of MEANDER program. Reprinted from [Briaud et al., 2007].

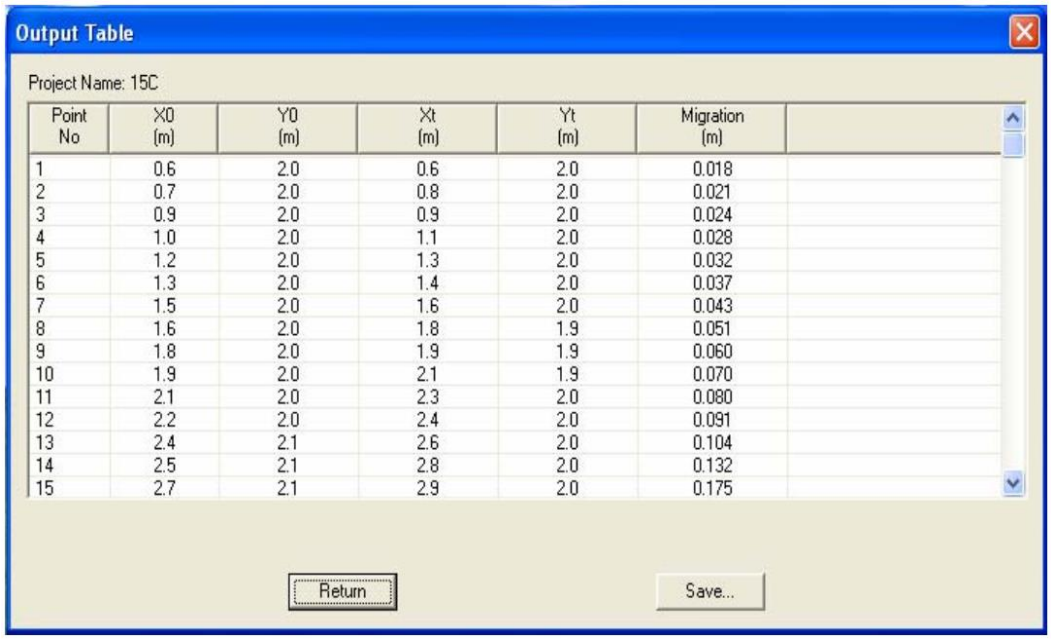

Figure 10. Output table of MEANDER program. Reprinted from [Briaud et al., 2007].

2.3.3.2. TAMU OMM

Texas A&M University – Observation Method for Meander (TAMU OMM) is developed by Montalvo-Bartolomei (2014). It is in form of two software programs: MATLAB and Microsoft Excel and it requires similar information as MEANDER does; river geometry, soil properties, and river flow data. River geometry is obtained from historical maps or aerial photos. Soil properties are represented by soil erosion rate obtained from erosion tests. River flow data is obtained from USGS database. Further explanation of this method is described in the next chapter.

3. OBSERVATION METHOD FOR MEANDER (OMM)

3.1. General Steps

Procedures to meander migration prediction using OMM are site selection, river hydrographs data collection, river movement observation, erosion tests, and calibration. This method can be verified by using MATLAB or Microsoft Excel software.

3.1.1. Site Selection

A meandering river can be selected for study according to presence of vital infrastructure surrounding the river and river stability which can be seen from its shape. Montalvo-Bartolomei (2014) studied meander migration at one channel bend from six different rivers in Texas where important highways lay above it. While this research studies meander migration at eight different channel bends of Brazos River crossing City of Sugarland. The site is close to residential areas and crossed by Interstate 69 (Figure 1).

3.1.2. River Hydrographs Data Collection

River hydrographs data are collected from USGS stations and these data can be retrieved from USGS website. Discharge data provided from USGS can be chosen based on time-series (daily or yearly) and statistics (average, minimum, or maximum). For this study, discharge data selected is average daily discharge and it needs to be converted to velocity before being used in further analysis. The accurate way to obtain velocity is using program to simulate river geometry and flow such as HEC-RAS and TAMU-FLOW (Montalvo-Bartolomei, 2014). Generated velocity versus time is called hydrograph.

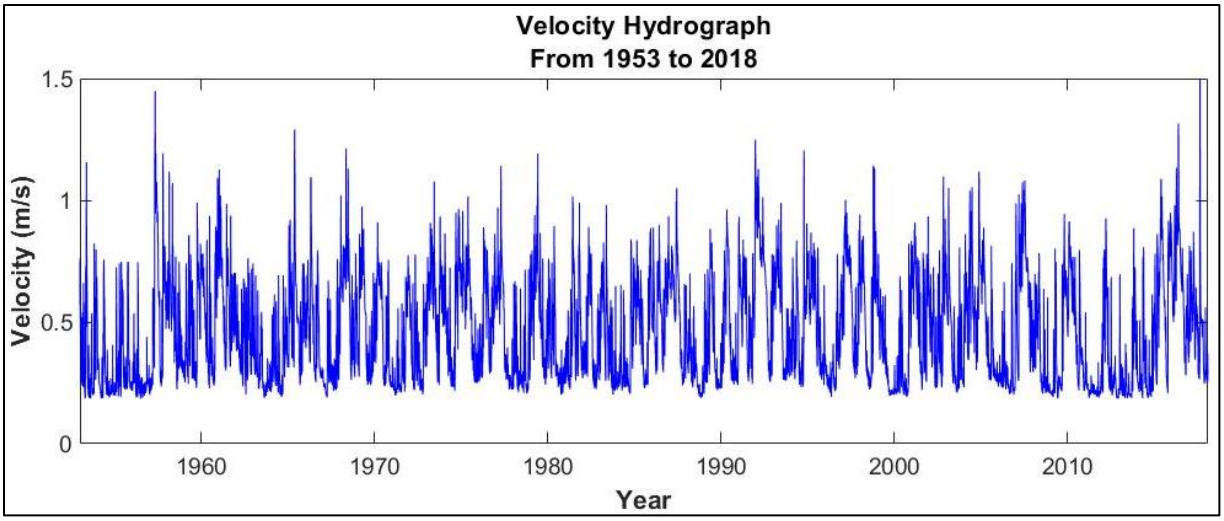

Figure 11. Velocity hydrograph of Brazos River from 1953 to 2018. Data retrieved from USGS website.

3.1.3. River Movement Observation

River movement observation is conducted in a similar way to time sequence map and extrapolation method by Lagasse et al. (2004). Delineation is conducted using drawing software such as AutoCAD and riverbank line of each year is represented by different color or styles. River movement of the period is calculated by drawing a reference line outwards from the bend centroid. Direction of the reference line should represent the migration of the meander during the period. Ideally, the line is perpendicular to the migration direction. However, as explained by Lagasse et al. (2004), a meander can have more than one movement type or rotation movement which makes the line drawing more difficult. Figure 12 shows that AOI 6 in Brazos River tends to have rotation movement move in two directions thus two references are drawn to find the direction which is more critical.

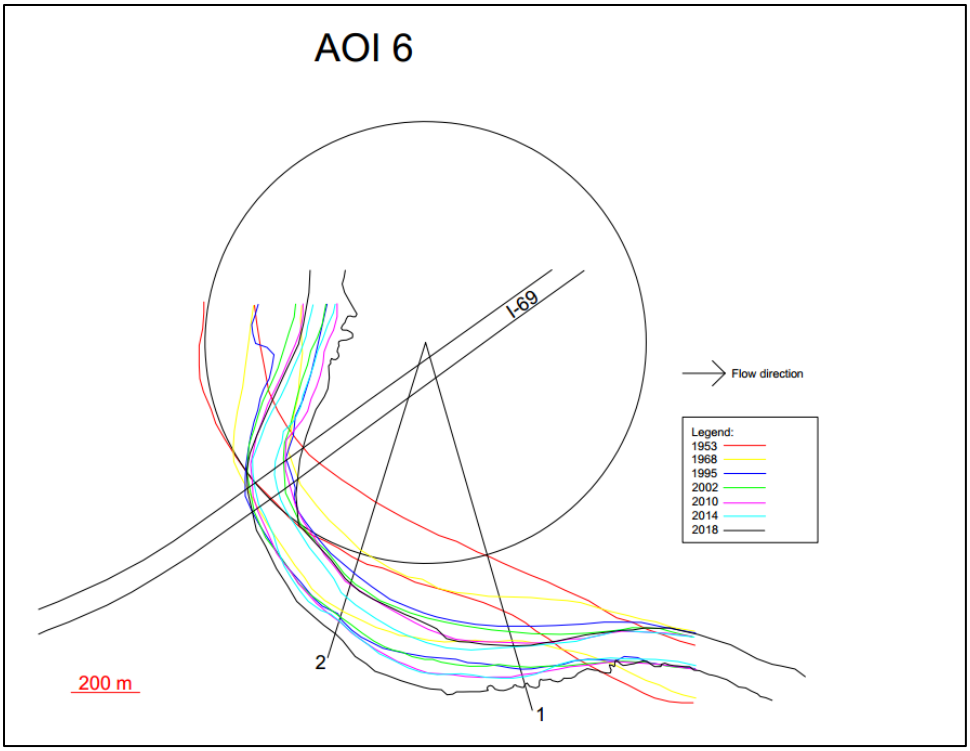

Figure 12. River movement observation at AOI 6 in Brazos River

3.1.4. Erosion Tests

Samples from the field are tested in laboratory to determine soil classification and erodibility. Erosion Function Apparatus (EFA) test is one of laboratory tests for erosion which was first developed in the early 1990s. Soil sample is put in Shelby tube and the tube is placed under a conduit with constant water velocity (Figure 13). The sample is pushed out by piston as it is being eroded. For each velocity, erosion rate ($\dot{z}$) is calculated by Eq. 9 and shear stress is calculated using Moody's chart.

$$\dot{z} = \frac{h}{t} \qquad \text{(Eq. 9)}$$

where $\dot{z}$ is erosion rate, h is length of sample eroded, and t is time required.

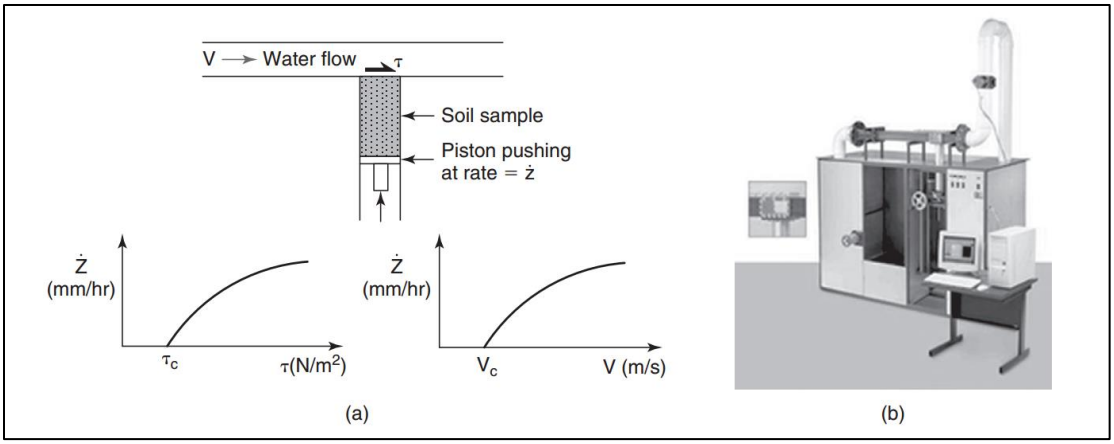

Figure 13. Erosion Function Apparatus (EFA); principle (a) and equipment (b). Reprinted from [Briaud, 2013].

After years of erosion testing experience, erosion categories chart for soils and rocks based on velocity and shear stress is proposed. If there is no sample for erosion tests, the soil erodibility can be determined by using the chart based on soil classification of the sample (Figure 14). Unit of erosion rate in the chart is mm/hr and it is required to be converted to m/s for analysis due to consistency in the unit of the data.

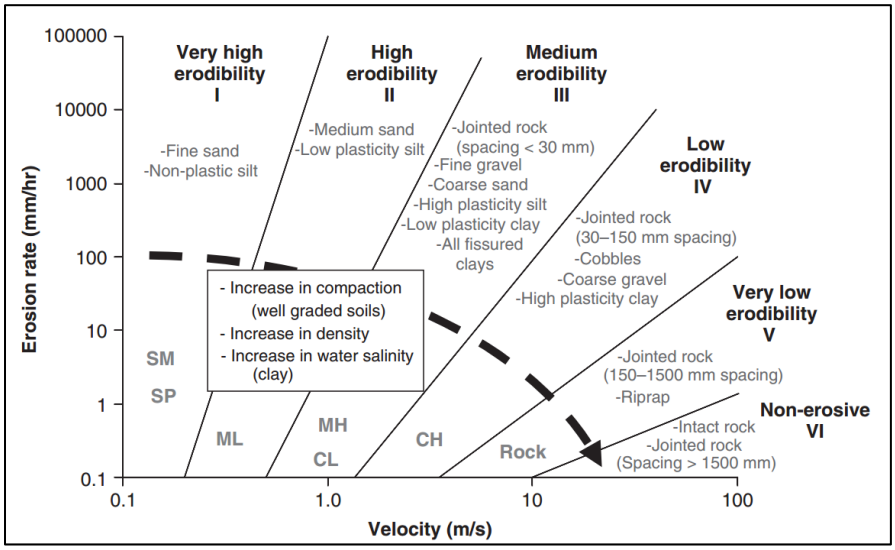

Figure 14. Erosion categories for soil and rocks based on velocity. Reprinted from [Briaud, 2013].

EFA test results from field samples in Brazos River shows that soil of the riverbank is in category III (medium erodibility) (Figure 15). Soil erosion function is presented by a straight line that divided two categories and it is defined by Eq. 10 as follows

$$\dot{z} = \alpha v^{\beta} \qquad \text{(Eq. 10)}$$

where $\dot{z}$ is erosion rate, v is velocity, α and β are soil parameters in erosion function. The equation is normalized to make both sides of the equation dimensionless and the model in OMM uses critical velocity (v_c) instead of velocity (Montalvo-Bartolomei, 2014). Critical velocity is defined as the velocity corresponding to a very low erosion rate of $\dot{z}_c$ = 0.1 mm/hr or 2.78x10^{-8} m/s.

$$\frac{\dot{z}}{v_c} = \alpha' \left(\frac{v}{v_c}\right)^{\beta} \qquad \text{(Eq. 11)}$$

the coefficient of α' is obtained from

$$\alpha' = \frac{\dot{z}_{c(0.1)}}{v_c} \qquad \text{(Eq. 12)}$$

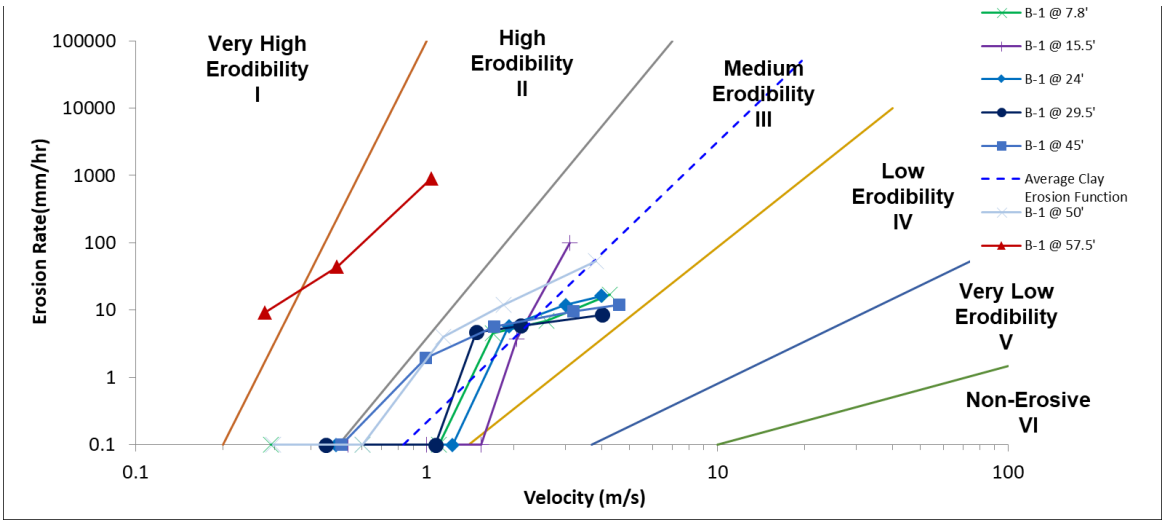

Figure 15. EFA test results from field samples in Brazos River

Critical velocity of soil sample can be calculated using the above equations. However, it cannot be directly used to predict erosion rate in the field due to various factors influencing differences between small-scale testing and actual river condition. Thus, critical velocity in the field must be obtained by calibration step with an assumption that β is same for soil sample and soil in the field.

3.1.5. Calibration

Critical velocity in the field is obtained by automation process using OMM spreadsheet or OMM code. Input data for this calibration step are average daily velocity during the period, β value from the previous step, and river movement observation data. During the process, the spreadsheet or the code will calculate an estimated magnitude of migration (ΔM) for each day using this equation

$$\Delta M = \alpha' \left(\frac{v}{v_{cfield}} \right)^{\beta} v_{cfield} \Delta t \qquad \text{(Eq. 13)}$$

where Δt is increment of time (in seconds). Because it uses average daily data, increment of time is 86400 seconds.

The OMM will compare observed data with estimated data for each critical velocity until obtaining the smallest difference which is presented by Ranking Index (RI). The RI is calculated by using the following equation

$$RI = |\mu(a)| + \sigma(a) \qquad \text{(Eq. 14)}$$

where μ is average of all values, a is ratio of calibrated migration to observed migration (M_c/M_o), and σ is standard deviation of a value.

Results of this method are migration (both calibrated migration and observed migration) versus time plot and critical velocity in the field which can be used for prediction.

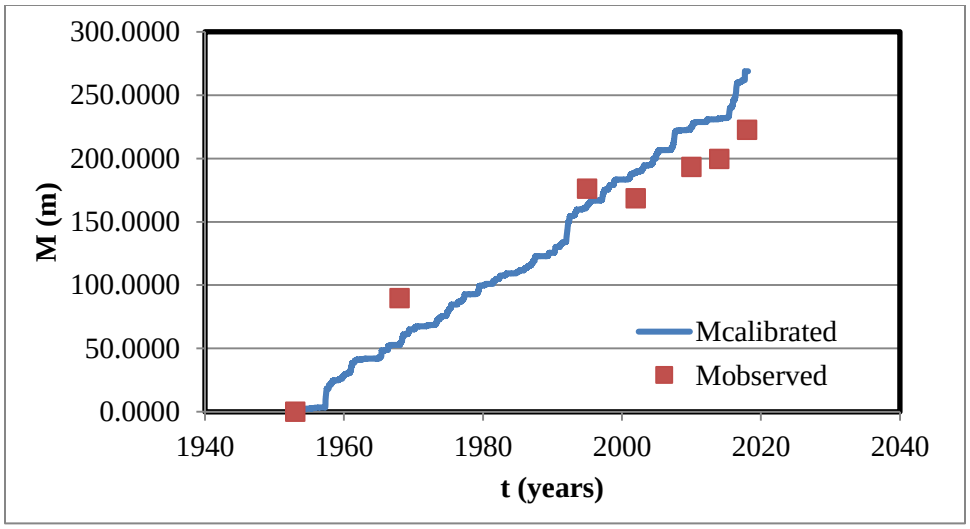

Figure 16. Calibrated and observed migration versus time plot for AOI 6 Direction 1

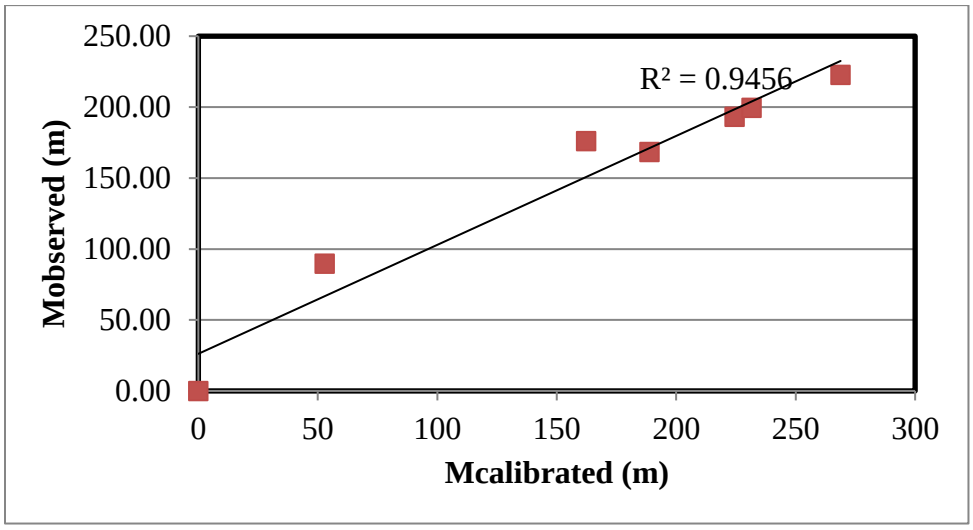

Figure 17. Observed migration versus calibrated migration plot for AOI 6 Direction 1

3.2. Deterministic Analysis

The procedures explained above is to obtain critical velocity in the field (v_c) and soil parameters (α' and β) from past to present river movement. These parameters are then used to predict river movement from present to future. In deterministic analysis, future hydrograph is in a single value which can be obtained from the past hydrograph with or without consideration of

flood. An example for 30-year future prediction, if it does not consider any flood, discharge values for future time period are copied from the last 30 years data. Meanwhile, if it considers flood such as 500-year flood, certain discharge of the flood is added in the middle of the future period.

3.3. Probabilistic Analysis

In probabilistic analysis, future hydrograph has a large number of possible values which each set of values should satisfy statistical distribution. Figure 18 shows that the flow hydrograph fits a lognormal distribution. Predicted future hydrograph can be generated using random sampling from cumulative density function (CDF) of the original data thus future and past flow hydrograph will have identical distribution.

If possible future hydrograph is generated 100 times, there will be 100 possible migration distances of the river. The distribution of these values is then plotted to determine the migration distance of each certain probability. The advantage of using probabilistic analysis is uncertainty related to each variable in meander migration is considered. However, generating future flow hydrograph must reasonably satisfy principles of hydrology and the existing OMM has not incorporated probabilistic analysis. Therefore, this study will mainly focus on these two problems.

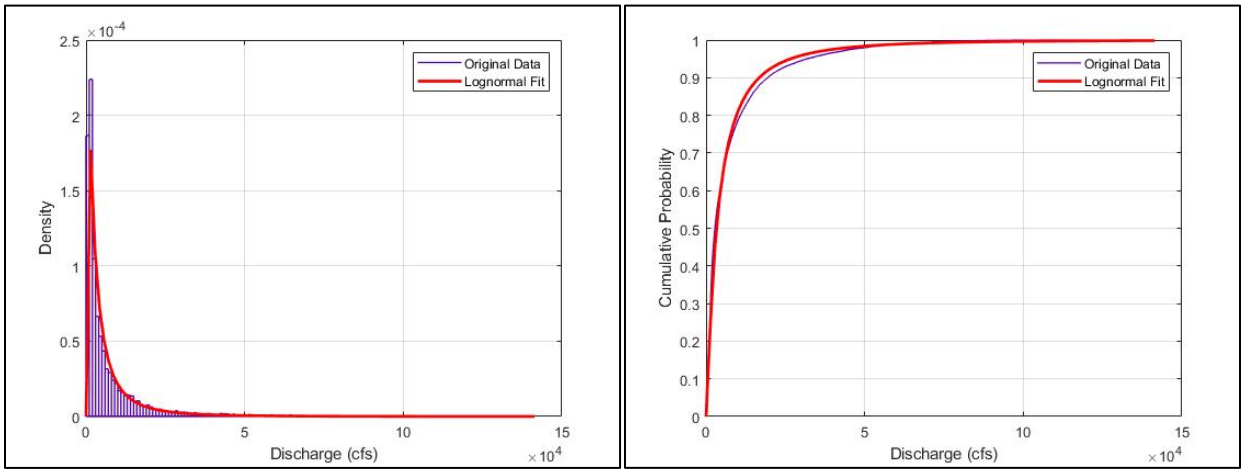

Figure 18. Probability density function (PDF) and cumulative density function (CDF) of original and fitted distribution

4. FIELD APPLICATION STUDY WITH PROBABILITY ANALYSIS

4.1. Description of Case Histories

The site for this study is located at Brazos River near City of Sugar Land, Texas and there are eight meanders as area of interest (AOI) starting from AOI 3 to AOI 10. Figure 1 shows the entire area for this study and Table 1 gives the detail location of each AOI. Period of time selected for this study is from 1953 to 2018 to obtain erosion parameters required for future prediction from 2018 to 2048. Degree of sinuosity of the study area is 1.36. In general, the area has meander migration problems and some meanders are close to residential area.

The nearest river gage station is Brazos River at Richmond, Texas with station ID 08114000 and it is about 6.3 km (4 miles) upstream of the AOI 10. The discharge data retrieved is average daily flow and it needs to be converted into velocity by dividing the flow by the cross-section area. However, because the cross-section area is not constant depending on the river geometry, the accurate way to obtain velocity is using programs such as HEC-RAS and TAMU-FLOW (Montalvo-Bartolomei, 2014). Hydraulic modelling using HEC-RAS was performed and resulted in discharge vs velocity curve and the fitted trendline equation.

$$v = -6 \times 10^{-30} Q^6 + 4 \times 10^{-24} Q^5 - 9 \times 10^{-19} Q^4 + 10^{-13} Q^3 - 6 \times 10^{-9} Q^2 + 0.0002Q + 0.8021 \quad \text{(Eq. 15)}$$

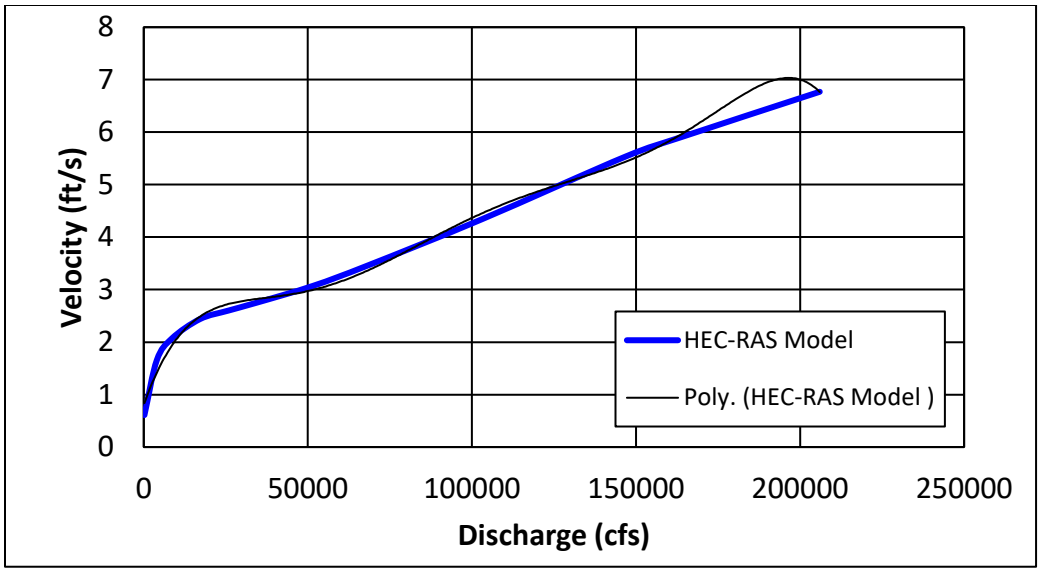

Figure 19. HEC-RAS discharge vs velocity curve for Brazos River

Linear interpolation can be used to get more precise result. For flow discharge less than 200 cfs, the velocity is assumed to be constant at 0.61 ft/s. Figure 20 shows the velocity hydrograph from 1953 to 2018 after being converted from flow discharge data.

Table 2. HEC-RAS interpolation

Flow (1,000 cfs)	206	164	147	103	68.7	51.5	34.3	25.7	17.2	8.6	4	0.2
Velocity (ft/s)	6.77	5.91	5.54	4.34	3.47	3.07	2.75	2.6	2.44	2.07	1.66	0.61

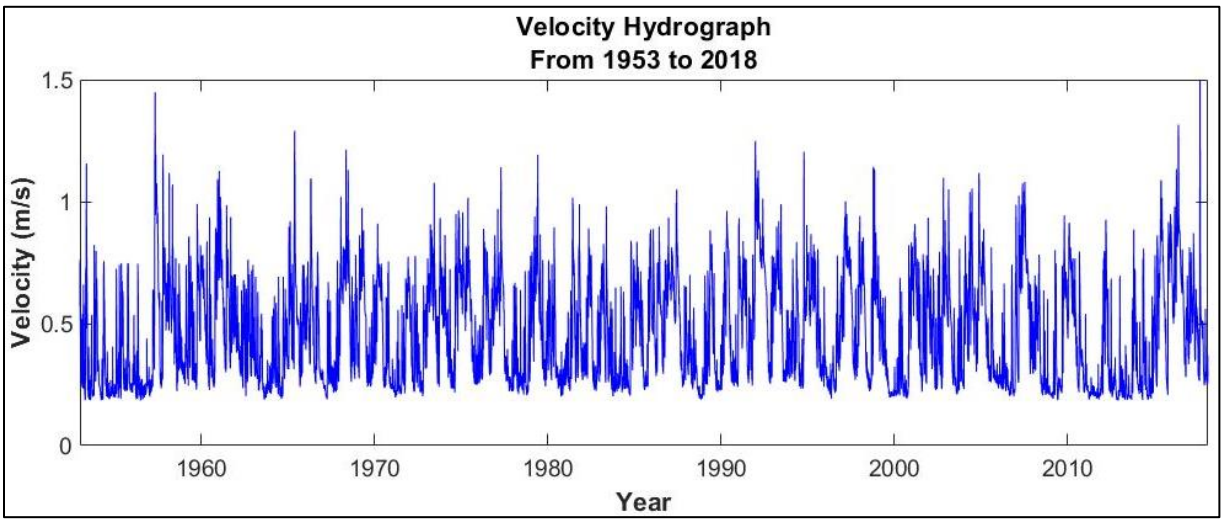

Figure 20. Velocity hydrograph of Brazos River from 1953 to 2018 after being converted from discharge data of USGS Gage 08114000.

The following figures show the result of river movement observation by using historical aerial photos. The number of observation is seven: 1953, 1968, 1995, 2002, 2010, 2014, and late 2017 or early 2018 (after Hurricane Harvey). Extrapolation of the aerial images and riverbank delineation were conducted by using AutoCAD. The directions lines were drawn to represent meander migration. Observed migration is measured along the direction lines and then it is used for input data of calibration steps.

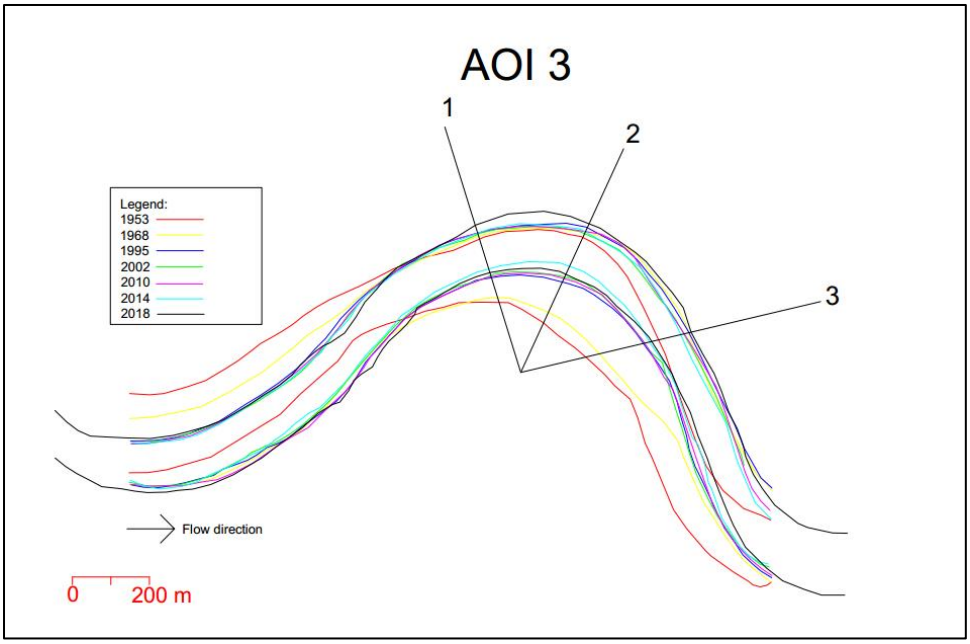

Figure 21. River movement observation at AOI 3

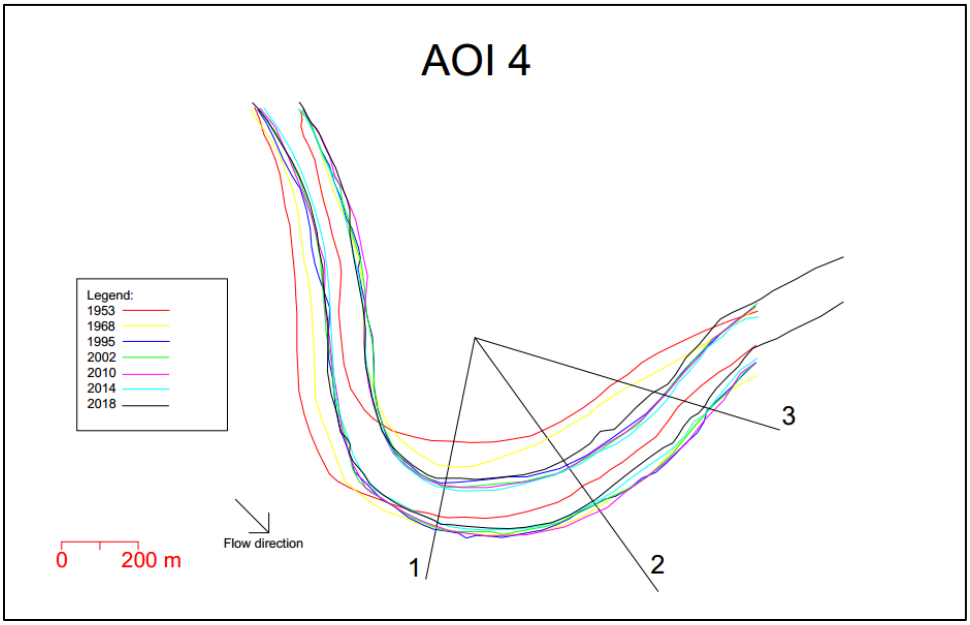

Figure 22. River movement observation at AOI 4

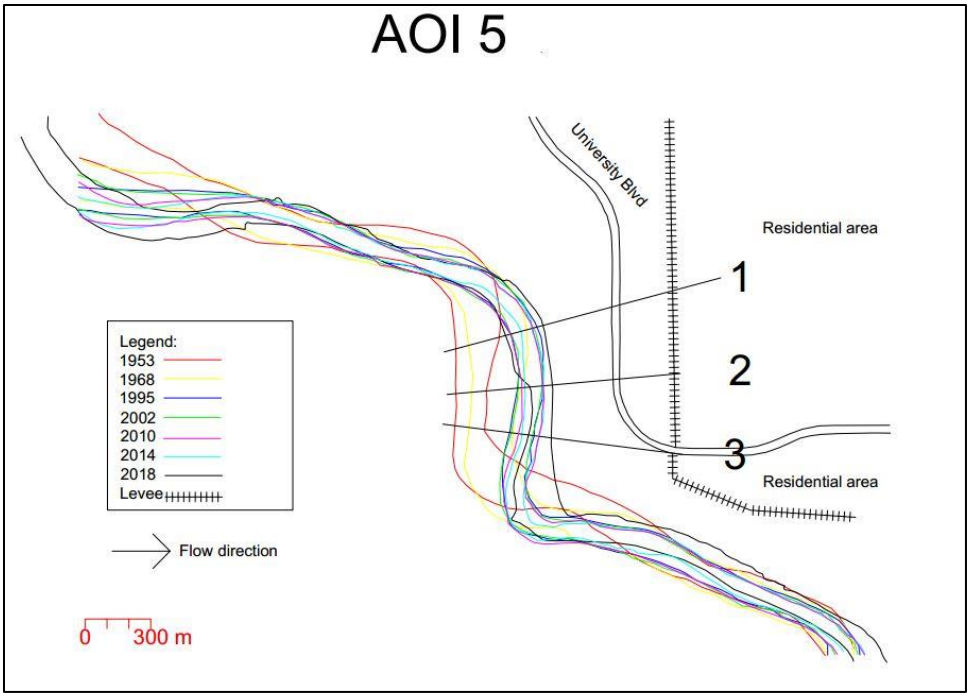

Figure 23. River movement observation at AOI 5

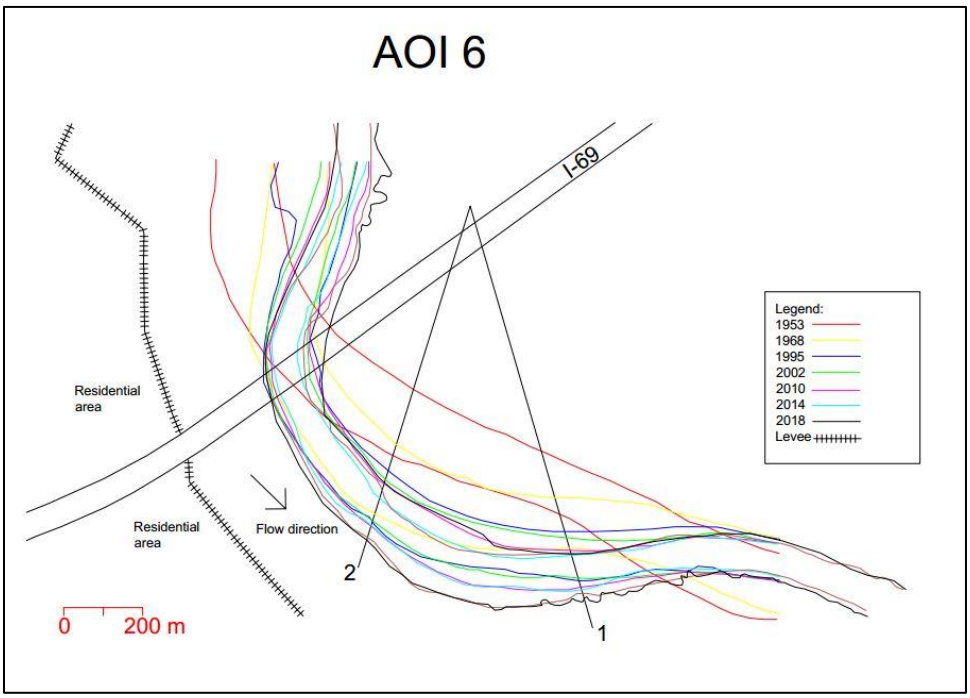

Figure 24. River movement observation at AOI 6

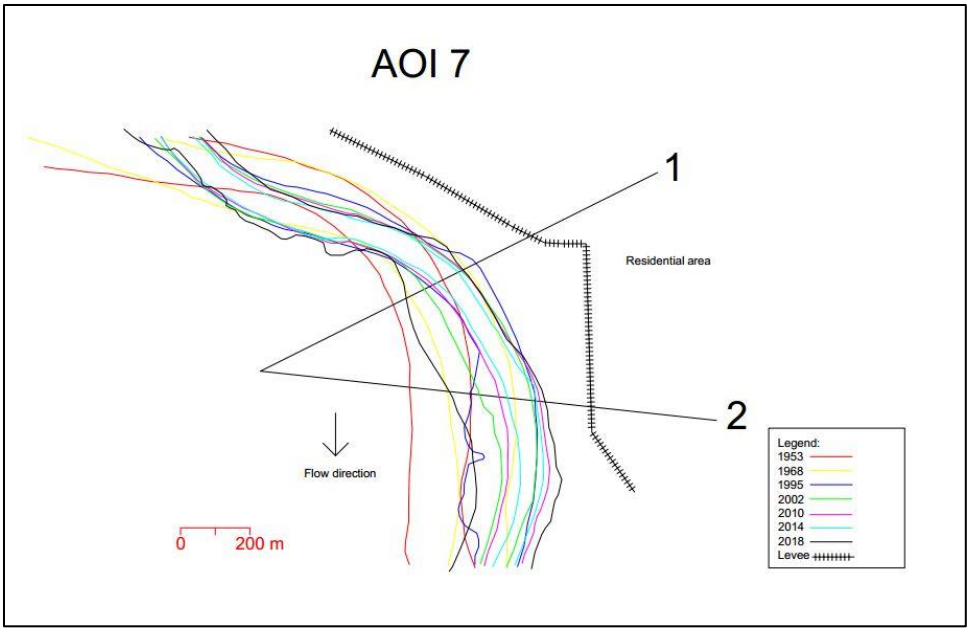

Figure 25. River movement observation at AOI 7

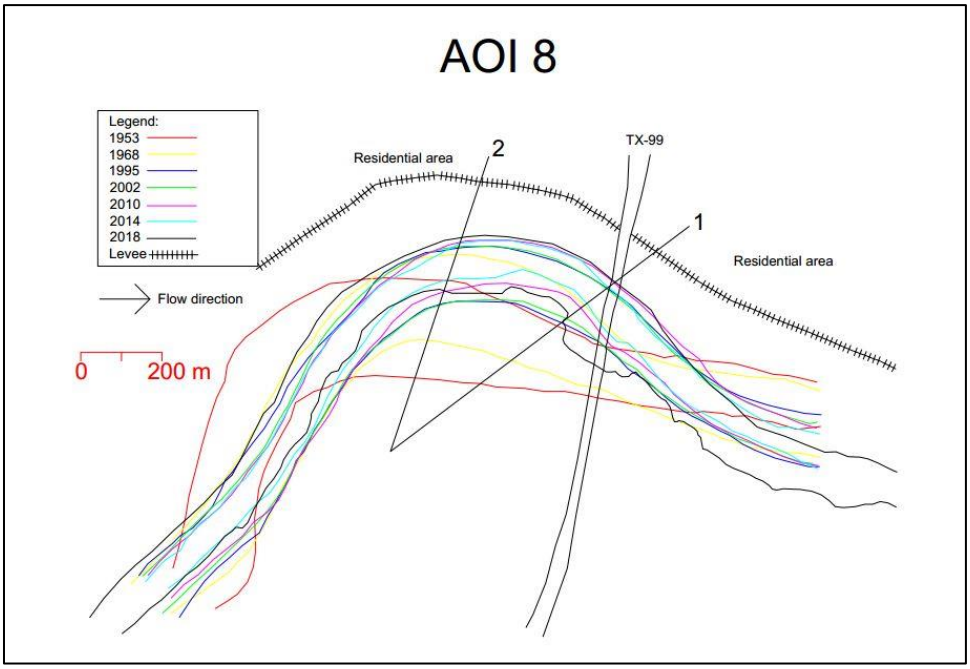

Figure 26. River movement observation at AOI 8

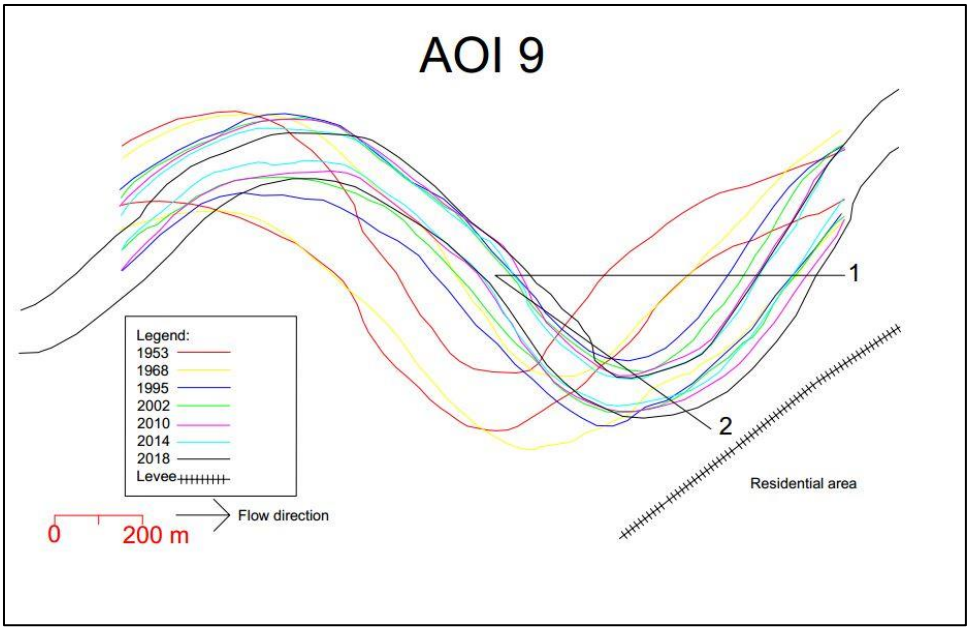

Figure 27. River movement observation at AOI 9

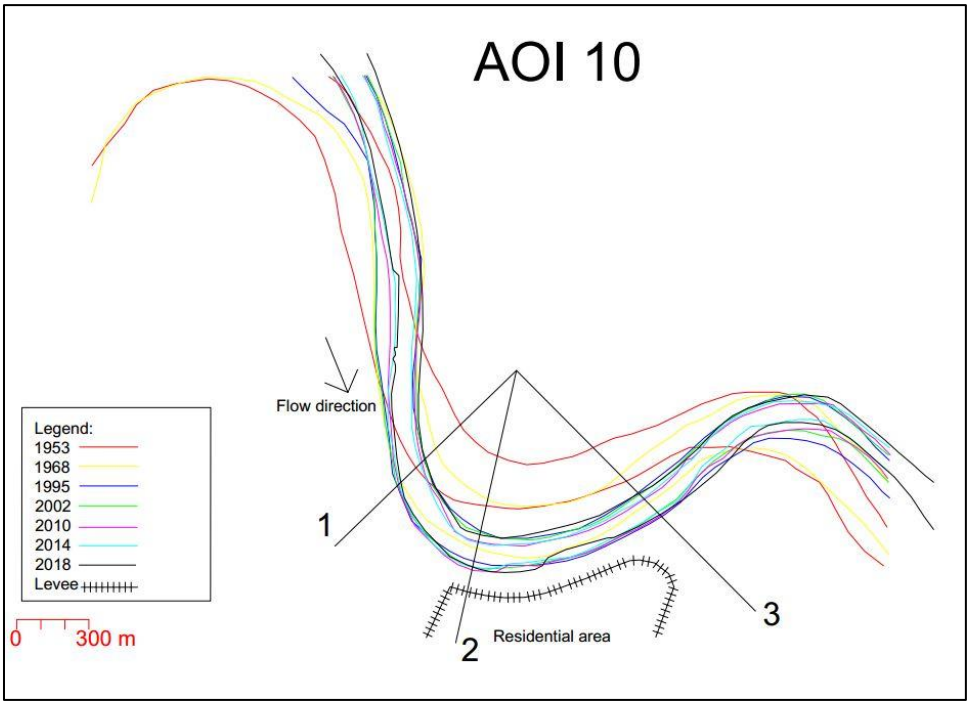

Figure 28. River movement observation at AOI 10

Seven samples from the field were tested as explained in Section 3.14 to obtain soil classification and soil erodibility. All of soil samples from depth above 50' are high plasticity clays (CH), sample at depth 50' is low plasticity clay (CL), and the lowest sample is poorly graded sand (SP). The result of EFA shows that soil of the riverbank is in category III (medium erodibility) for the clay and category II (high erodibility) for the sand (Figure 29). The gray line dividing category II and III is considered as the average erosion function for all the samples. The slope of the line is β = 5.24. This value is used for all meanders in the study area because the soil stratigraphy of the riverbank is assumed to be equal.

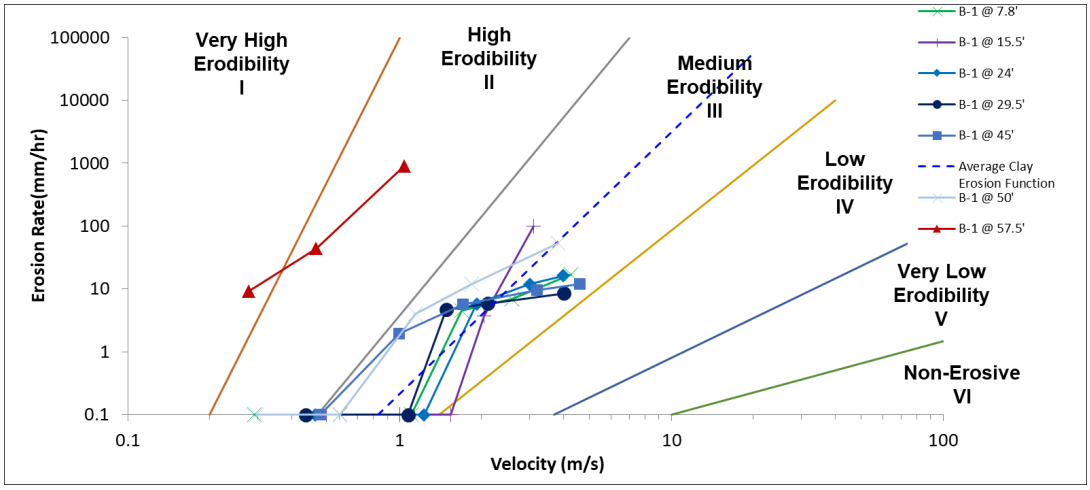

Figure 29. EFA test results from field samples in Brazos River

4.2. Calibration Step

Calibration step is conducted by using OMM spreadsheet or OMM code. The main result of the calibration step is critical velocity in the field (v_c) which is the lowest velocity at which the erosion starts to occur. Critical velocity value will be different for each meander and it is an important variable for meander prediction.

The following tables and figures show the results of calibration step for each meander of each AOI. The results consist of α' value, critical velocity in the field (v_c), Ranking Index (RI), observed migration (Mo), and calibrated migration (Mc).

4.2.1. Area of Interest (AOI) 3

Table 3. Calibration data of AOI 3 Direction 1

α'	3.9714×10^{-8}	
v_c	0.7 m/s	
RI	0.3163	
Time (years)	**Mo (m)**	**Mc (m)**
1953	0.00	0.00
1968	7.45	5.42
1995	16.22	15.06
2002	13.24	17.32
2010	16.50	20.58
2014	15.95	21.16
2018	37.43	24.65

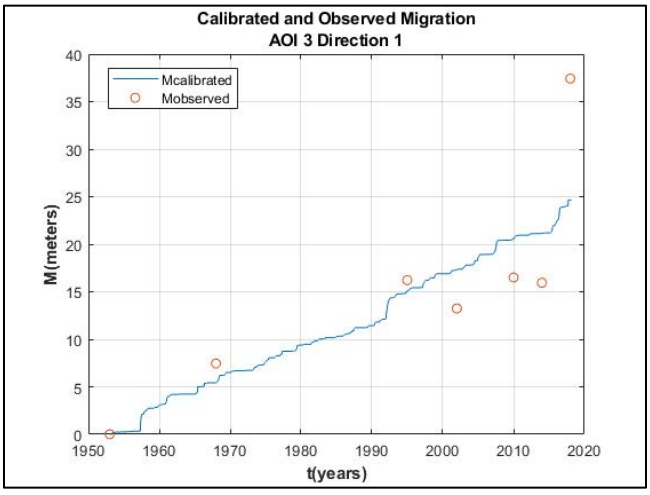

Figure 30. Calibrated and observed migration of AOI 3 Direction 1

Table 4. Calibration data of AOI 3 Direction 2

α’	4.088×10^{-8}	
v_c	0.68 m/s	
RI	0.6196	
Time (years)	**Mo (m)**	**Mc (m)**
1953	0.00	0.00
1968	15.05	6.56
1995	27.64	18.42
2002	10.72	21.23
2010	16.58	25.16
2014	15.69	25.88
2018	38.87	30.03

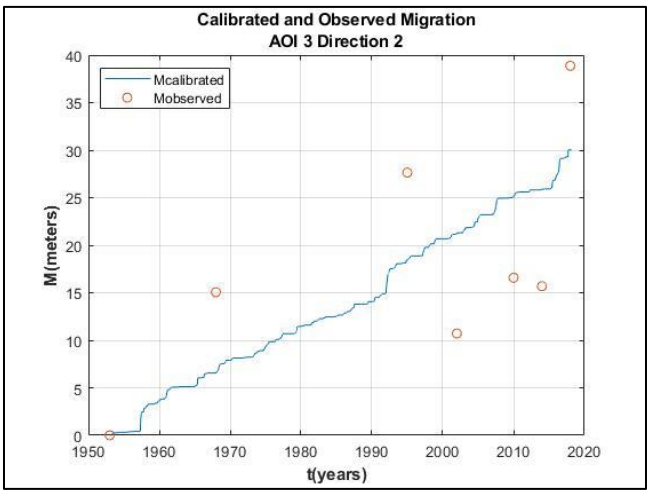

Figure 31. Calibrated and observed migration of AOI 3 Direction 2

Table 5. Calibration data of AOI 3 Direction 3

α’	5.0545×10^{-8}	
v_c	0.55 m/s	
RI	0.6632	
Time (years)	**Mo (m)**	**Mc (m)**
1953	0.00	0.00
1968	80.19	23.48
1995	81.42	67.83
2002	67.17	78.38
2010	68.85	92.36
2014	59.21	95.09
2018	87.00	108.76

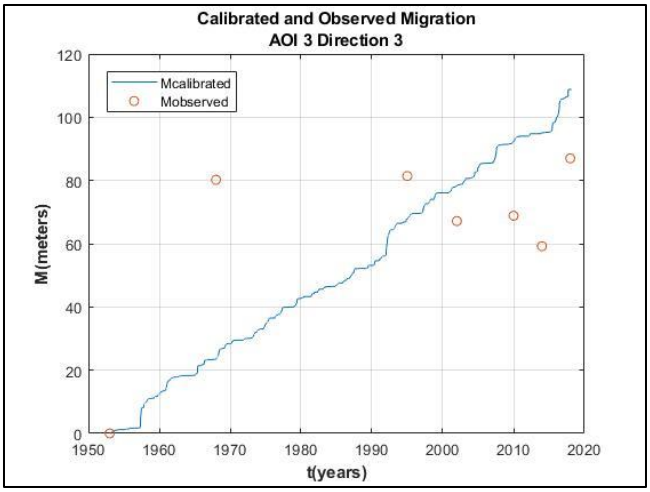

Figure 32. Calibrated and observed migration of AOI 3 Direction 3

4.2.2. Area of Interest (AOI) 4

Table 6. Calibration data of AOI 4 Direction 1

α'	4.2121×10^{-8}	
v_c	0.66 m/s	
RI	0.8472	
Time (years)	**Mo (m)**	**Mc (m)**
1953	0.00	0.00
1968	30.76	7.96
1995	35.30	22.59
2002	29.83	26.10
2010	26.52	30.85
2014	14.97	31.74
2018	15.96	36.70

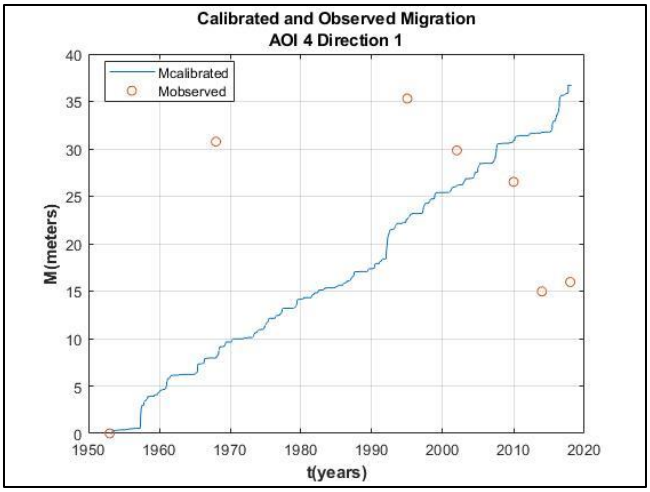

Figure 33. Calibrated and observed migration of AOI 4 Direction 1

Table 7. Calibration data of AOI 4 Direction 2

α'	4.8772×10^{-8}	
v_c	0.57 m/s	
RI	0.7014	
Time (years)	**Mo (m)**	**Mc (m)**
1953	0.00	0.00
1968	68.01	19.11
1995	58.35	55.25
2002	58.64	63.85
2010	78.73	75.35
2014	52.82	77.55
2018	47.29	88.80

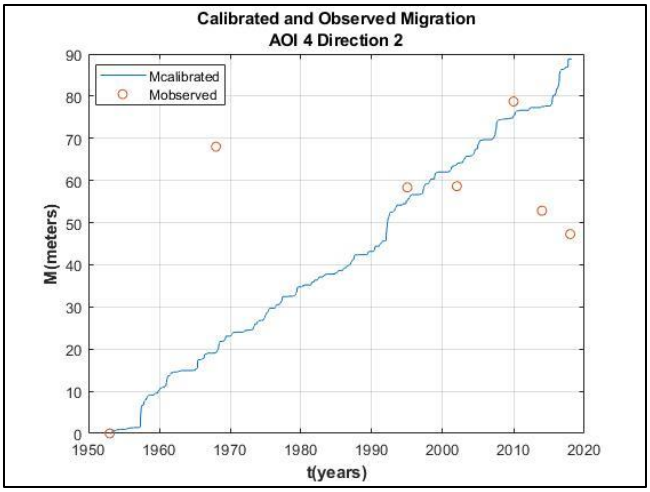

Figure 34. Calibrated and observed migration of AOI 4 Direction 2

Table 8. Calibration data of AOI 4 Direction 3

α'	5.0545×10^{-8}	
v_c	0.55 m/s	
RI	0.6268	
Time (years)	**Mo (m)**	**Mc (m)**
1953	0.00	0.00
1968	67.13	23.48
1995	66.92	67.83
2002	70.48	78.38
2010	81.48	92.36
2014	68.20	95.09
2018	53.73	108.79

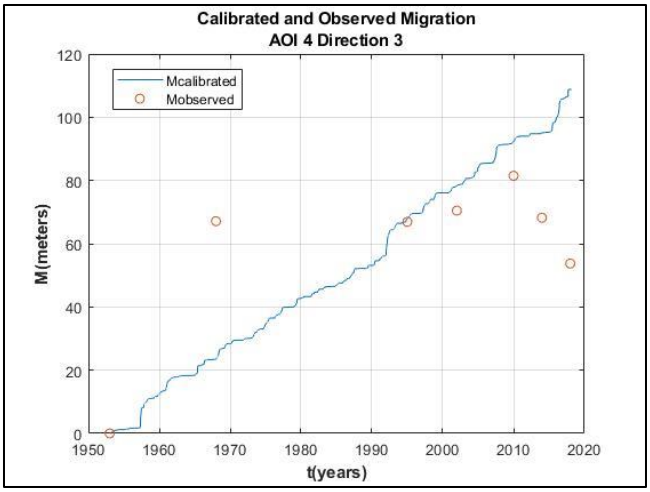

Figure 35. Calibrated and observed migration of AOI 4 Direction 3

4.2.3. Area of Interest (AOI) 5

Table 9. Calibration data of AOI 5 Direction 1

α'	5.9149×10^{-8}	
v_c	0.47 m/s	
RI	0.4804	
Time (years)	**Mo (m)**	**Mc (m)**
1953	0.00	0.00
1968	128.99	55.83
1995	178.37	161.28
2002	161.03	186.33
2010	156.63	219.64
2014	154.40	226.22
2018	207.00	258.18

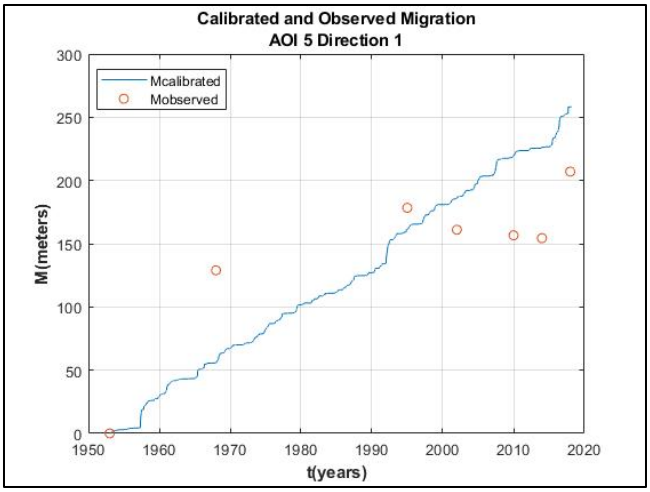

Figure 36. Calibrated and observed migration of AOI 5 Direction 1

Table 10. Calibration data of AOI 5 Direction 2

α'	6.3182 x 10^{-8}	
v_c	0.44 m/s	
RI	0.3863	
Time (years)	**Mo (m)**	**Mc (m)**
1953	0.00	0.00
1968	159.79	79.23
1995	258.27	228.93
2002	257.64	264.49
2010	261.07	311.72
2014	262.97	321.09
2018	303.49	366.39

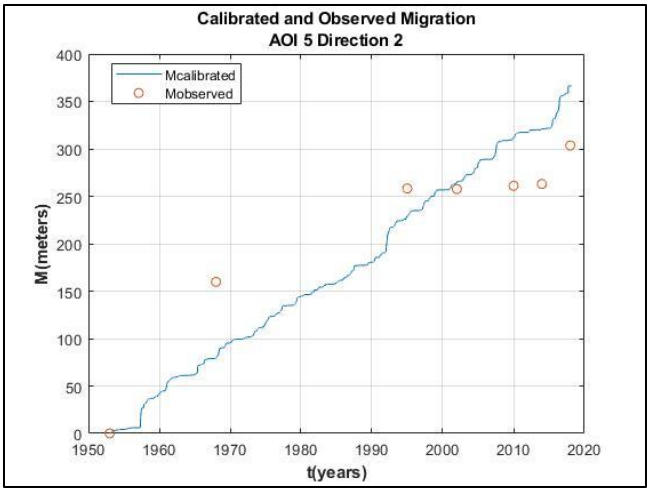

Figure 37. Calibrated and observed migration of AOI 5 Direction 2

Table 11. Calibration data of AOI 5 Direction 3

α'	6.3182 x 10^{-8}	
v_c	0.44 m/s	
RI	0.3377	
Time (years)	**Mo (m)**	**Mc (m)**
1953	0.00	0.00
1968	130.04	79.23
1995	227.32	228.93
2002	220.59	264.49
2010	249.58	311.72
2014	252.10	321.09
2018	307.58	366.39

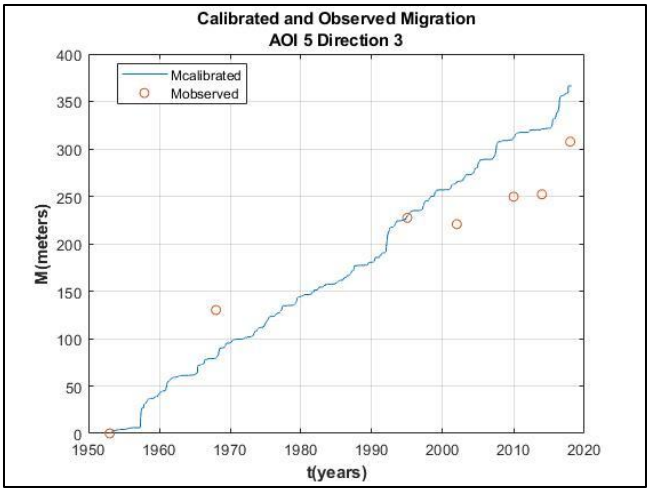

Figure 38. Calibrated and observed migration of AOI 5 Direction 3

4.2.4. Area of Interest (AOI) 6

Table 12. Calibration data of AOI 6 Direction 1

α'	5.9149 x 10^{-8}	
v_c	0.47 m/s	
RI	0.2535	
Time (years)	**Mo (m)**	**Mc (m)**
1953	0.00	0.00
1968	89.71	55.83
1995	176.16	161.28
2002	168.48	186.33
2010	193.21	219.64
2014	199.64	226.22
2018	222.70	258.18

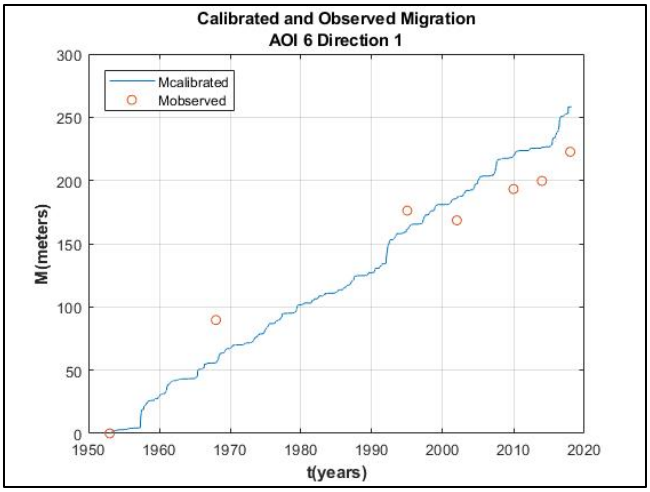

Figure 39. Calibrated and observed migration of AOI 6 Direction 1

Table 13. Calibration data of AOI 6 Direction 2

α'	6.0435 x 10^{-8}	
v_c	0.46 m/s	
RI	0.4903	
Time (years)	**Mo (m)**	**Mc (m)**
1953	0.00	0.00
1968	155.86	62.60
1995	175.89	180.85
2002	174.27	208.95
2010	187.69	246.28
2014	185.81	253.67
2018	225.12	289.47

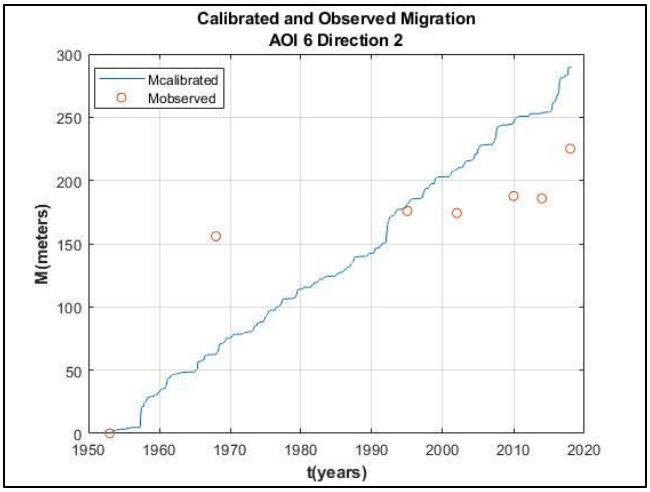

Figure 40. Calibrated and observed migration of AOI 6 Direction 2

4.2.5. Area of Interest (AOI) 7

Table 14. Calibration data of AOI 7 Direction 1

α'	5.0545 x 10^{-8}	
v_c	0.55 m/s	
RI	0.7337	
Time (years)	**Mo (m)**	**Mc (m)**
1953	0.00	0.00
1968	75.98	23.48
1995	107.15	67.83
2002	59.51	78.33
2010	63.16	92.36
2014	49.99	95.09
2018	65.22	108.79

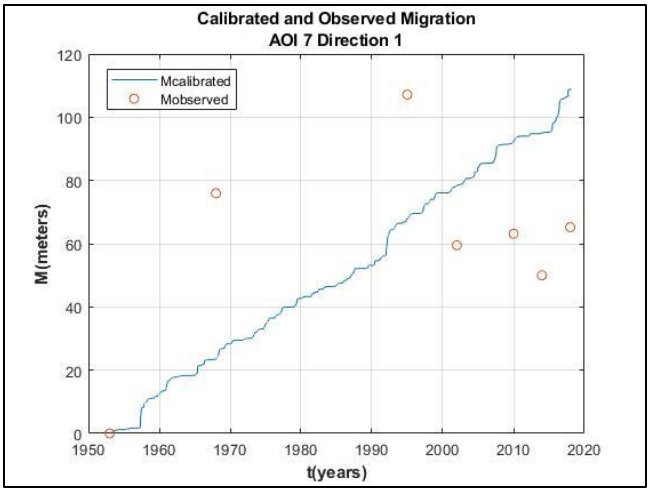

Figure 41. Calibrated and observed migration of AOI 7 Direction 1

Table 15. Calibration data of AOI 7 Direction 2

α'	6.0435×10^{-8}	
v_c	0.46 m/s	
RI	0.4240	
Time (years)	**Mo (m)**	**Mc (m)**
1953	0.00	0.00
1968	124.84	62.60
1995	185.06	180.85
2002	175.75	208.95
2010	198.99	246.28
2014	188.35	253.66
2018	214.63	289.47

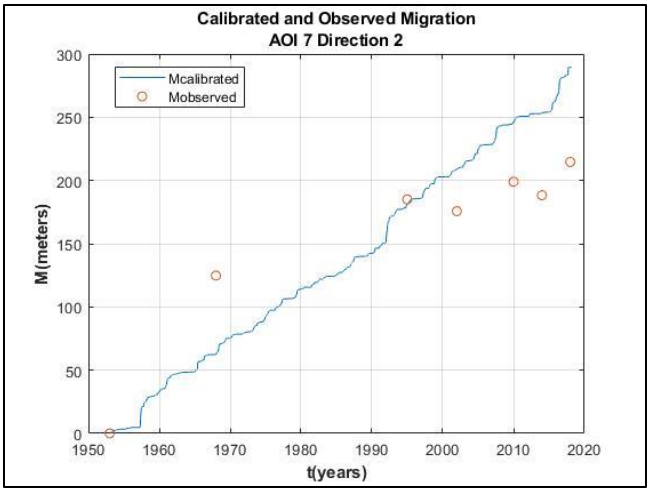

Figure 42. Calibrated and observed migration of AOI 7 Direction 2

4.2.6. Area of Interest (AOI) 8

Table 16. Calibration data of AOI 8 Direction 1

α'	5.7917 x 10^{-8}	
v_c	0.48 m/s	
RI	0.3106	
Time (years)	**Mo (m)**	**Mc (m)**
1953	0.00	0.00
1968	84.33	49.91
1995	154.08	144.16
2002	150.96	166.56
2010	175.79	196.34
2014	158.22	202.23
2018	179.11	230.81

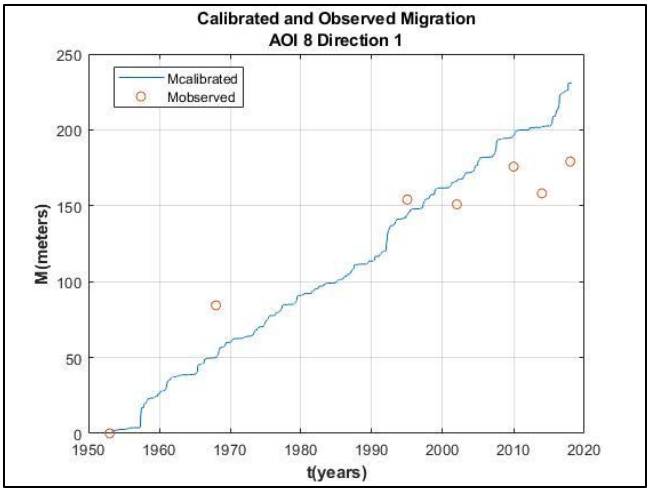

Figure 43. Calibrated and observed migration of AOI 8 Direction 1

Table 17. Calibration data of AOI 8 Direction 2

α'	5.2453 x 10^{-8}	
v_c	0.53 m/s	
RI	0.4445	
Time (years)	**Mo (m)**	**Mc (m)**
1953	0.00	0.00
1968	67.98	28.96
1995	84.17	83.77
2002	87.76	96.77
2010	98.96	114.10
2014	96.09	117.50
2018	111.52	134.26

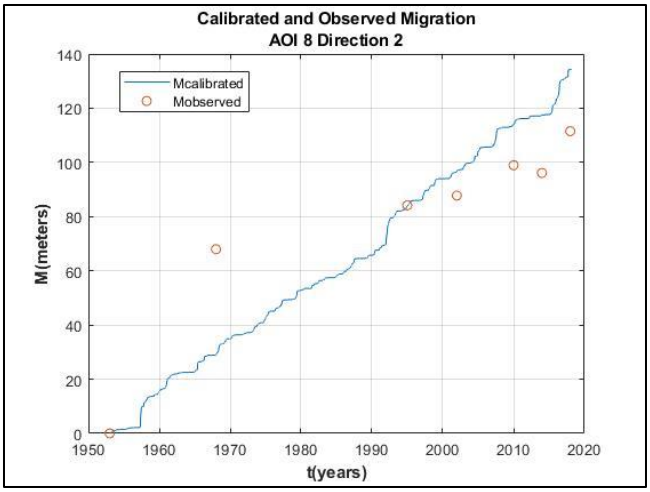

Figure 44. Calibrated and observed migration of AOI 8 Direction 2

4.2.7. Area of Interest (AOI) 9

Table 18. Calibration data of AOI 9 Direction 1

α'	6.4651×10^{-8}	
v_c	0.43 m/s	
RI	0.5852	
Time (years)	**Mo (m)**	**Mc (m)**
1953	0.00	0.00
1968	248.33	89.54
1995	238.13	258.62
2002	244.50	298.78
2010	270.59	352.11
2014	238.75	362.70
2018	292.14	413.83

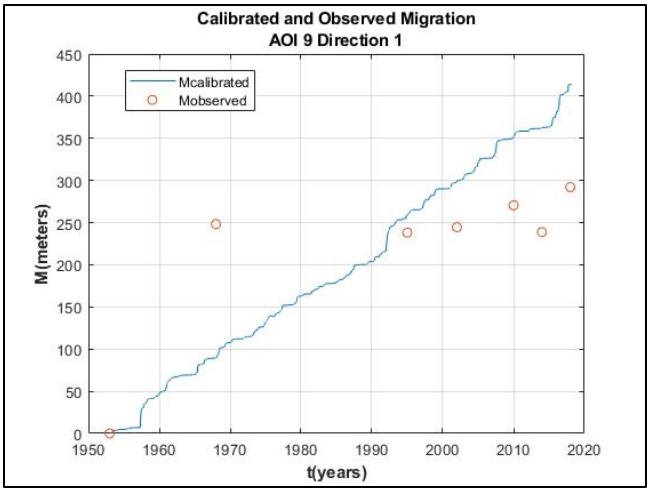

Figure 45. Calibrated and observed migration of AOI 9 Direction 1

Table 19. Calibration data of AOI 9 Direction 2

α'	5.9149 x 10^{-8}	
v_c	0.47 m/s	
RI	0.4391	
Time (years)	**Mo (m)**	**Mc (m)**
1953	0.00	0.00
1968	117.79	55.83
1995	160.18	161.28
2002	166.01	186.33
2010	174.29	219.64
2014	153.52	226.22
2018	207.61	258.18

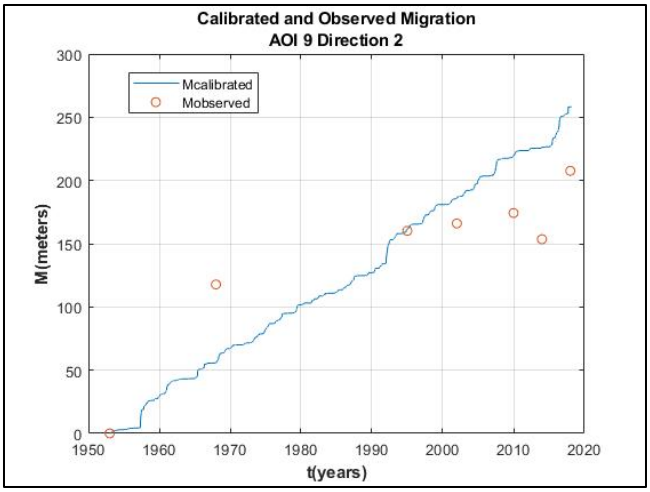

Figure 46. Calibrated and observed migration of AOI 9 Direction 2

4.2.8. Area of Interest (AOI) 10

Table 20. Calibration data of AOI 10 Direction 1

α'	5.2453 x 10^{-8}	
v_c	0.53 m/s	
RI	0.6650	
Time (years)	**Mo (m)**	**Mc (m)**
1953	0.00	0.00
1968	84.53	28.96
1995	108.78	83.77
2002	106.64	96.77
2010	100.17	114.10
2014	94.53	117.50
2018	60.95	134.26

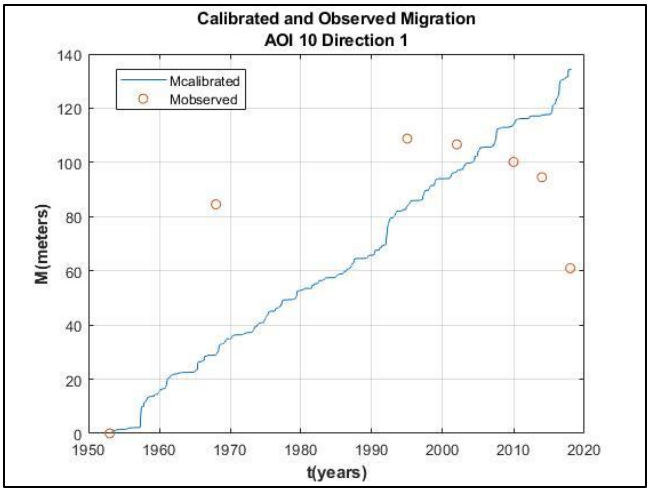

Figure 47. Calibrated and observed migration of AOI 10 Direction 1

Table 21. Calibration data of AOI 10 Direction 2

α'	6.3182 x 10^{-8}	
v_c	0.44 m/s	
RI	0.4385	
Time (years)	**Mo (m)**	**Mc (m)**
1953	0.00	0.00
1968	181.25	79.23
1995	231.08	228.93
2002	260.54	264.49
2010	273.75	311.72
2014	262.66	321.10
2018	261.02	366.39

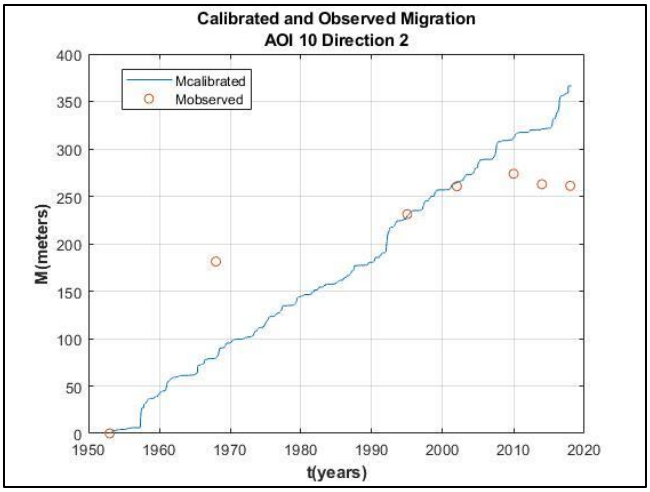

Figure 48. Calibrated and observed migration of AOI 10 Direction 2

Table 22. Calibration data of AOI 10 Direction 3

α'	6.0435×10^{-8}	
v_c	0.46 m/s	
RI	0.4432	
Time (years)	**Mo (m)**	**Mc (m)**
1953	0.00	0.00
1968	129.86	62.60
1995	208.14	180.85
2002	183.27	208.95
2010	200.92	246.28
2014	183.43	253.66
2018	197.14	289.47

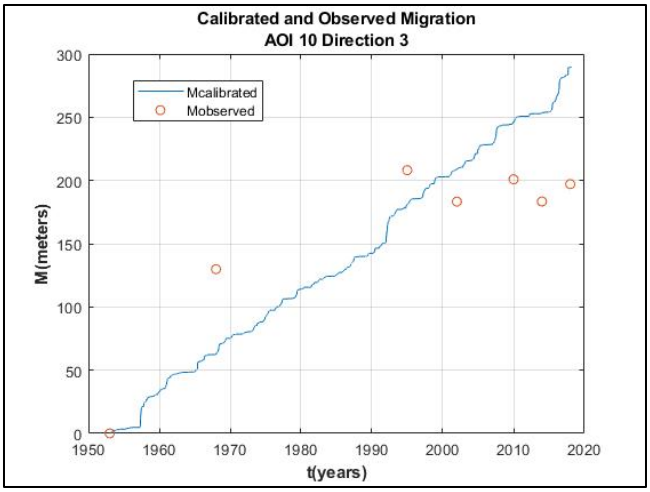

Figure 49. Calibrated and observed migration of AOI 10 Direction 3

4.3. Deterministic Prediction

Previous OMM for prediction step only used spreadsheet. In this study, OMM code is improved for prediction step because there is any limitation using spreadsheet particularly for probabilistic prediction. Input data for this step are critical velocity in the field (v_c) and soil parameters (α' and β) from calibration steps, and future flow discharge. The difference between deterministic and probabilistic prediction comes from future flow discharge data. In deterministic prediction, future hydrograph is in a single value which can be obtained from the past hydrograph with or without consideration of flood.

Deterministic prediction for this study is carried out in two analyses. First, by using last 30 years hydrograph and the second is by using last 30 years hydrograph with a 500-year flood. The flood discharge, Q_{500} = 206,000 cfs is applied for a week (seven days) in the middle of the future period (21 to 27 July 2033). The results of the deterministic prediction are shown by the following figures and tables. Because the prediction uses the copied flow hydrograph, the future migration duplicates the past migration and all the meanders have the same pattern of future migration line.

Table 23. Future predicted position and migration distance by deterministic prediction

Meander Name	Last Position (in 2018) (m)	Without Flood		With 500-Year Flood	
		Predicted Position (in 2048) (m)	Migration Distance (m)	Predicted Position (in 2048) (m)	Migration Distance (m)
AOI 3 Direction 1	37.43	51.20	14.54	56.06	18.63
AOI 3 Direction 2	38.87	55.53	16.66	61.18	22.31
AOI 3 Direction 3	87.00	145.20	58.20	162.39	75.39
AOI 4 Direction 1	15.96	36.13	20.17	42.74	26.78
AOI 4 Direction 2	47.29	94.98	47.69	109.23	61.94
AOI 4 Direction 3	53.73	111.93	58.20	129.12	75.39
AOI 5 Direction 1	207.00	344.32	137.32	383.48	176.48
AOI 5 Direction 2	303.49	498.25	194.76	553.59	250.10
AOI 5 Direction 3	307.58	502.34	194.76	557.68	250.10
AOI 6 Direction 1	222.70	360.02	137.32	399.18	176.48
AOI 6 Direction 2	225.12	379.04	153.92	422.88	197.76
AOI 7 Direction 1	65.22	123.42	58.20	140.61	75.39
AOI 7 Direction 2	214.63	368.56	153.93	412.39	197.76
AOI 8 Direction 1	179.11	301.92	122.81	337.00	157.89
AOI 8 Direction 2	111.52	183.20	71.68	204.07	92.55
AOI 9 Direction 1	292.14	512.08	219.94	574.49	282.35
AOI 9 Direction 2	207.61	344.92	137.31	348.09	140.48
AOI 10 Direction 1	60.95	132.62	71.67	153.50	92.55
AOI 10 Direction 2	261.02	455.79	194.77	511.11	250.09
AOI 10 Direction 3	197.14	351.07	153.93	394.90	197.76

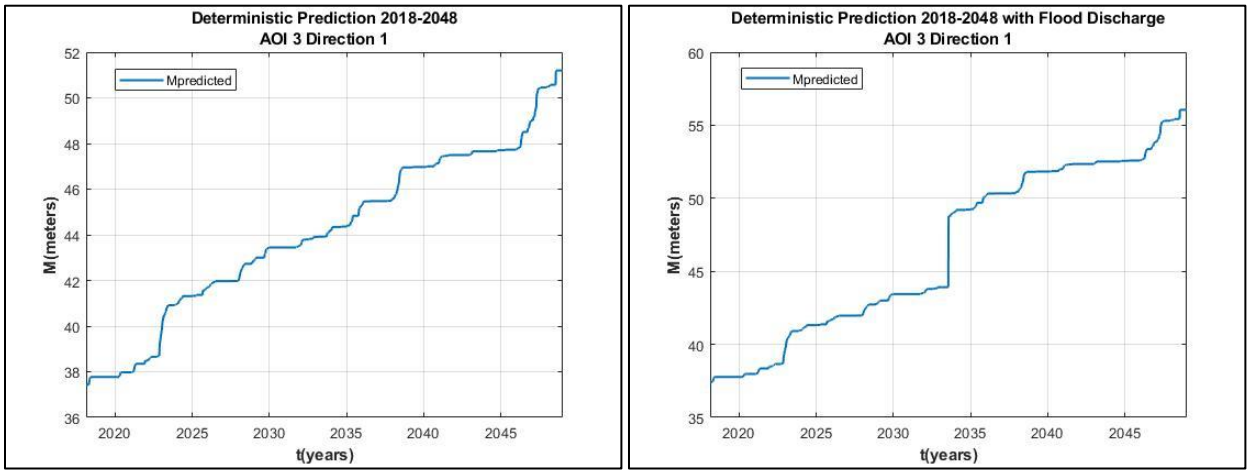

Figure 50. Deterministic prediction of AOI 3 Direction 1

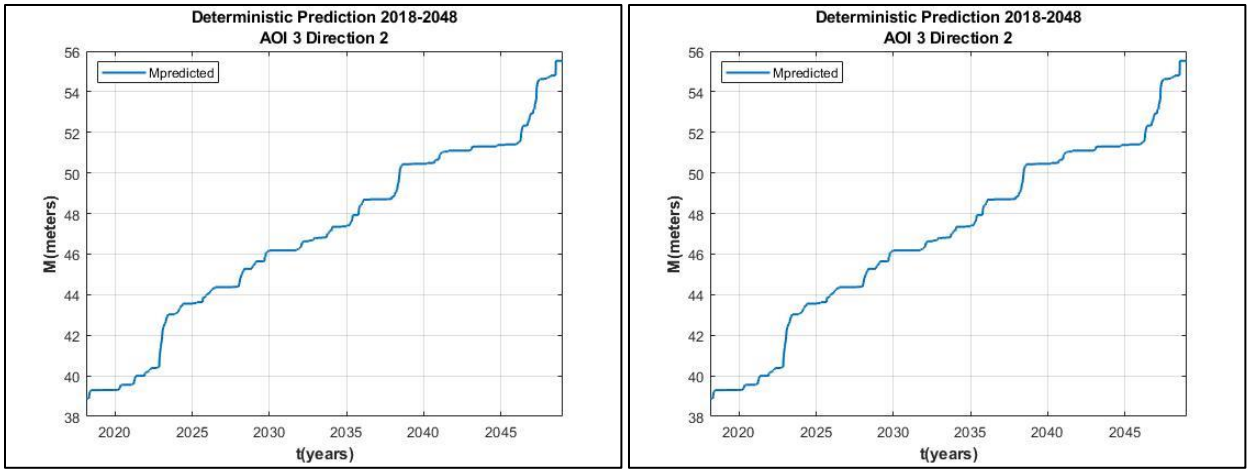

Figure 51. Deterministic prediction of AOI 3 Direction 2

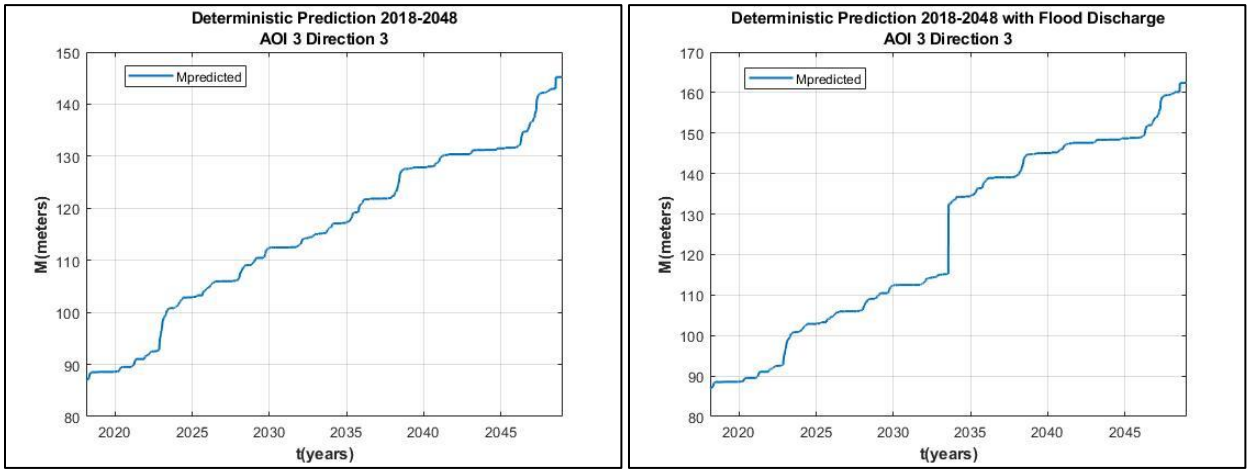

Figure 52. Deterministic prediction of AOI 3 Direction 3

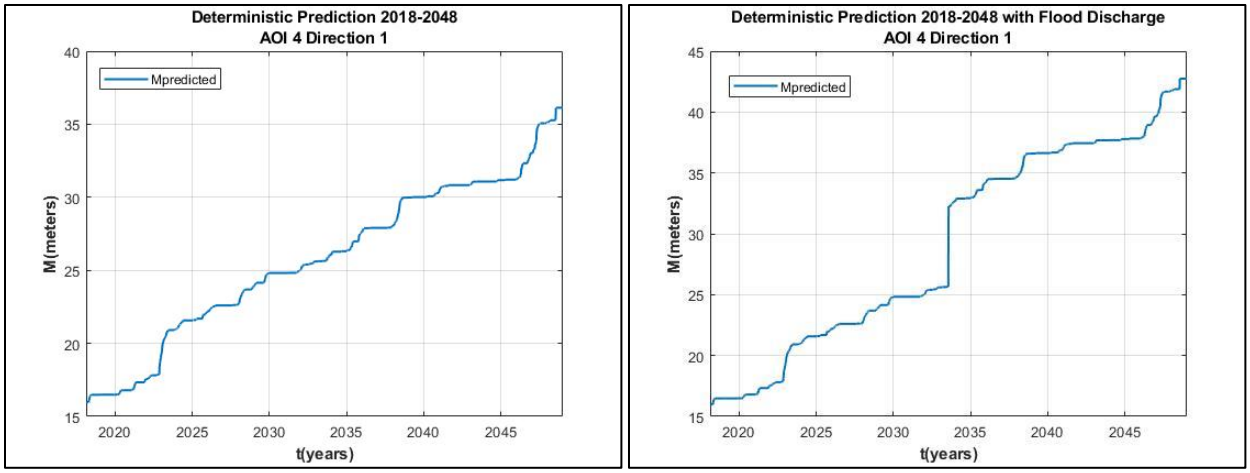

Figure 53. Deterministic prediction of AOI 4 Direction 1

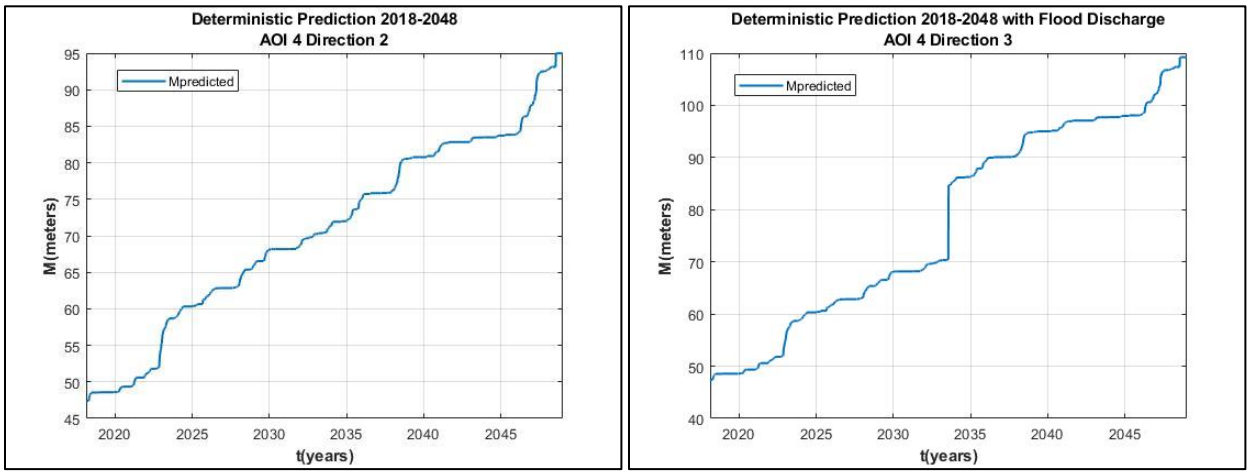

Figure 54. Deterministic prediction of AOI 4 Direction 2

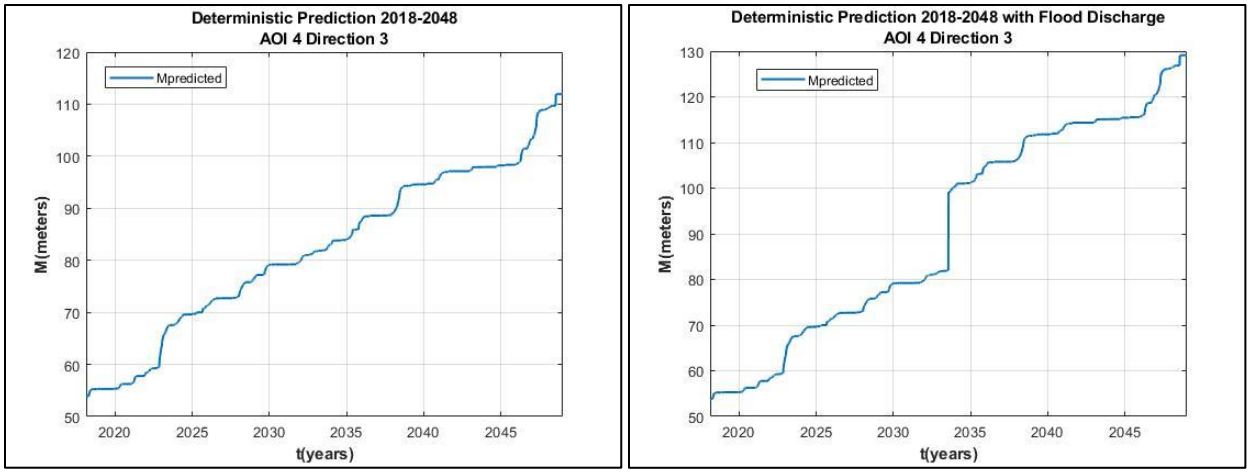

Figure 55. Deterministic prediction of AOI 4 Direction 3

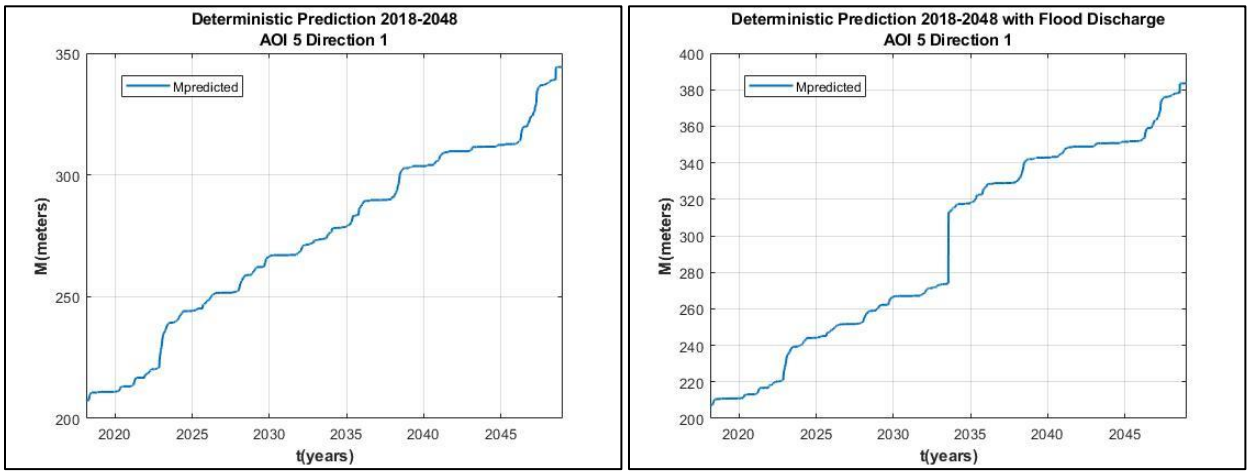

Figure 56. Deterministic prediction of AOI 5 Direction 1

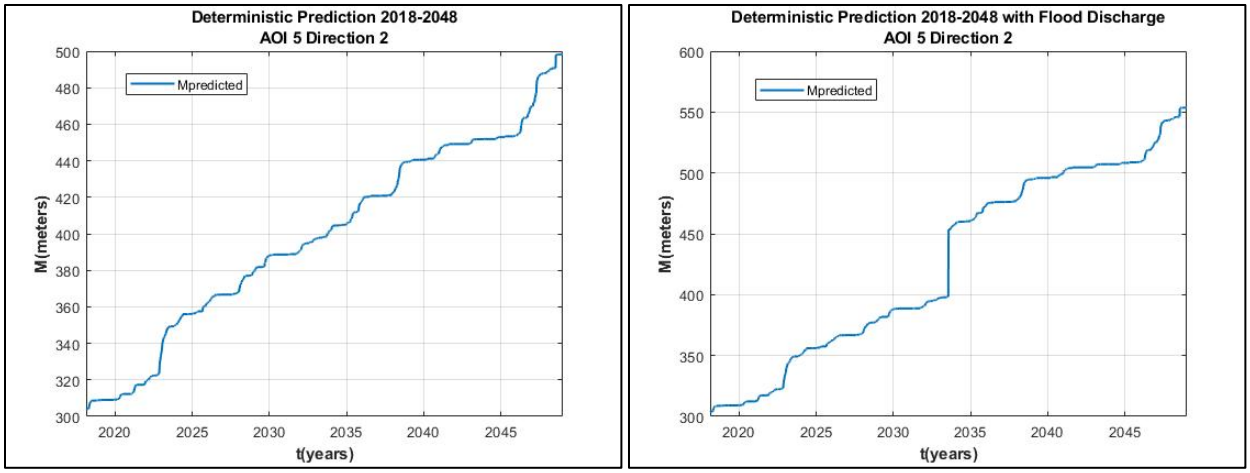

Figure 57. Deterministic prediction of AOI 5 Direction 2

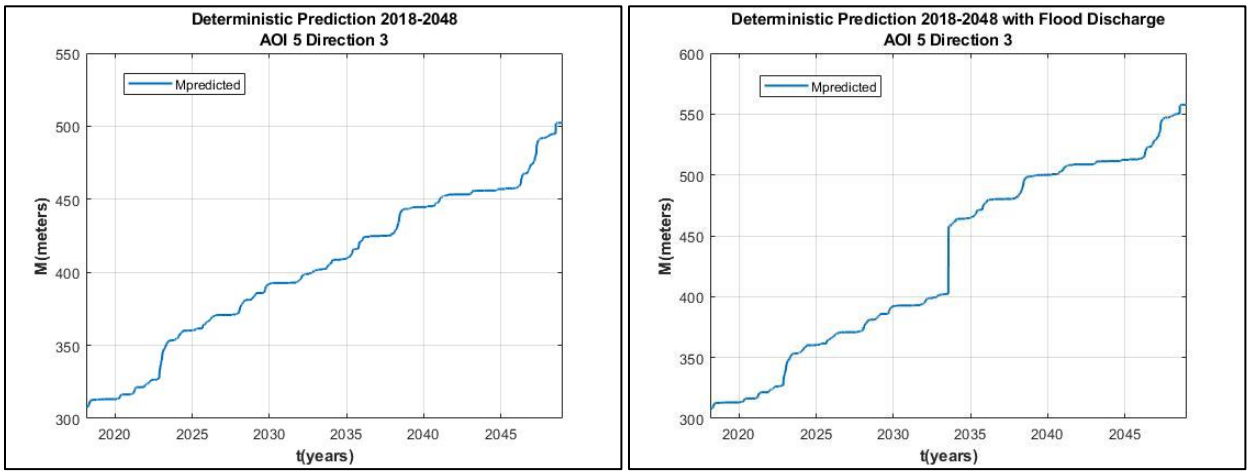

Figure 58. Deterministic prediction of AOI 5 Direction 3

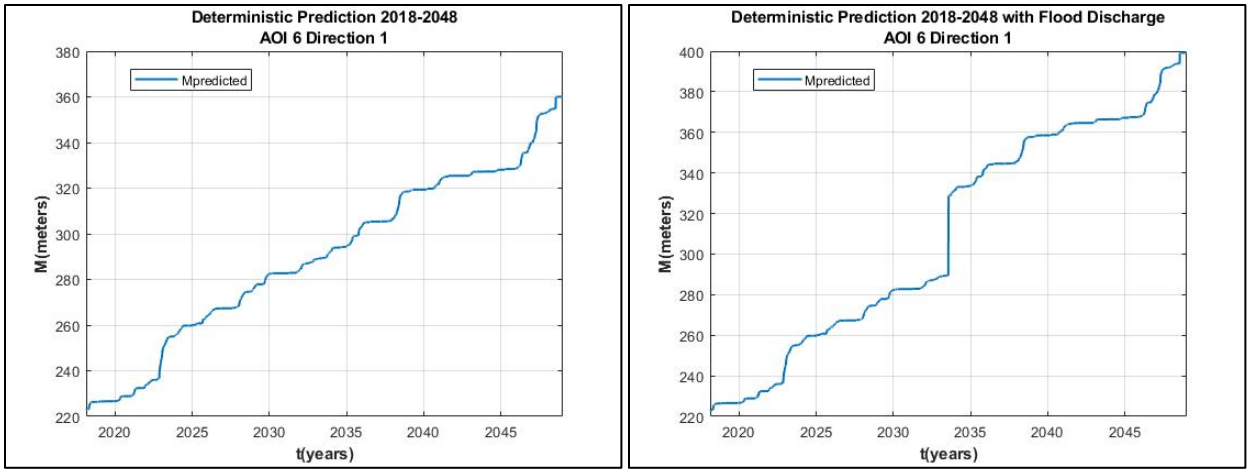

Figure 59. Deterministic prediction of AOI 6 Direction 1

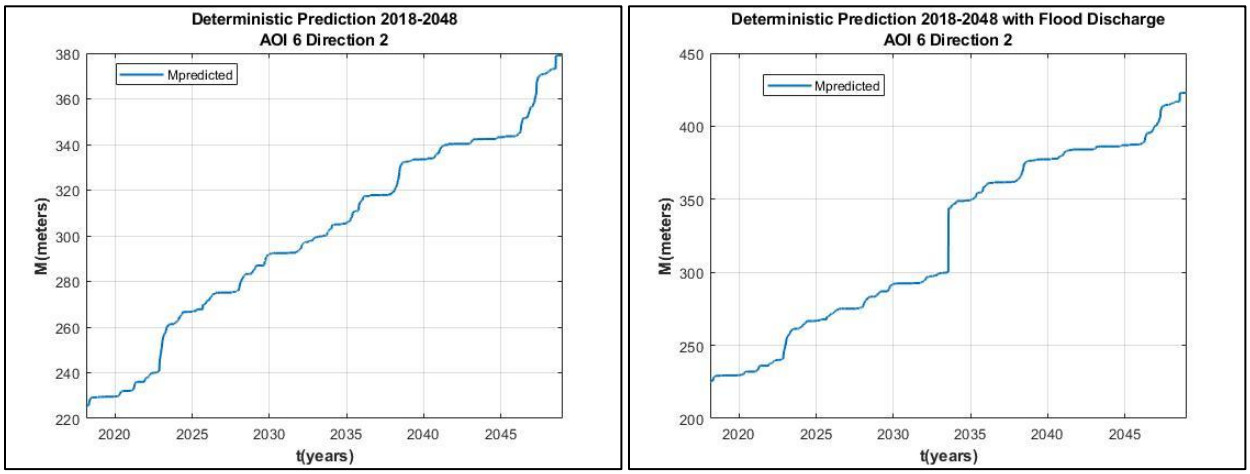

Figure 60. Deterministic prediction of AOI 6 Direction 2

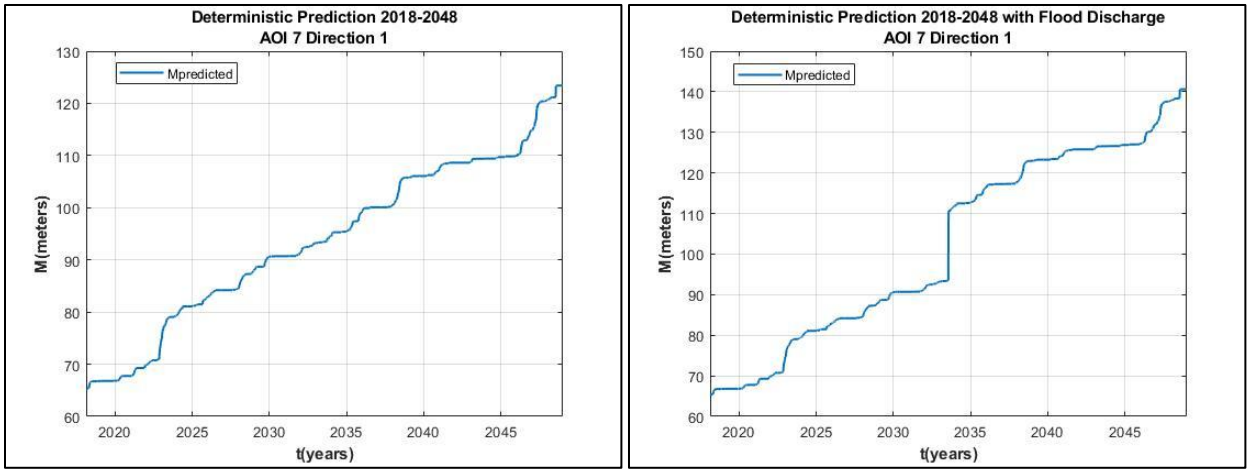

Figure 61. Deterministic prediction of AOI 7 Direction 1

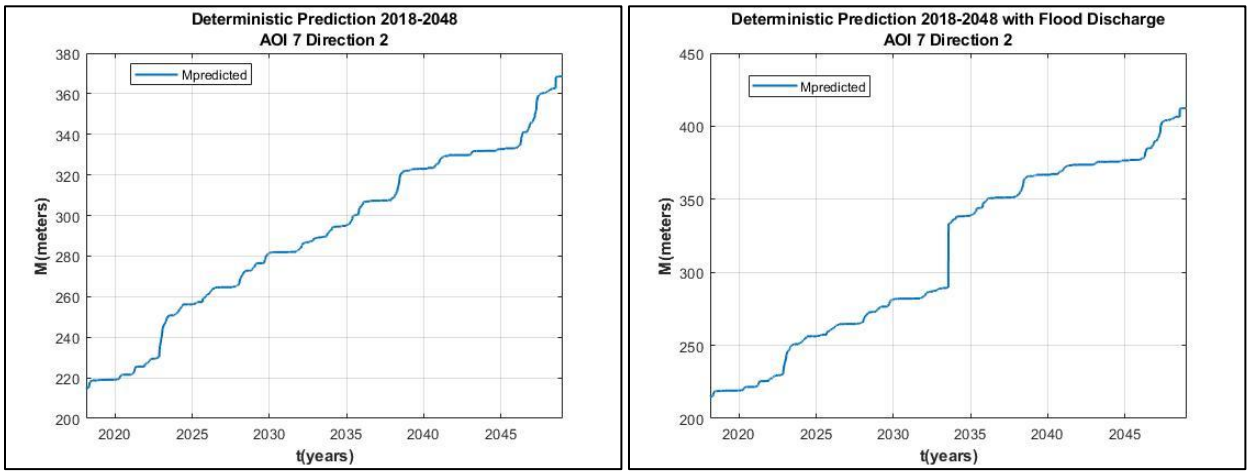

Figure 62. Deterministic prediction of AOI 7 Direction 2

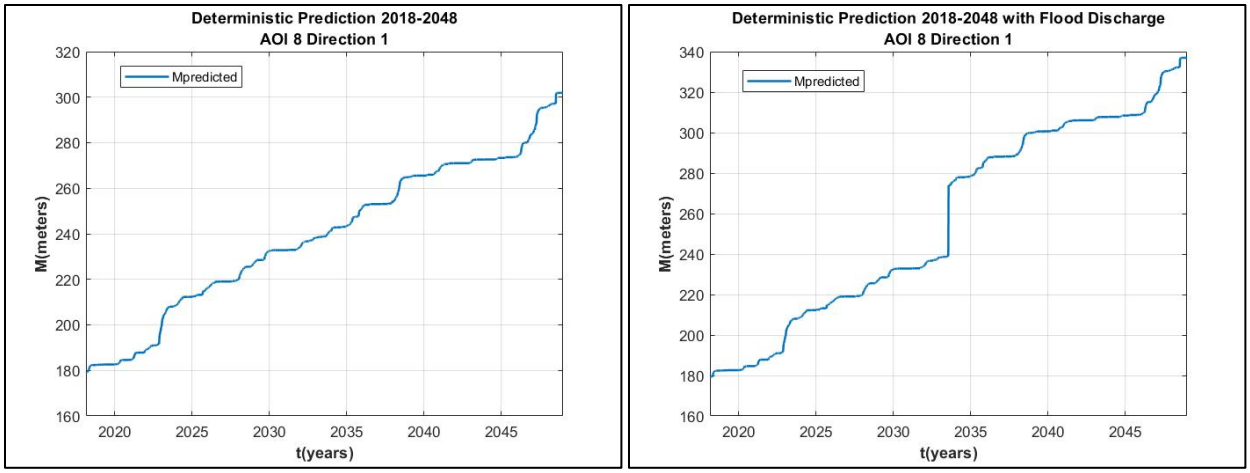

Figure 63. Deterministic prediction of AOI 8 Direction 1

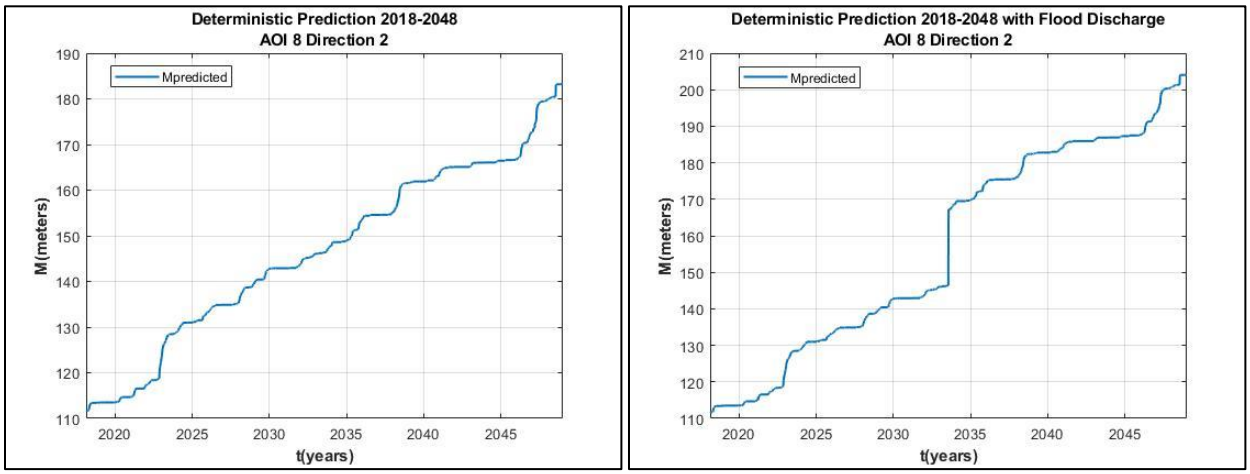

Figure 64. Deterministic prediction of AOI 8 Direction 2

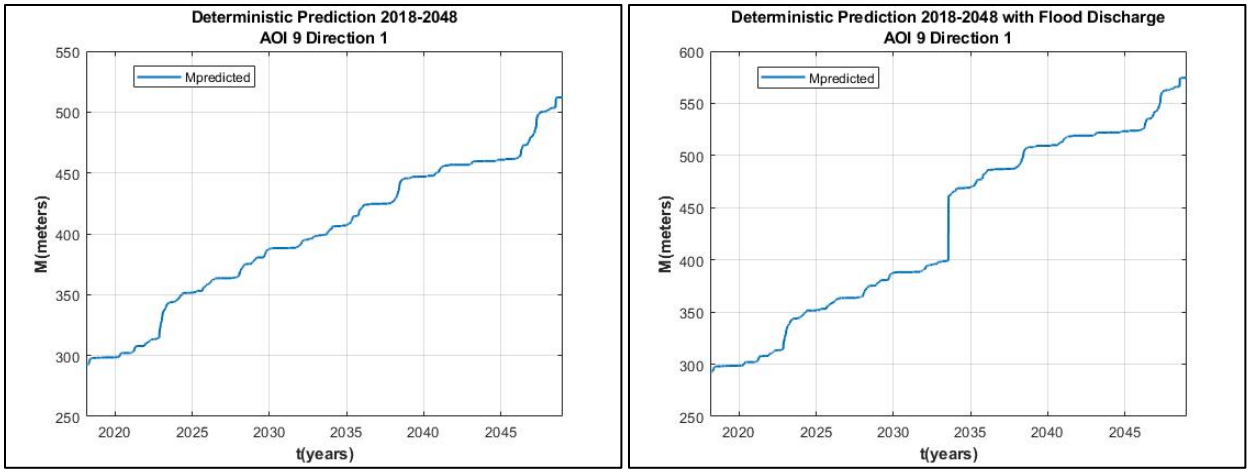

Figure 65. Deterministic prediction of AOI 9 Direction 1

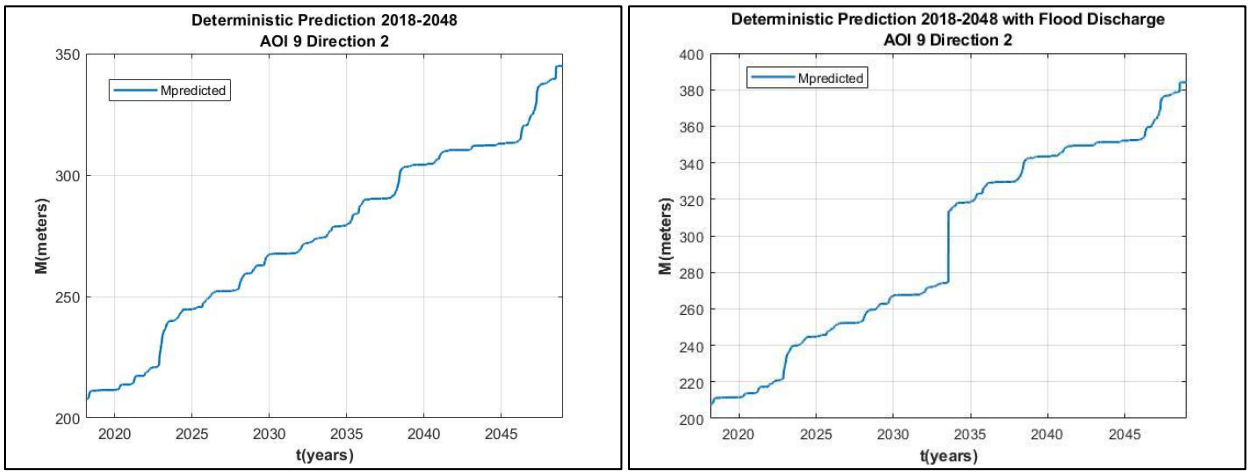

Figure 66. Deterministic prediction of AOI 9 Direction 2

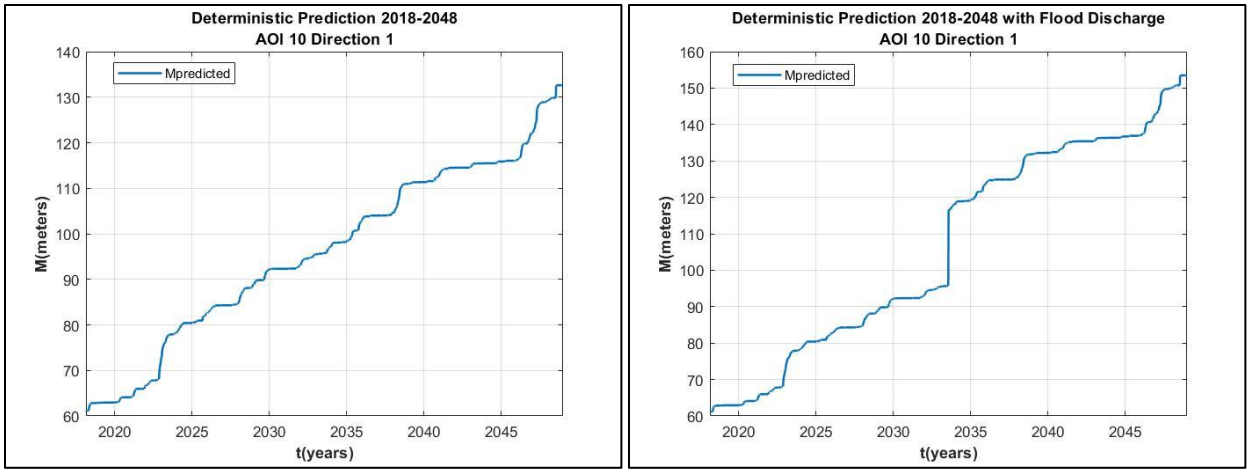

Figure 67. Deterministic prediction of AOI 10 Direction 1

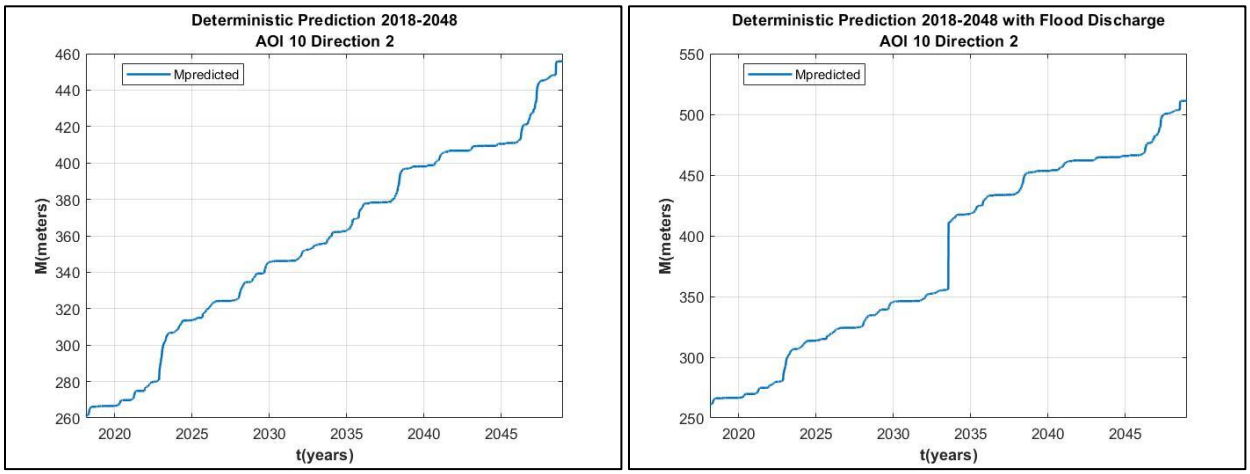

Figure 68. Deterministic prediction of AOI 10 Direction 2

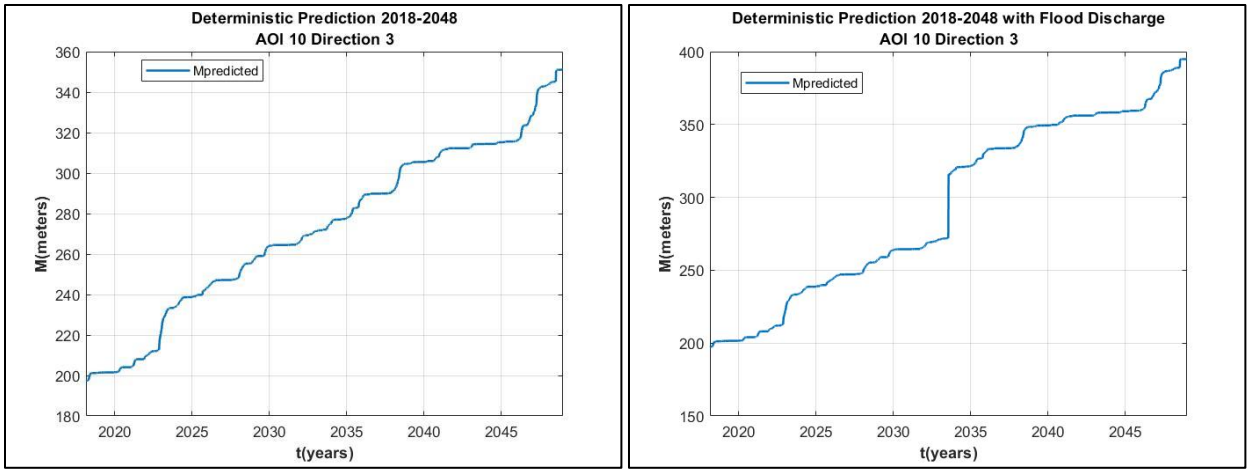

Figure 69. Deterministic prediction of AOI 10 Direction 3

After the migration distance is obtained from deterministic prediction, the predicted outer riverbank line can be drawn to find out whether the river will be likely to migrate beyond levee or to move until reaching residential areas by the river. The geometry of the predicted riverbank line in 2048 is assumed to follow the geometry of the current riverbank because this prediction does not consider any changes in geometry that might happen during the future period.

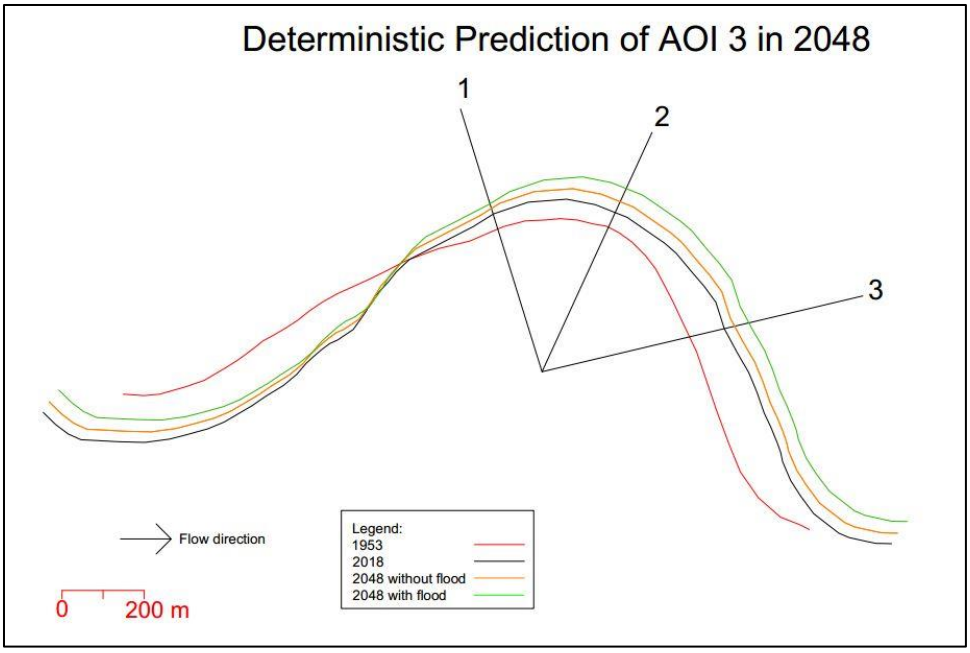

Figure 70. River position of AOI 3 in 2048 based on deterministic prediction

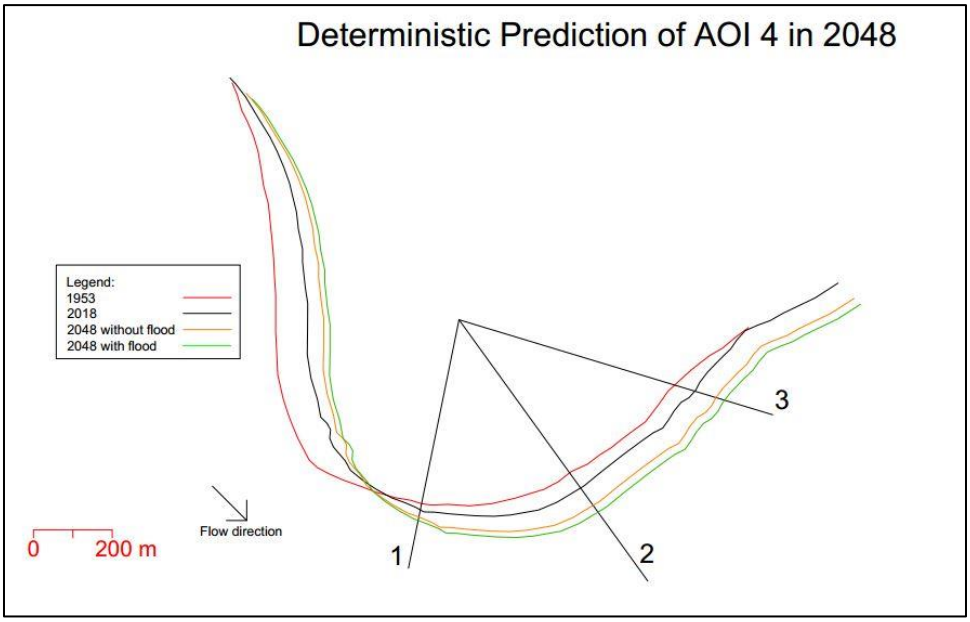

Figure 71. River position of AOI 4 in 2048 based on deterministic prediction

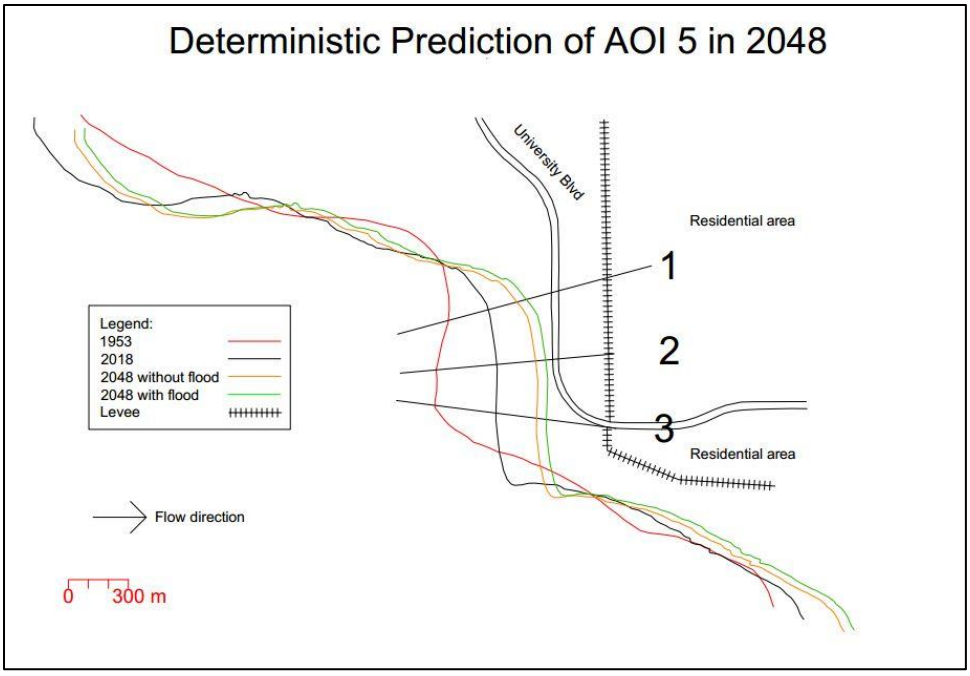

Figure 72. River position of AOI 5 in 2048 based on deterministic prediction

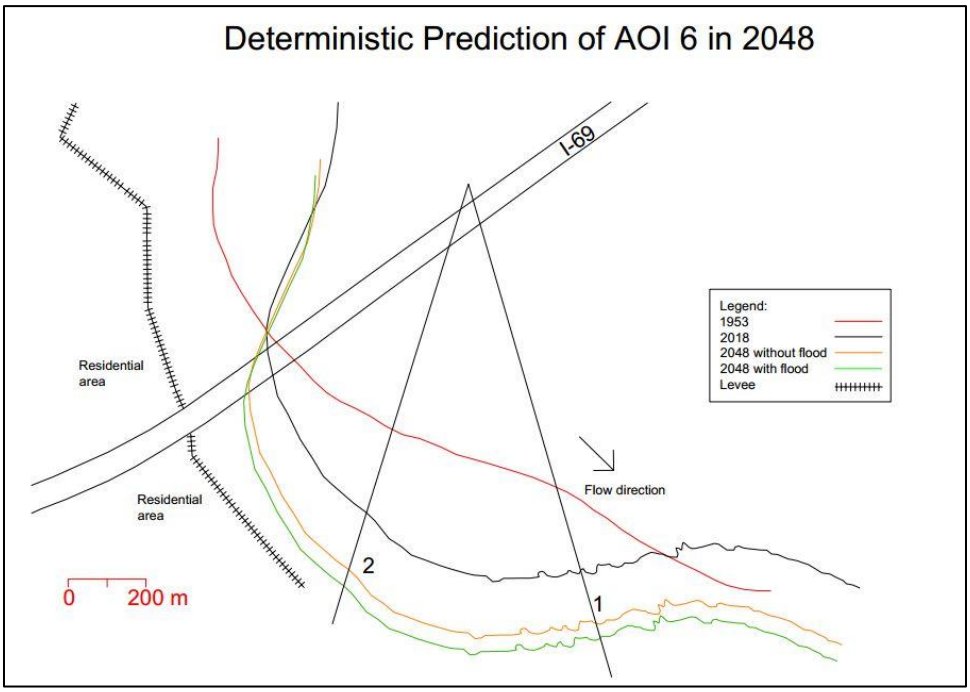

Figure 73. River position of AOI 6 in 2048 based on deterministic prediction

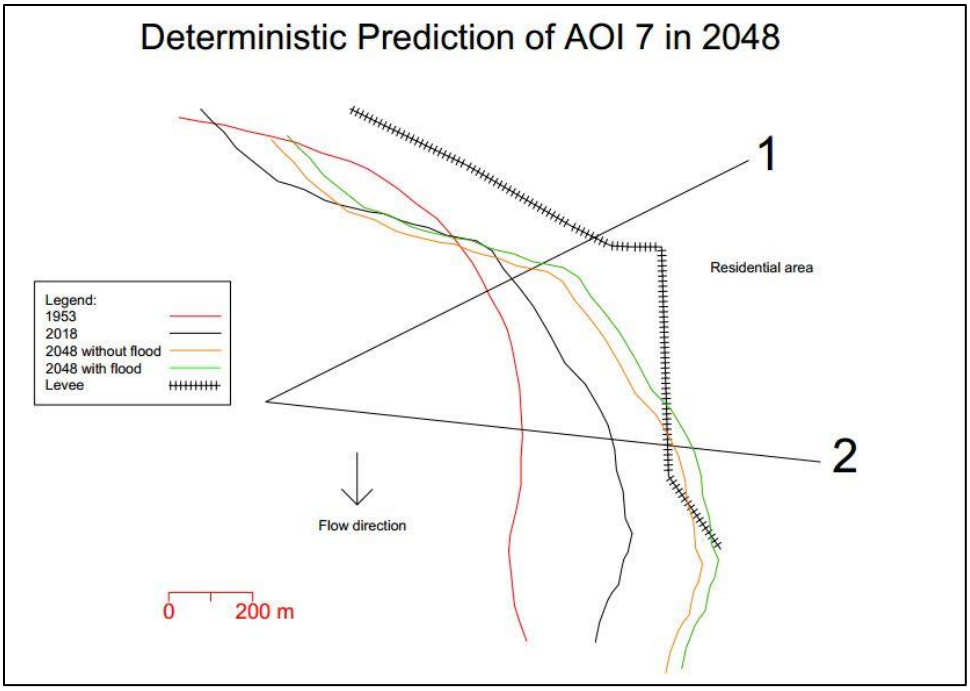

Figure 74. River position of AOI 7 in 2048 based on deterministic prediction

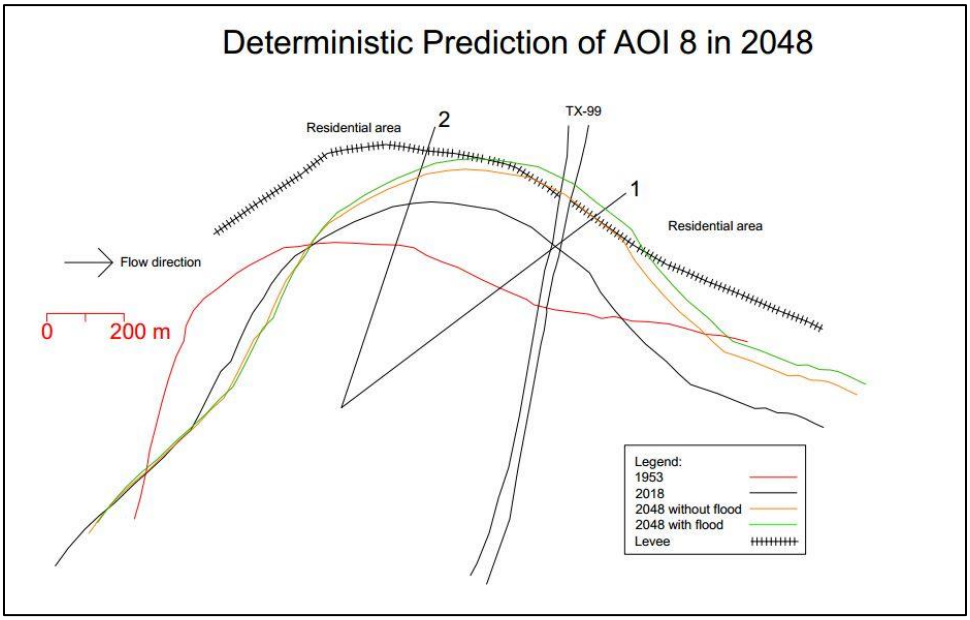

Figure 75. River position of AOI 8 in 2048 based on deterministic prediction

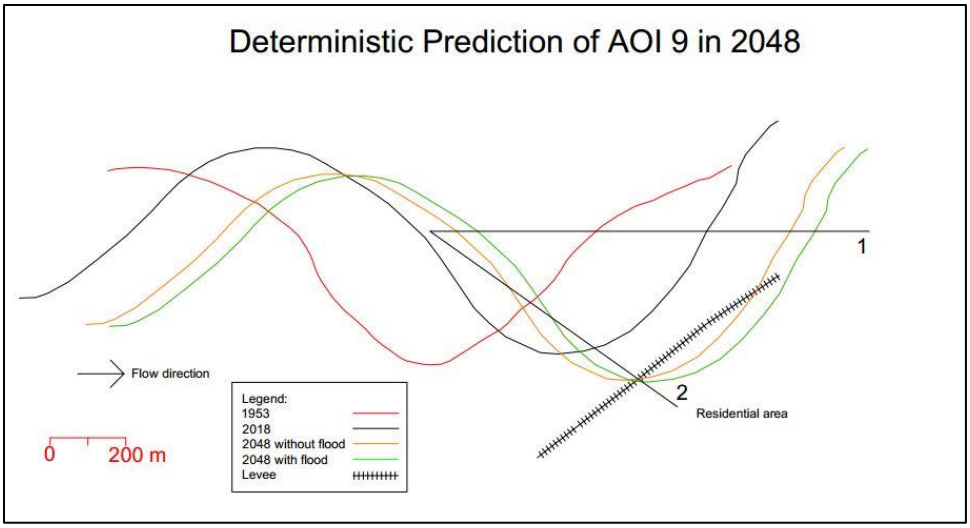

Figure 76. River position of AOI 9 in 2048 based on deterministic prediction

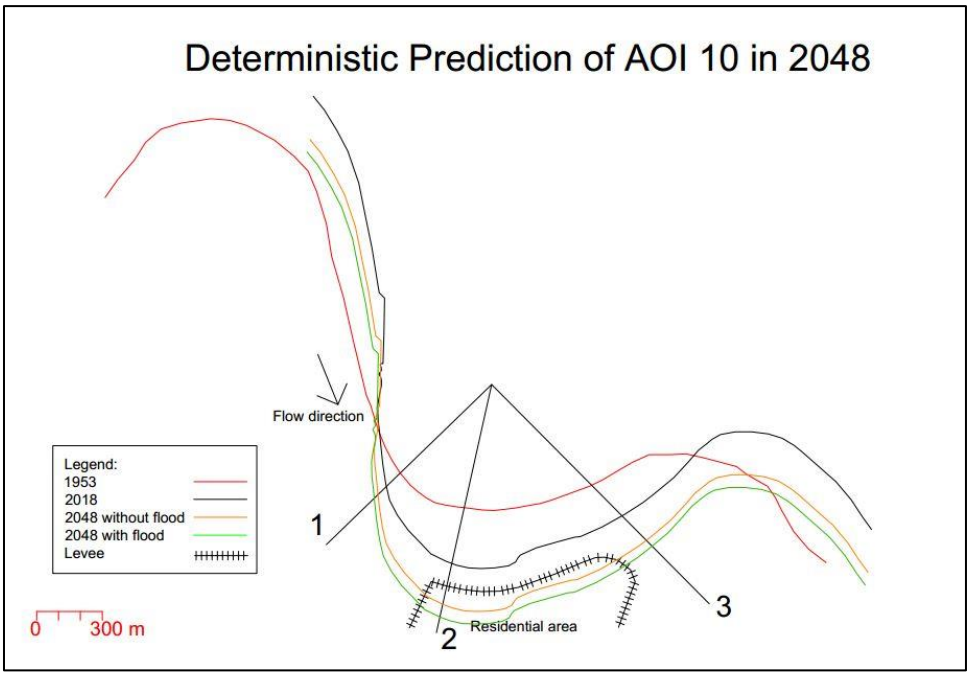

Figure 77. River position of AOI 10 in 2048 based on deterministic prediction

4.4. Probabilistic Prediction

4.4.1. Future Hydrograph

Probabilistic prediction is conducted by improving the previous code. Input data for probabilistic prediction are same with the data for deterministic prediction except the future flow discharge. Numerous studies of river flow prediction have been improved by using various methods. In this study, it is conducted by extracting the statistical properties of the past flow hydrograph. Additional parameters such as rainfall and potential evapotranspiration are not considered.

First, the distribution of past flow discharge is plotted. Figure 78 shows that past flow hydrograph fits a lognormal distribution. It is common that data from measurements will have lognormal distribution. If Q is lognormally distributed, then Y = ln(Q) is a normal random variable. The probability density function (PDF) of Q is

$$f(Q|\mu,\sigma) = \frac{1}{Q\sigma\sqrt{2\pi}} e^{-\frac{(\ln Q-\mu)^2}{2\sigma^2}} \quad \text{(Eq. 16)}$$

where μ and σ are the mean and standard deviation of Y respectively. If *m* and *s* are the mean and standard deviation of Q, they can be calculated as follows

$$m = e^{\mu+\frac{\sigma^2}{2}} \quad \text{(Eq. 17)}$$

$$s = \sqrt{\left(e^{2\mu+\sigma^2}\right)\left(e^{\sigma^2}-1\right)} \quad \text{(Eq. 18)}$$

$$\mu = \ln\left(\frac{m^2}{\sqrt{m^2+s^2}}\right) \quad \text{(Eq. 19)}$$

$$\sigma = \sqrt{\ln\left(\frac{s}{m}\right)^2 + 1} \quad \text{(Eq. 20)}$$

The lognormal fitting and the calculation of each parameters are executed by the code. Mean and standard deviation of the original data from the past hydrograph are symbolized by m_Q and s_Q respectively, while mean and standard deviation of its normal distribution are symbolized by μ_Y and σ_Y respectively. The parameters for the fitted distribution are also calculated and the comparison between original and fitted distribution is shown by Table 24. For confidence level of 99%, the confidence intervals of μ_Y and σ_Y for the fitted distribution are $\mu_Y \in (8.078, 8.120)$ and $\sigma_Y \in (1.256, 1.286)$.

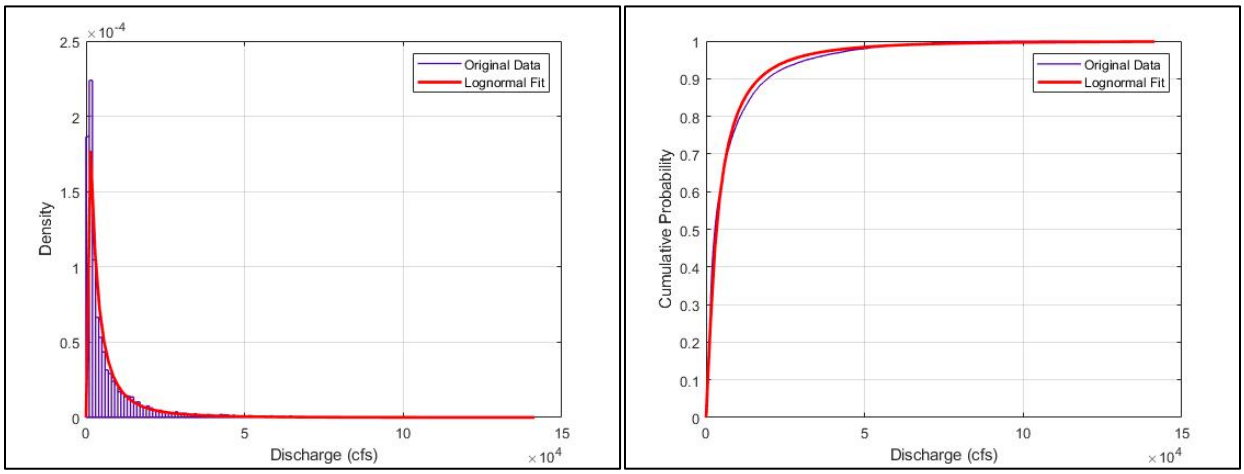

Figure 78. Probability density function (PDF) and cumulative density function (CDF) of original and fitted distribution of the past flow hydrograph

Table 24. Comparison of statistical parameters of original data and fitted lognormal distribution

Parameters	Original Data (cfs)	Fitted Distribution (cfs)	% Error
μ_Y	8.3013	8.0992	2.43
σ_Y	1.1232	1.2704	13.10
m_Q	7571.7	7377.3	2.57
s_Q	12047	14796	22.82

The error percentage of the standard deviation s_Q is 22.82% and the original data μ_Y and σ_Y are outside of the 99% confidence level of the fitted distribution. It shows that the past flow hydrograph does not fit closely to lognormal distribution. Therefore, prediction of future flow hydrograph using cumulative density function (CDF) of fitted lognormal distribution will be overestimated. Therefore, the better approach to generate future flow discharge for probabilistic prediction is by using random sampling from cumulative density function (CDF) of the original data.

Table 25. Comparison of random sampling from lognormal distribution and original data

Random sampling	Using CDF of Lognormal Distribution (in cfs)	Using CDF of Original Data (in cfs)
Mean 1	7600.1	7241.5
Standard deviation 1	19404	13084
Mean 2	7548.4	7443.8
Standard deviation 2	14358	14171

Future flow hydrograph will have identical distribution with past hydrograph regardless the number of random sampling and repetition (Figure 79). Both predicted and past hydrograph fit to lognormal distribution. The greater number of random sampling, the smoother fitted curve of future hydrograph. However, the code will take a longer time to run. For this study, the future hydrograph is generated 100 times.

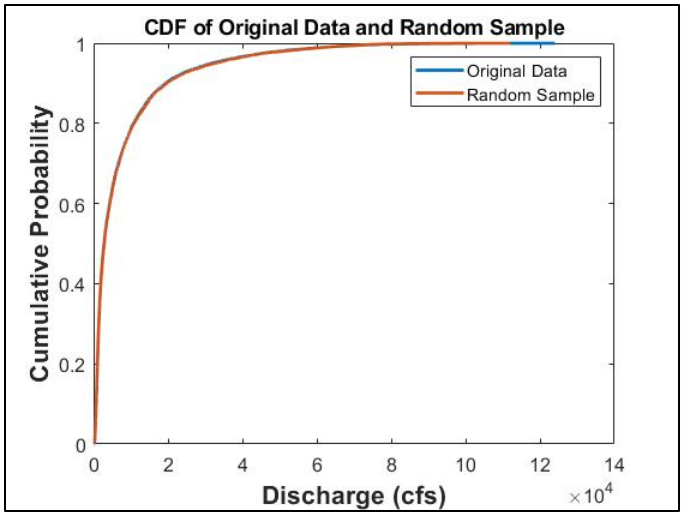

Figure 79. CDF of original data and random sample

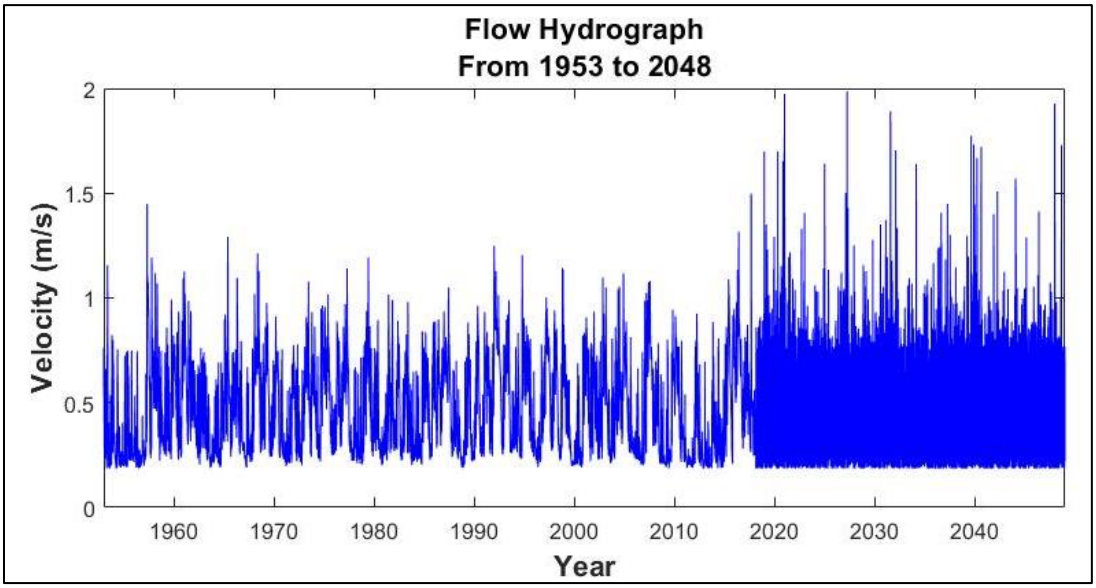

Figure 80. Past and predicted flow hydrograph

4.4.2. Future Migration

After being generated by using CDF of original data, each future hydrograph is applied to determine future migration of the meanders. The number of future migrations depends on the number of generated future hydrograph. The code will continue to plot histogram and cumulative

probability of future migrations of each meander or direction. The distribution relatively fits to normal distribution (Figure 81).

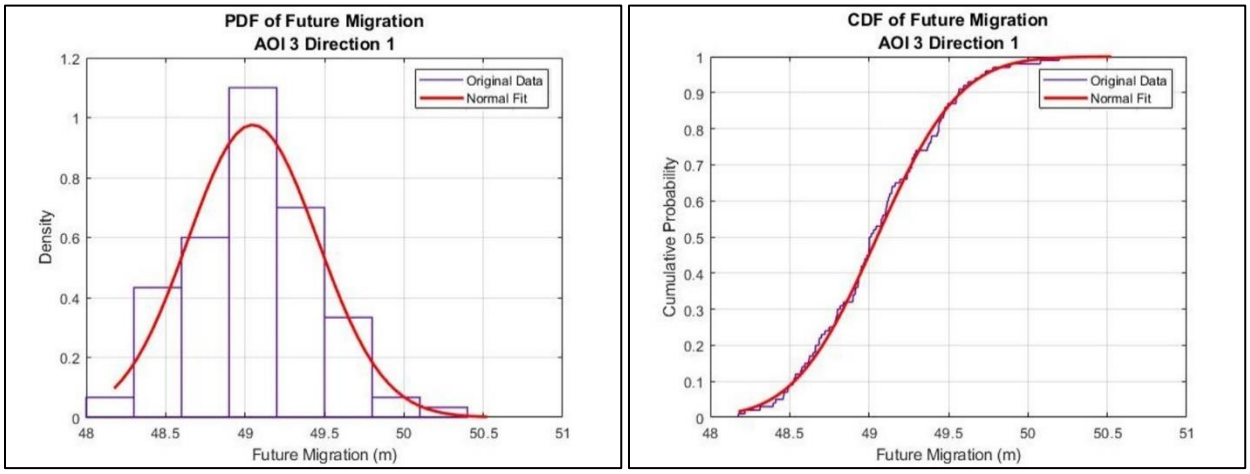

Figure 81. PDF and CDF of future migration prediction

The inverse cumulative distribution function is then calculated to determine the probability of exceedance curve and it is obtained by subtracting the CDF from 1 (Figure 82). A point (*x*, *y*) means that it has *y* probability to be equal or exceed the future distance *x*. The exceedance curve is used to determine future migration with probability of 50%, 10%, and 1%.

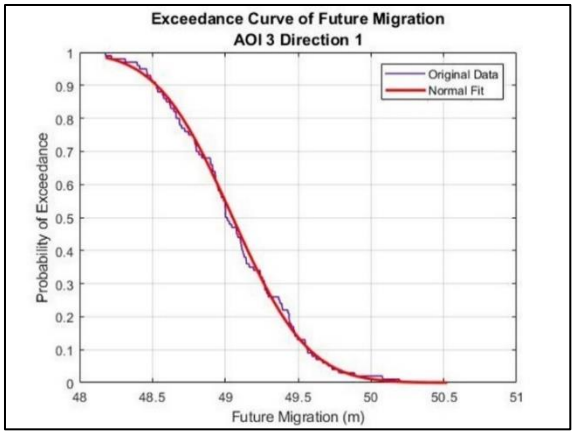

Figure 82. Exceedance curve of future migration

The following table and figures present the future migration of each probability of exceedance from all meanders in the study area.

Table 26. Future predicted position and migration distance by probabilistic prediction

Meander Name	Latest Position in 2018 (m)	Exceedance Probability	Predicted Position (in 2048) (m)	Migration Distance (m)
AOI 3 Direction 1	37.43	0.5	49.05	11.62
		0.1	49.57	12.14
		0.01	50.00	12.57
AOI 3 Direction 2	38.87	0.5	53.05	14.18
		0.1	53.62	14.75
		0.01	54.03	15.16
AOI 3 Direction 3	87.00	0.5	138.50	51.50
		0.1	140.40	53.40
		0.01	142.00	55.00
AOI 4 Direction 1	15.96	0.5	33.30	17.34
		0.1	33.90	17.94
		0.01	34.45	18.49
AOI 4 Direction 2	47.29	0.5	89.30	42.01
		0.1	90.94	43.65
		0.01	92.25	44.96
AOI 4 Direction 3	53.73	0.5	105.06	51.33
		0.1	106.90	53.17
		0.01	108.40	54.67
AOI 5 Direction 1	207.00	0.5	328.64	121.64

Table 26. Continued

Meander Name	Latest Position in 2018 (m)	Exceedance Probability	Predicted Position (in 2048) (m)	Migration Distance (m)
AOI 5 Direction 1	207.00	0.1	333.00	126.00
		0.01	336.80	129.80
AOI 5 Direction 2	303.49	0.5	476.80	173.31
		0.1	482.00	178.51
		0.01	486.20	182.71
AOI 5 Direction 3	307.58	0.5	480.89	173.31
		0.1	487.10	179.52
		0.01	492.30	184.72
AOI 6 Direction 1	222.70	0.5	344.42	121.72
		0.1	348.30	125.60
		0.01	351.80	129.10
AOI 6 Direction 2	225.12	0.5	361.90	136.78
		0.1	366.40	141.28
		0.01	370.20	145.08
AOI 7 Direction 1	65.22	0.5	116.55	51.33
		0.1	118.40	53.18
		0.01	119.90	54.68
AOI 7 Direction 2	214.63	0.5	351.23	136.60
		0.1	355.09	140.46
		0.01	359.80	145.17
AOI 8 Direction 1	179.11	0.5	287.86	108.75
		0.1	291.90	112.79
		0.01	295.20	116.09
AOI 8 Direction 2	111.52	0.5	175.02	63.50
		0.1	177.00	65.48
		0.01	178.80	67.28
AOI 9 Direction 1	292.14	0.5	487.46	195.32
		0.1	494.10	201.96
		0.01	499.70	207.56
AOI 9 Direction 2	207.61	0.5	329.26	121.65
		0.1	333.70	126.09
		0.01	337.50	129.89
AOI 10 Direction 1	60.95	0.5	124.45	63.50
		0.1	126.50	65.55
		0.01	128.10	67.15
AOI 10 Direction 2	261.02	0.5	434.33	173.31
		0.1	440.50	179.48
		0.01	445.70	184.68
AOI 10 Direction 3	197.14	0.5	335.60	138.46
		0.1	338.00	140.86
		0.01	341.80	144.66

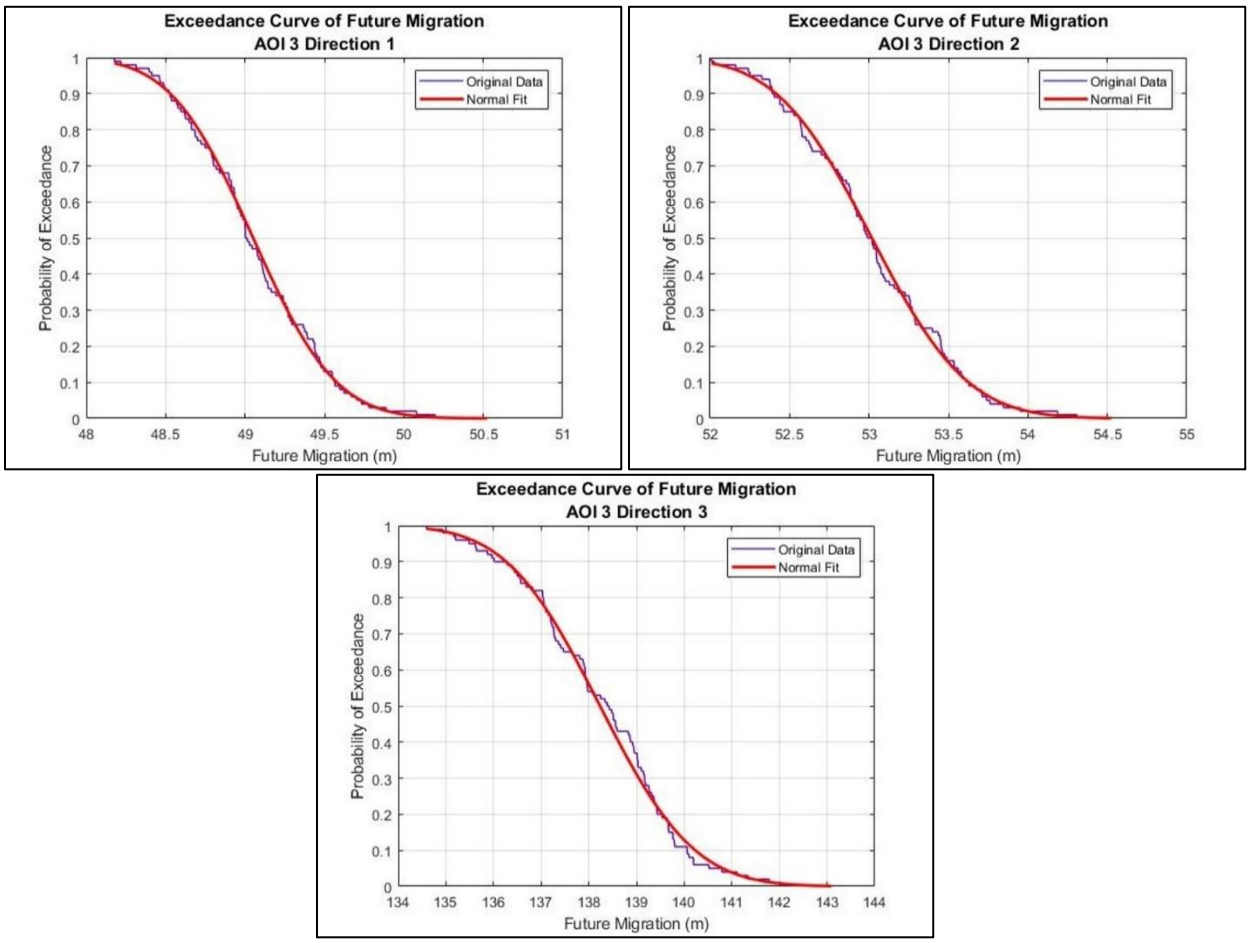

Figure 83. Exceedance curve of future migration in AOI 3

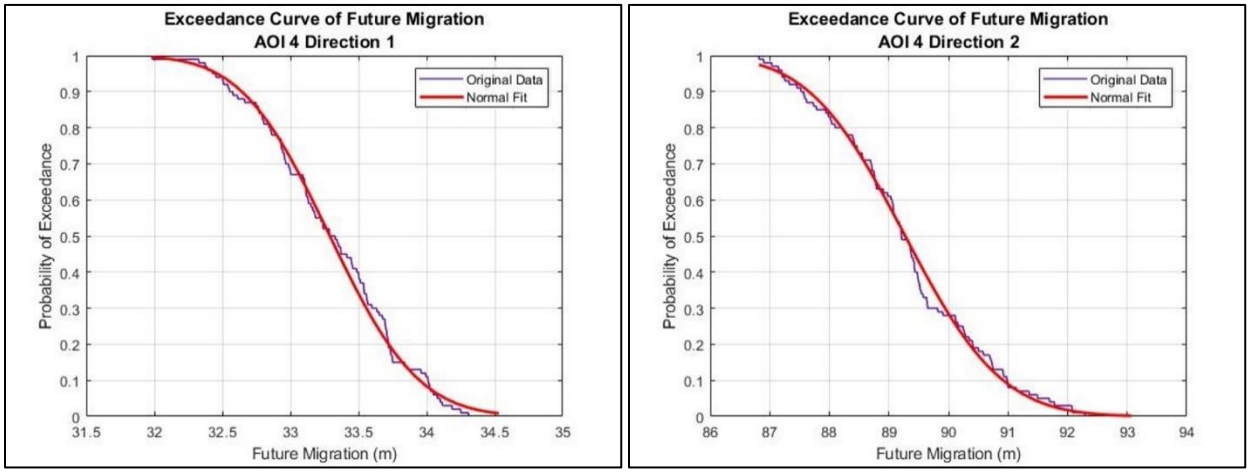

Figure 84. Exceedance curve of future migration in AOI 4

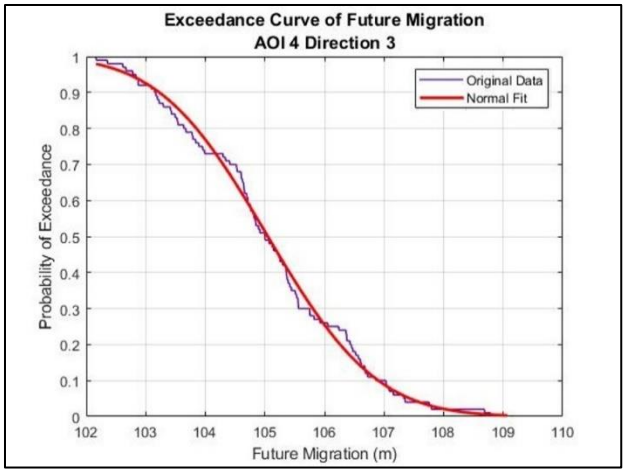

Figure 84. Continued

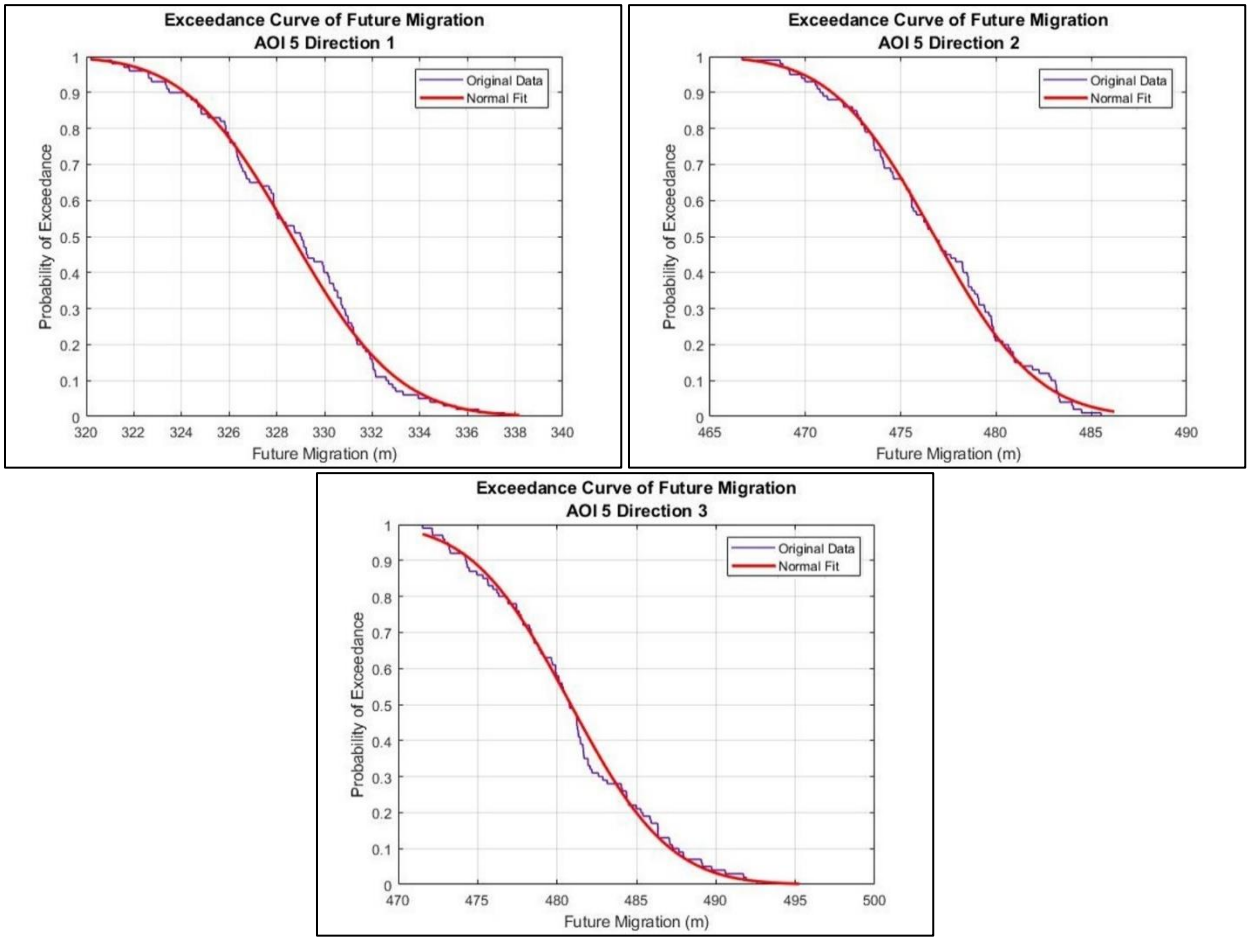

Figure 85. Exceedance curve of future migration in AOI 5

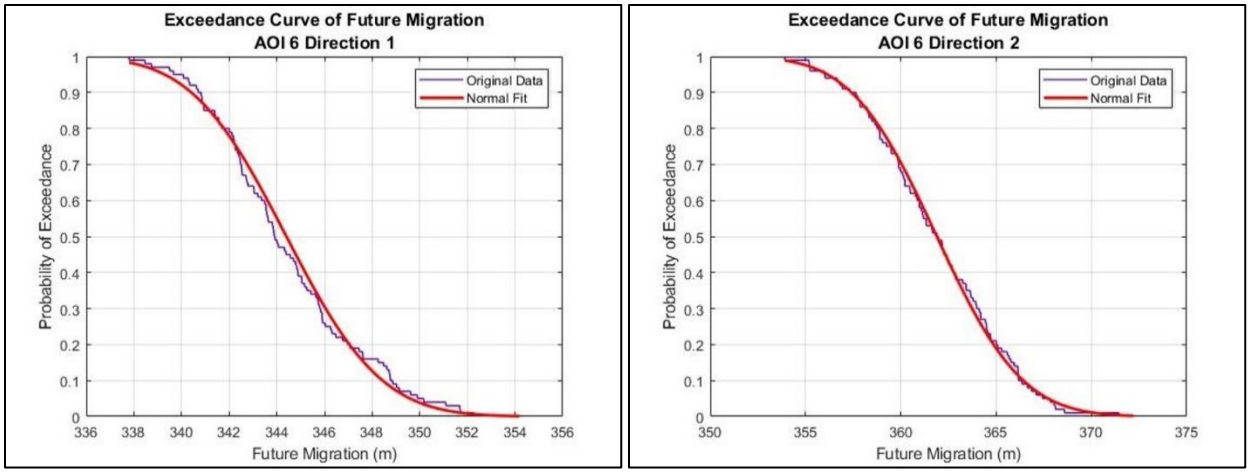

Figure 86. Exceedance curve of future migration in AOI 6

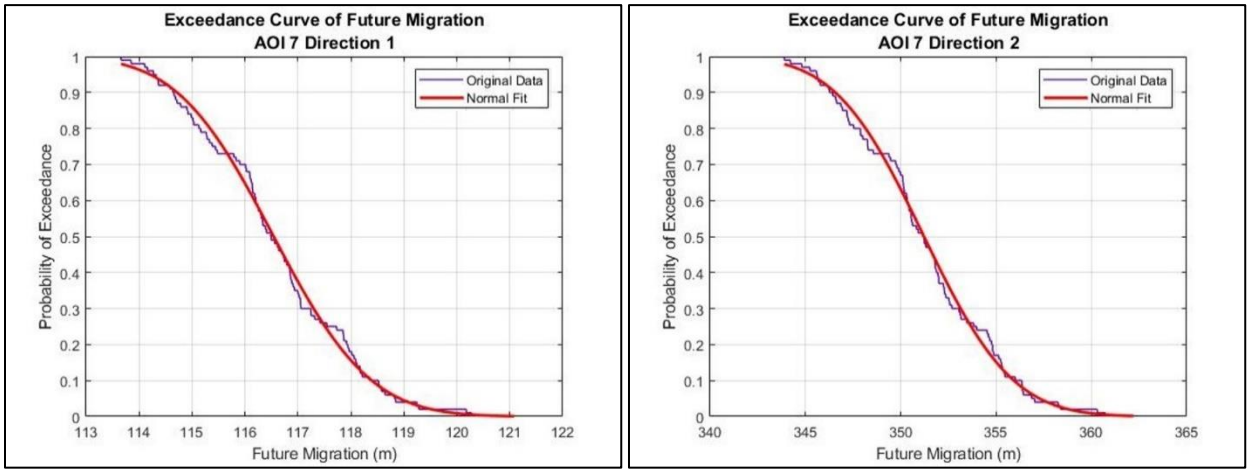

Figure 87. Exceedance curve of future migration in AOI 7

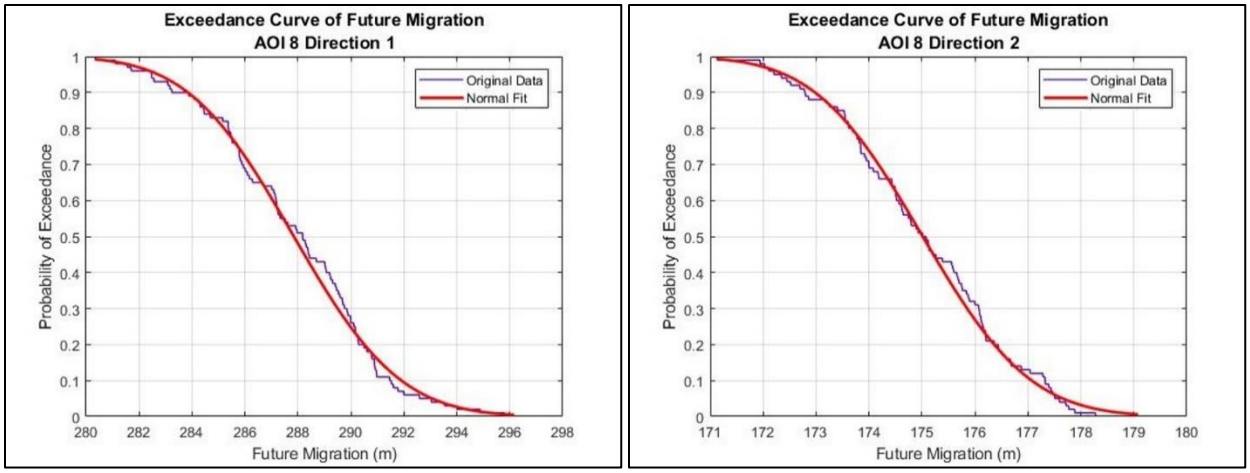

Figure 88. Exceedance curve of future migration in AOI 8

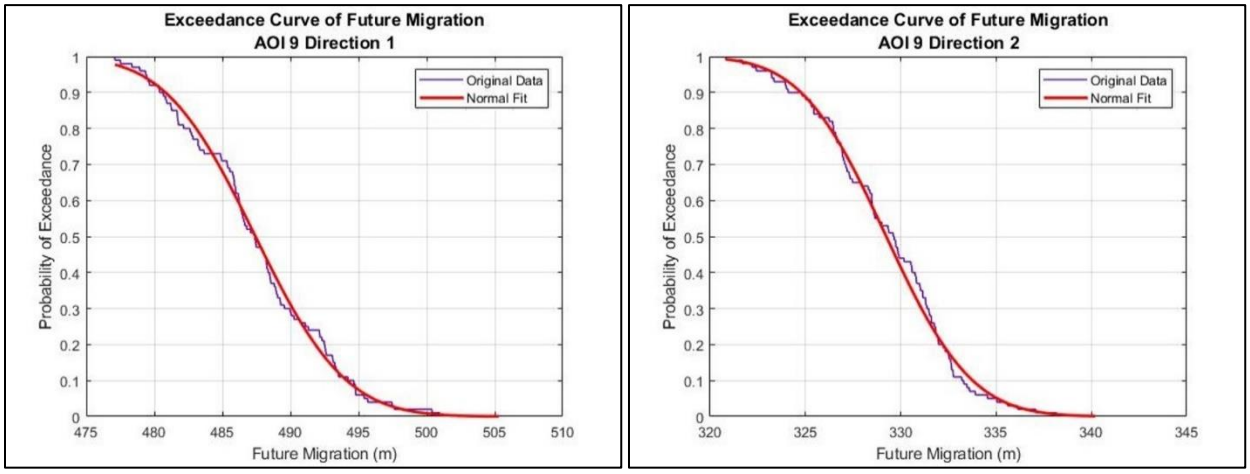

Figure 89. Exceedance curve of future migration in AOI 9

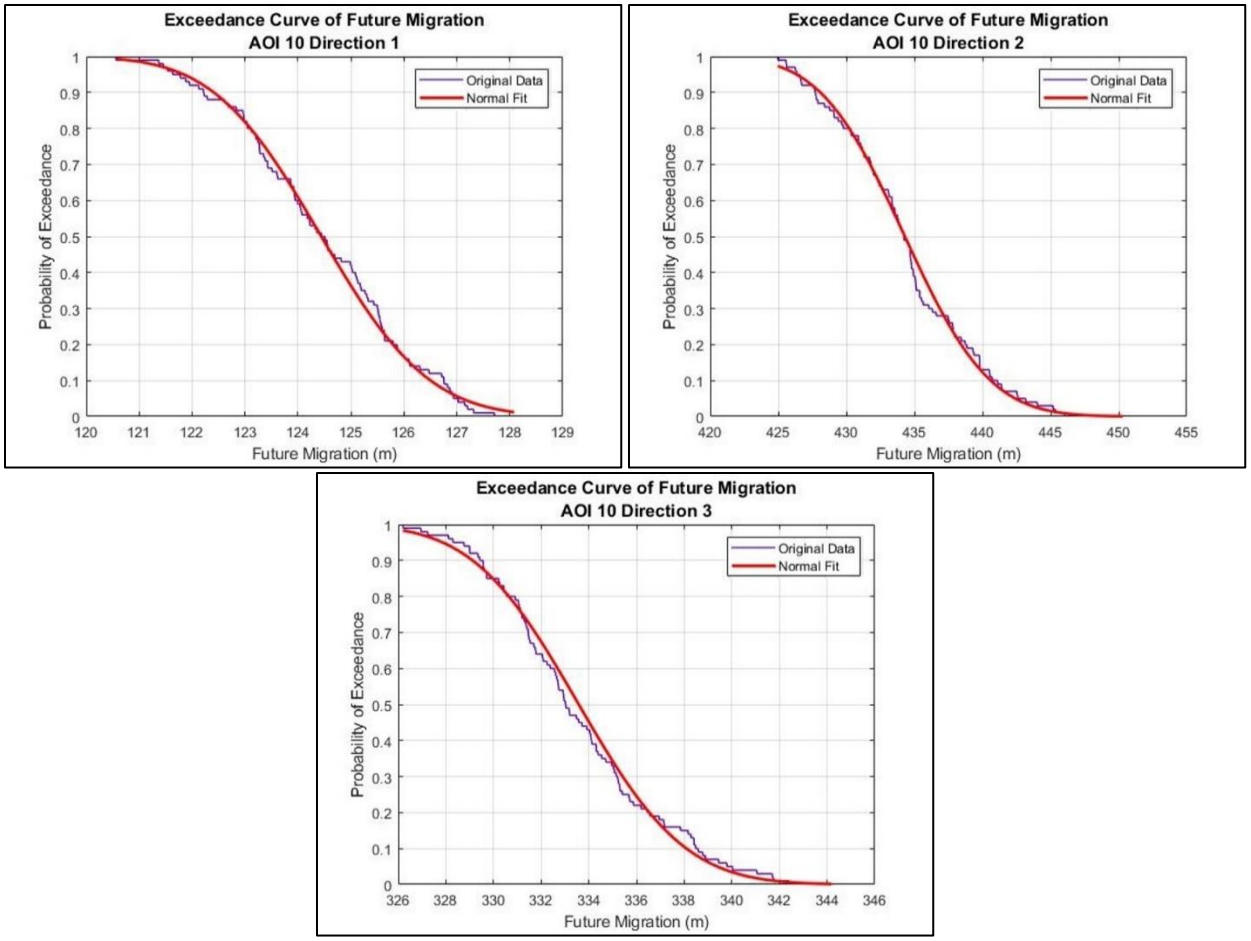

Figure 90. Exceedance curve of future migration in AOI 10

The following step is similar to deterministic prediction; drawing the predicted outer riverbank line to estimate whether the river will be likely to migrate beyond levee or to move until reaching residential areas by the river. The geometry of the predicted riverbank line in 2048 is assumed to follow the geometry of the current riverbank because this prediction does not consider any changes in geometry that might happen during the prediction time.

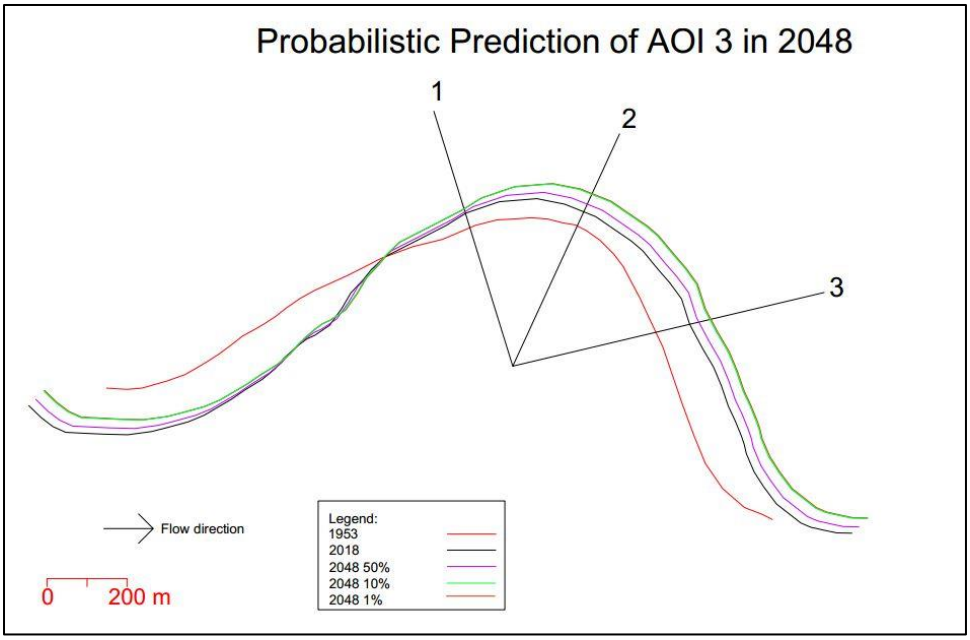

Figure 91. River position of AOI 3 in 2048 based on probabilistic prediction

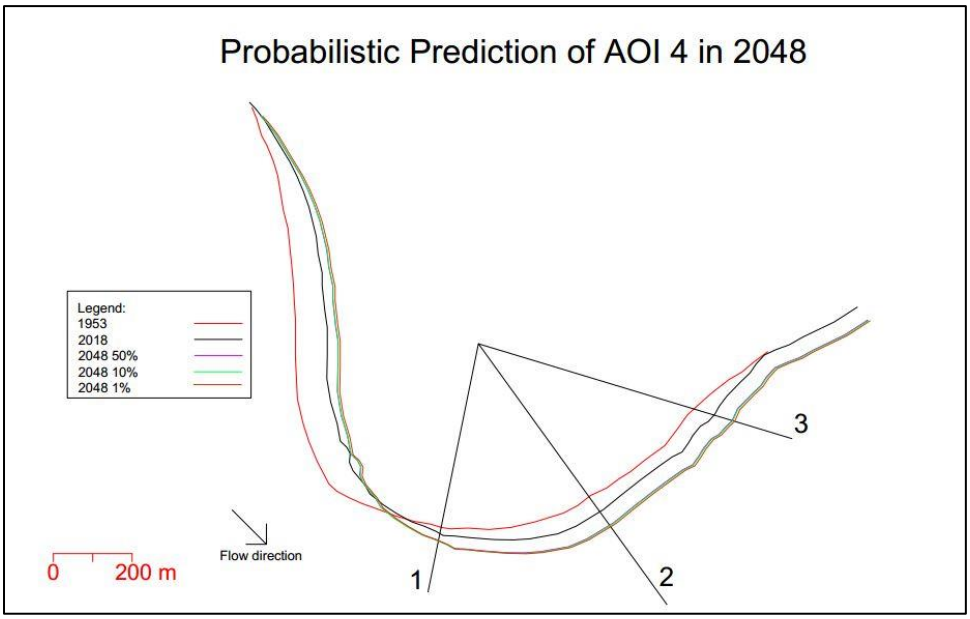

Figure 92. River position of AOI 4 in 2048 based on probabilistic prediction

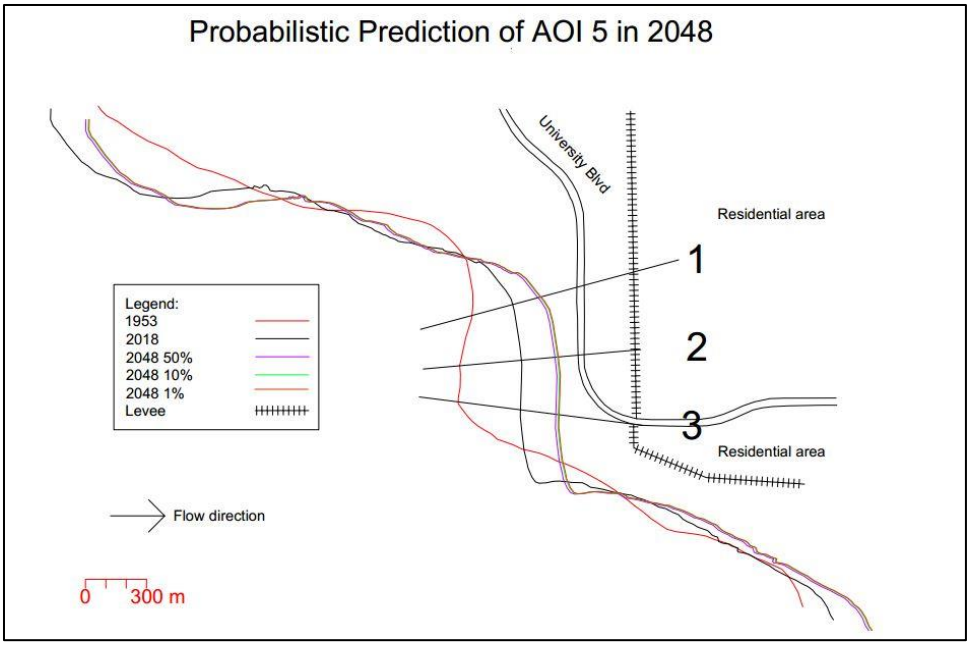

Figure 93. River position of AOI 5 in 2048 based on probabilistic prediction

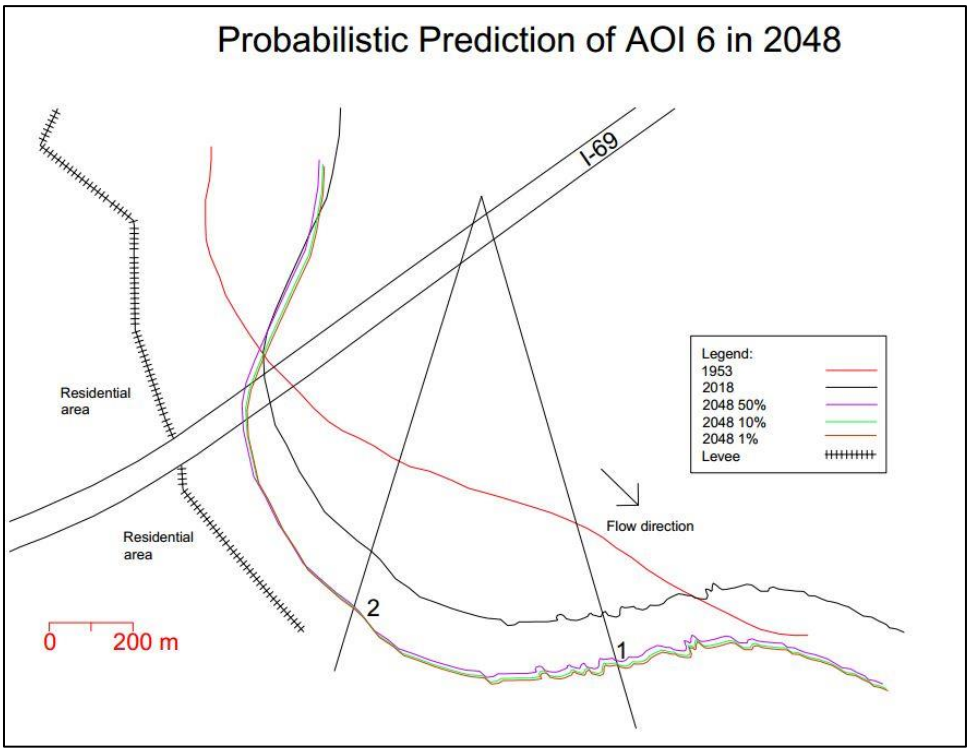

Figure 94. River position of AOI 6 in 2048 based on probabilistic prediction

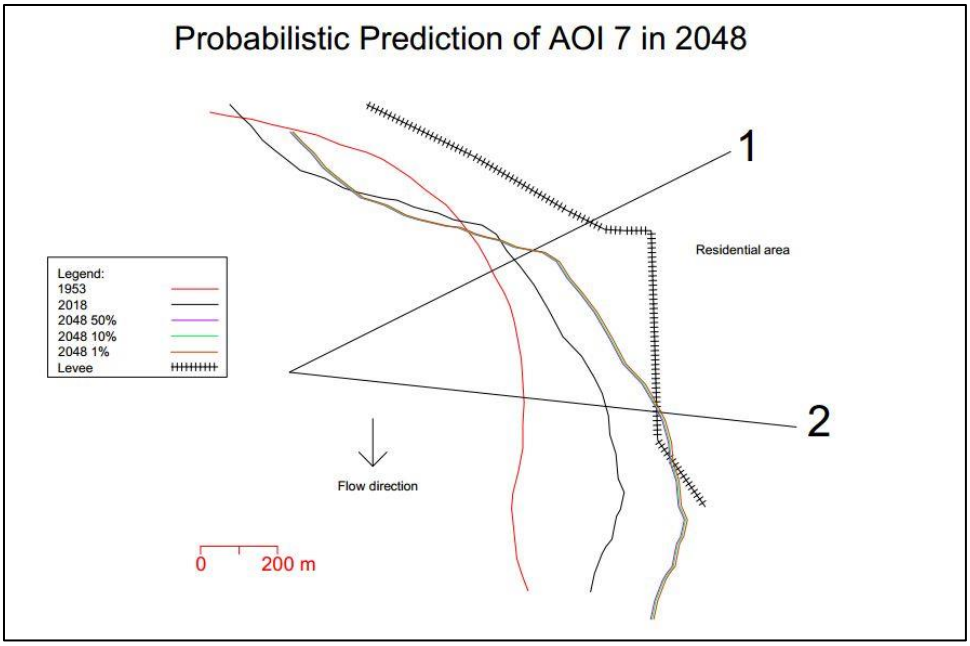

Figure 95. River position of AOI 7 in 2048 based on probabilistic prediction

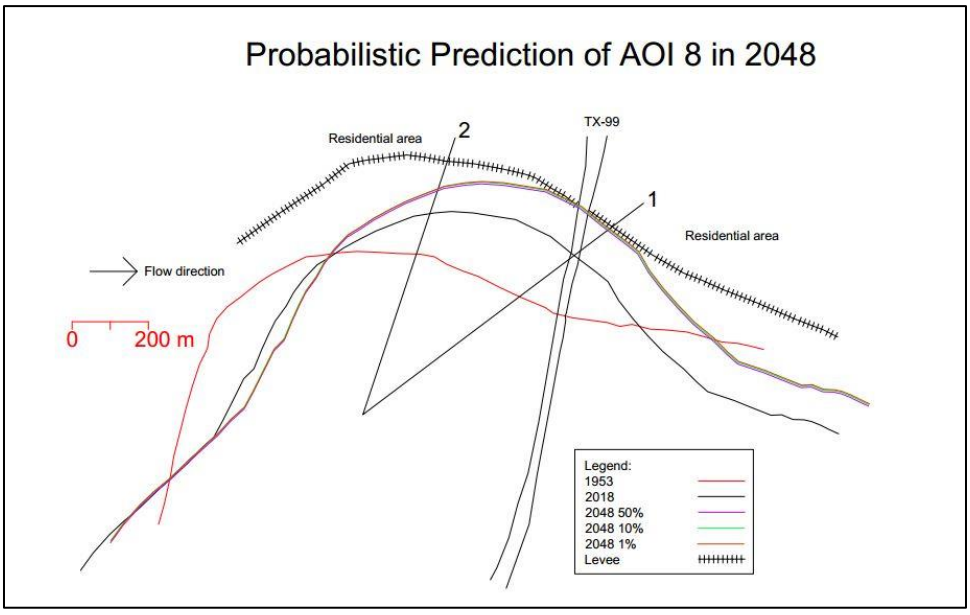

Figure 96. River position of AOI 8 in 2048 based on probabilistic prediction

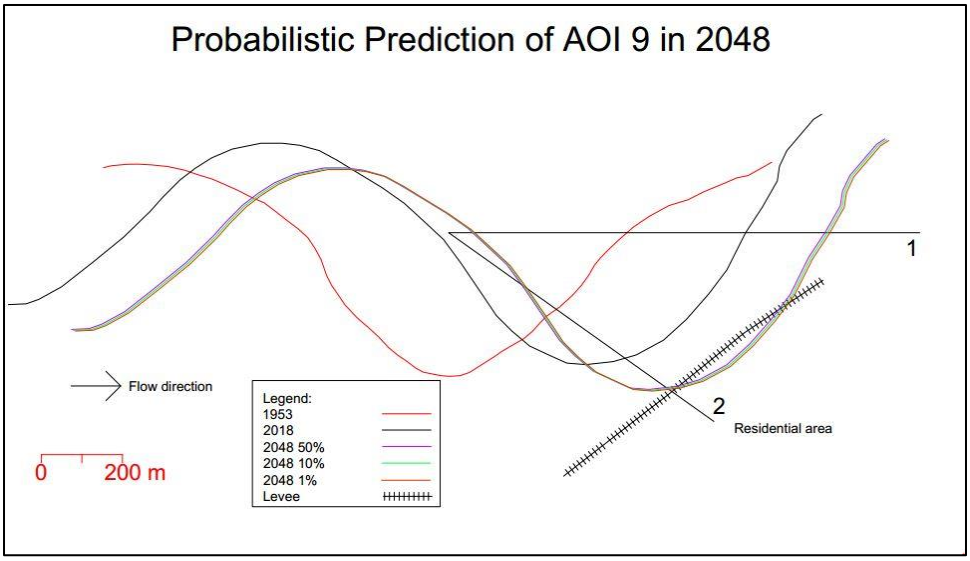

Figure 97. River position of AOI 9 in 2048 based on probabilistic prediction

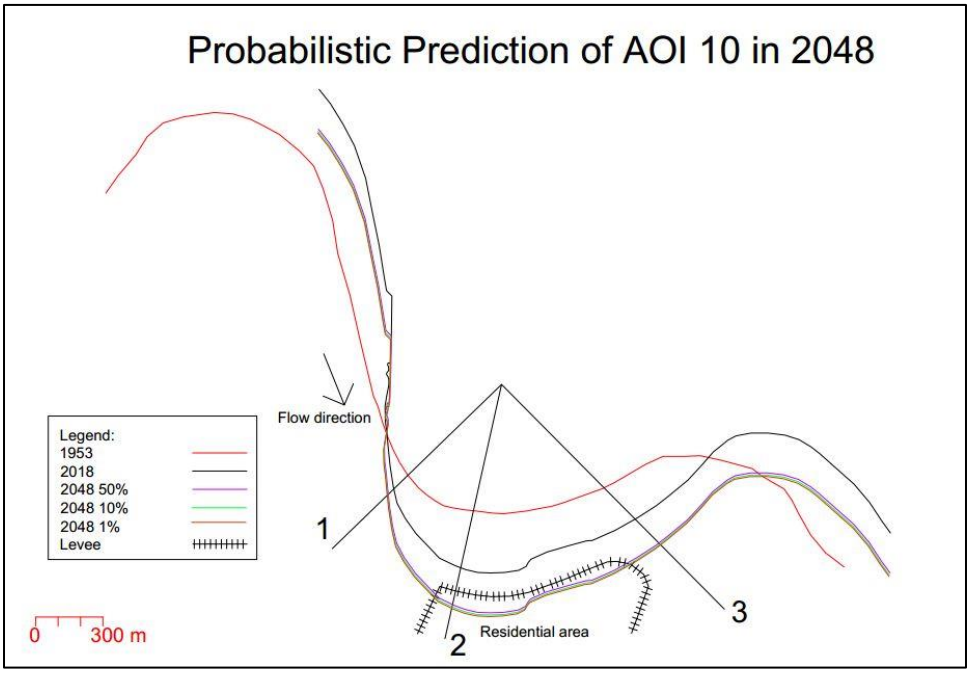

Figure 98. River position of AOI 10 in 2048 based on probabilistic prediction

4.5. Comparison of Deterministic Prediction with Probabilistic Prediction

Section 4.3 and 4.4. present the result of deterministic and probabilistic prediction respectively. Beside the number of migration distance resulted, the noticeable difference between those two approaches is deterministic prediction gives the higher migration distance than the probabilistic does, even the maximum distance from probabilistic prediction is still smaller than the result from the deterministic prediction without flood. This problem comes because the difference of future flow hydrograph used in prediction.

In deterministic prediction, the future flow duplicates the last 30 years of past flow, including the flow during Hurricane Harvey in August 2017. Mean of the data is 8258 cfs or about 9% higher than the mean of the original past flow from 1953 to 2018. Meanwhile, in probabilistic prediction, the future flow used in migration calculation is the flow which is generated from CDF of the original data and has the lower mean than the original data (Table 25).

4.6. Discussion of Results

Deterministic and probabilistic prediction using OMM can give reasonable result of future migration. However, in the calibration step, the OMM gives relatively high value of calibrated migration and does not fit perfectly to the observed migration. Compared to the Ranking Index (RI) value in Montalvo-Bartolomei (2014) which is quite low, the calibration step in this study results in higher value averaging 0.51. If the value of RI is closer to 0, the prediction result is more optimized (Briaud & Montalvo-Bartolomei, 2017). The high value of RI in this study is influenced by different migration rate between 1953-1968 period and 1968-2018 period. The OMM does not consider this issue and it only calculates erosion parameters that represent the entire period.

4.7. Prediction for 65-Year Period

Deterministic prediction result should be similar to probabilistic prediction with 50% of exceedance probability. However, because this study uses different period between past data and future prediction, the result of deterministic prediction is higher as explained in Section 4.5. If the prediction period is changed to be 65 years, there is a slight difference of result from both prediction. The following table and figures show the result of future prediction for next 65 years.

Table 27. Future predicted position from deterministic and probabilistic prediction for next 65 years

Location	Deterministic Prediction (m)	Probabilistic Prediction (m)		
		50% Probability	10% Probability	1% Probability
AOI 3 Direction 1	62.08	61.90	62.75	63.30
AOI 3 Direction 2	68.90	68.80	69.80	70.26
AOI 3 Direction 3	195.80	195.20	198.00	200.20
AOI 4 Direction 1	52.66	52.50	53.49	54.19
AOI 4 Direction 2	136.09	135.20	137.40	139.70
AOI 4 Direction 3	162.53	162.00	164.70	167.00
AOI 5 Direction 1	465.20	463.10	470.00	475.30
AOI 5 Direction 2	667.00	668.00	677.00	684.00
AOI 5 Direction 3	674.00	673.10	680.50	687.20
AOI 6 Direction 1	480.90	478.80	485.70	490.90
AOI 6 Direction 2	514.62	513.90	520.10	525.10
AOI 7 Direction 1	174.02	173.00	176.40	178.30
AOI 7 Direction 2	504.13	501.60	509.60	517.20
AOI 8 Direction 1	409.93	408.30	413.80	418.90
AOI 8 Direction 2	245.79	245.40	249.10	251.50
AOI 9 Direction 1	706.01	703.70	714.30	723.30
AOI 9 Direction 2	465.81	463.70	470.20	474.50
AOI 10 Direction 1	195.22	194.90	197.80	199.60
AOI 10 Direction 2	627.45	624.50	633.60	641.90
AOI 10 Direction 3	486.63	485.90	492.00	497.10

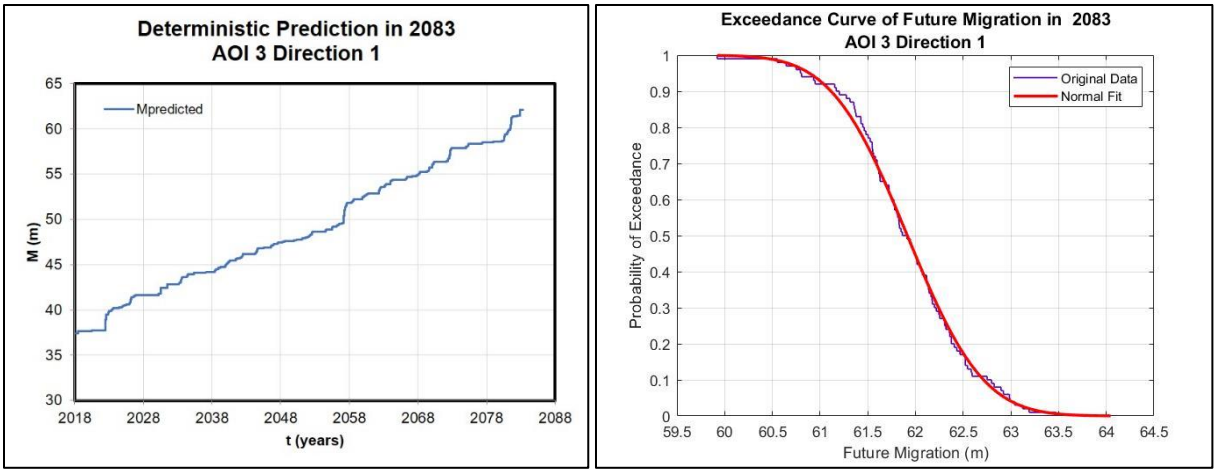

Figure 99. Future position of AOI 3 Direction 1 in 2083

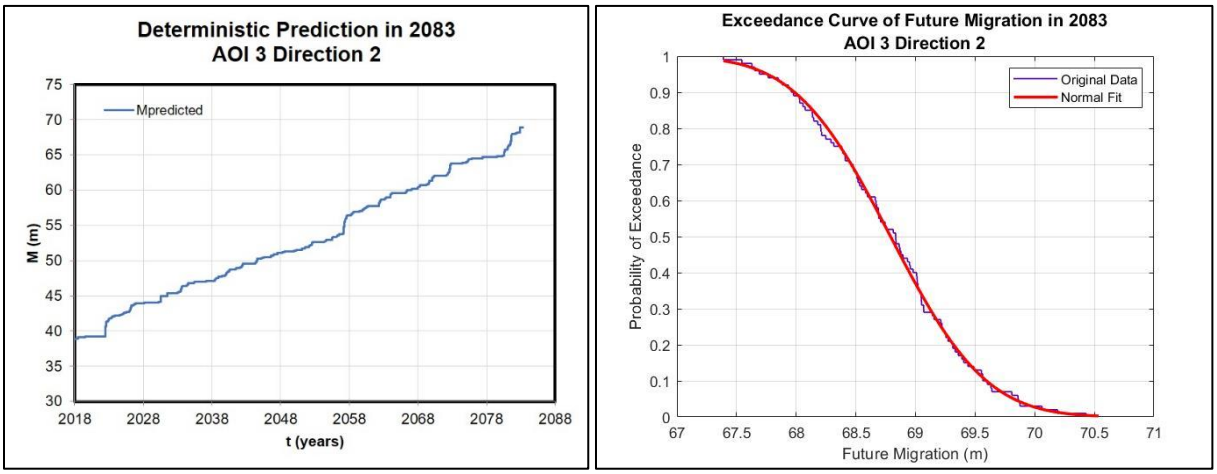

Figure 100. Future position of AOI 3 Direction 2 in 2083

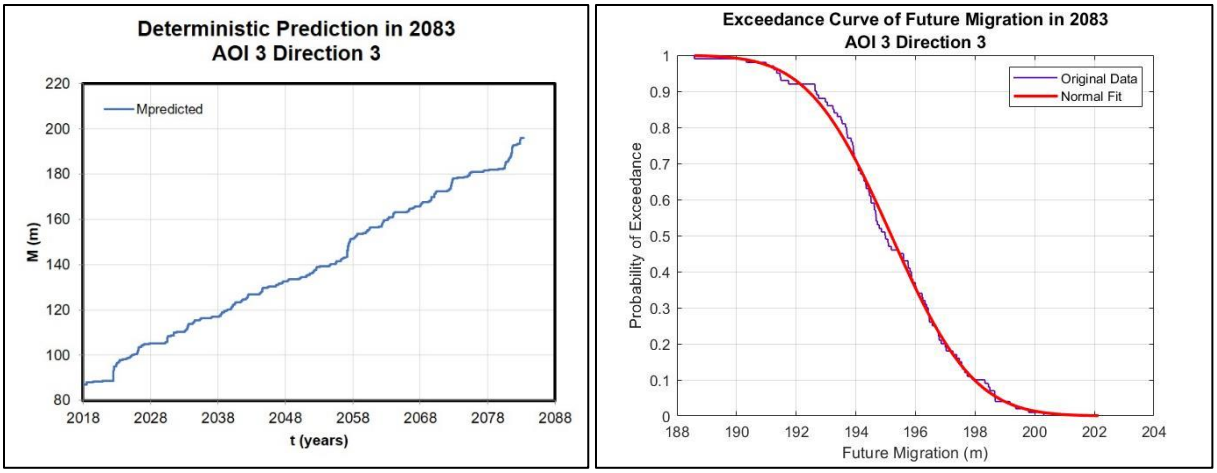

Figure 101. Future position of AOI 3 Direction 3 in 2083

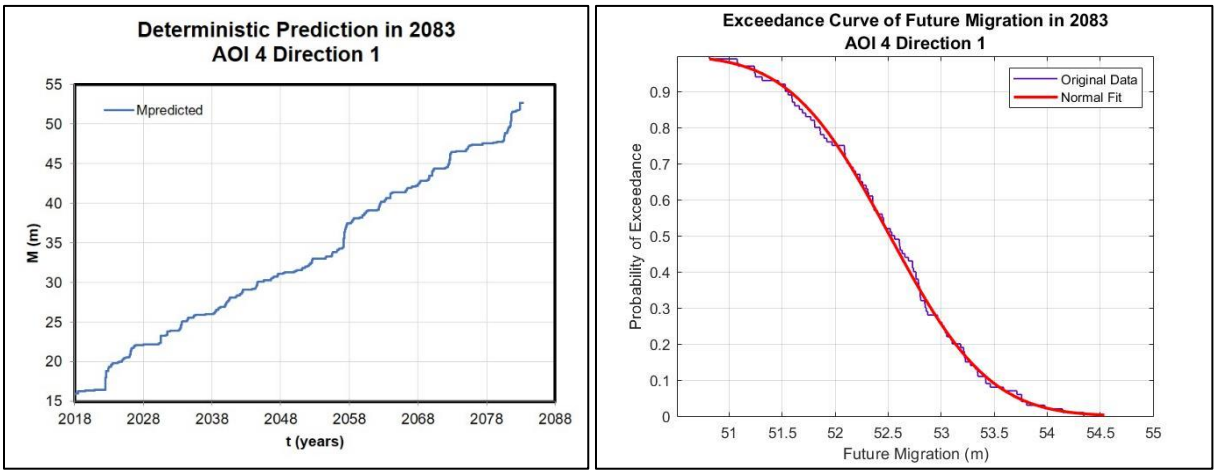

Figure 102. Future position of AOI 4 Direction 1 in 2083

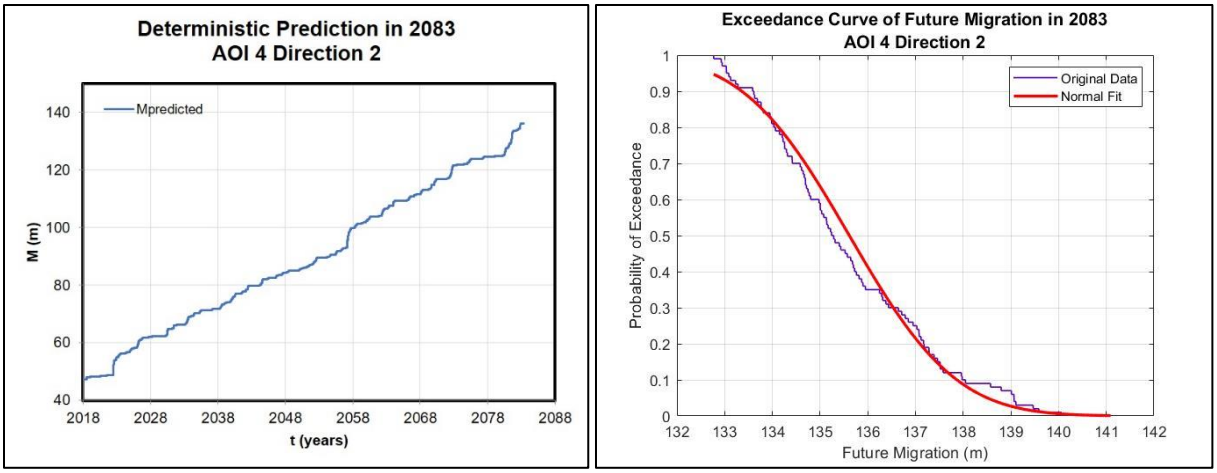

Figure 103. Future position of AOI 4 Direction 2 in 2083

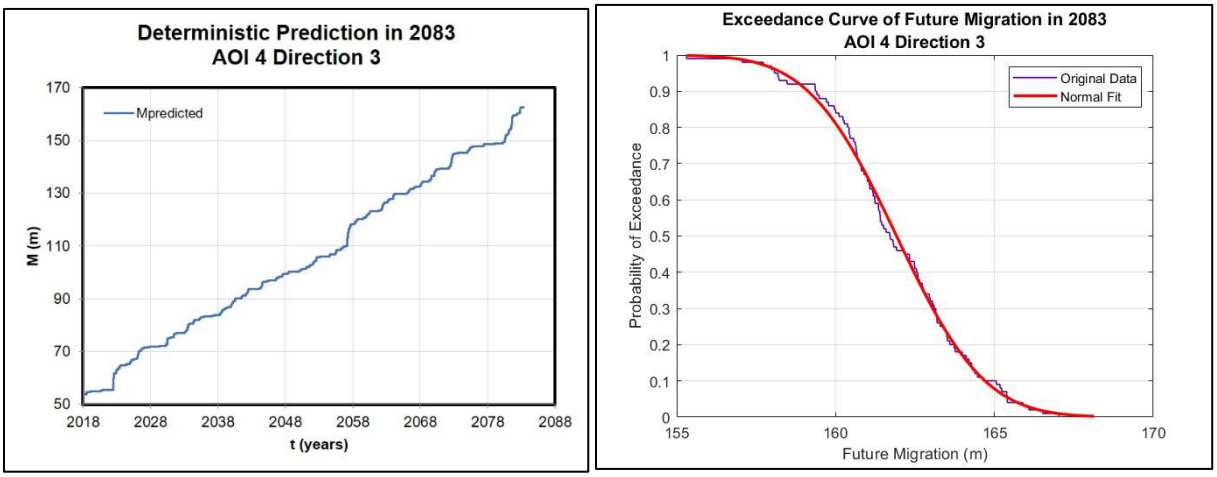

Figure 104. Future position of AOI 4 Direction 3 in 2083

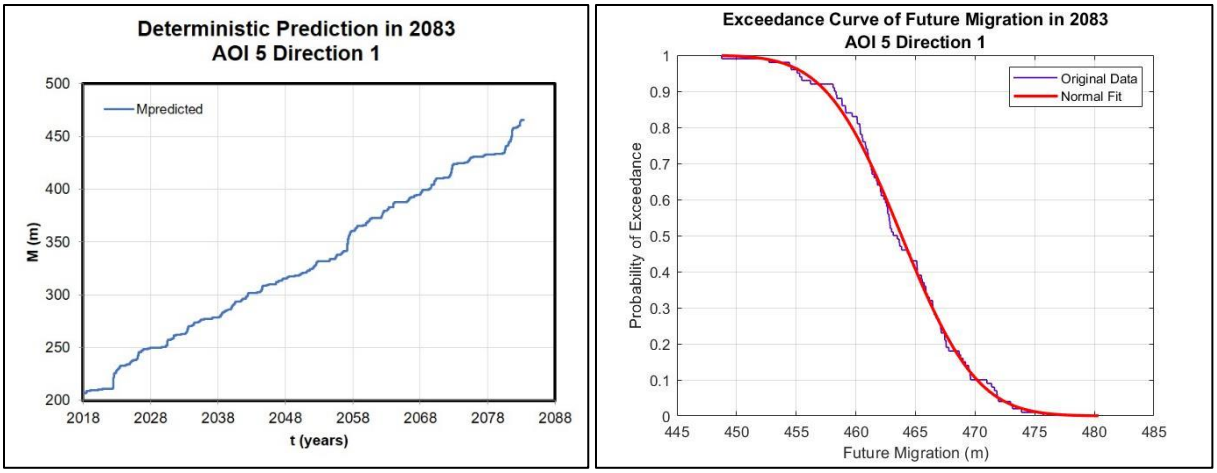

Figure 105. Future position of AOI 5 Direction 1 in 2083

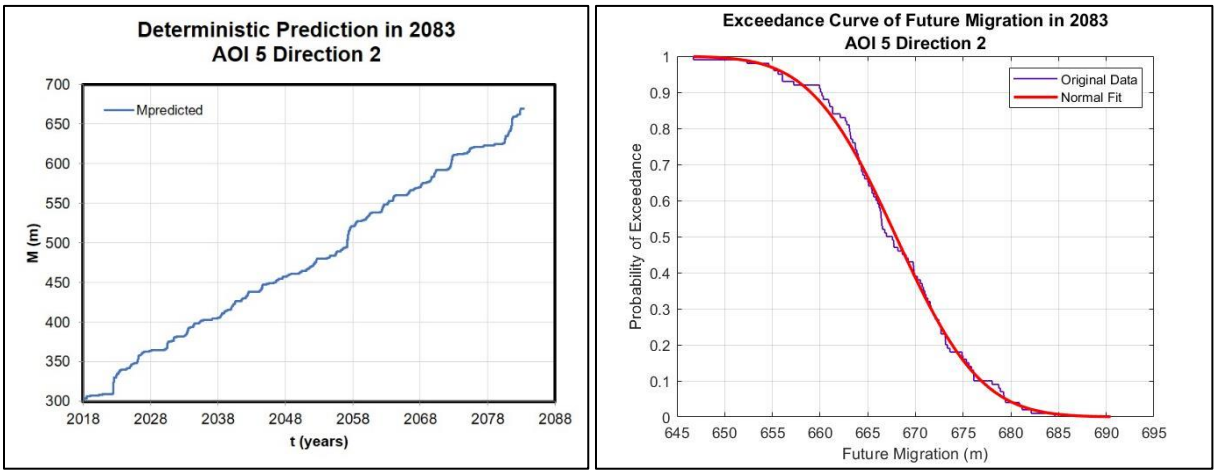

Figure 106. Future position of AOI 5 Direction 2 in 2083

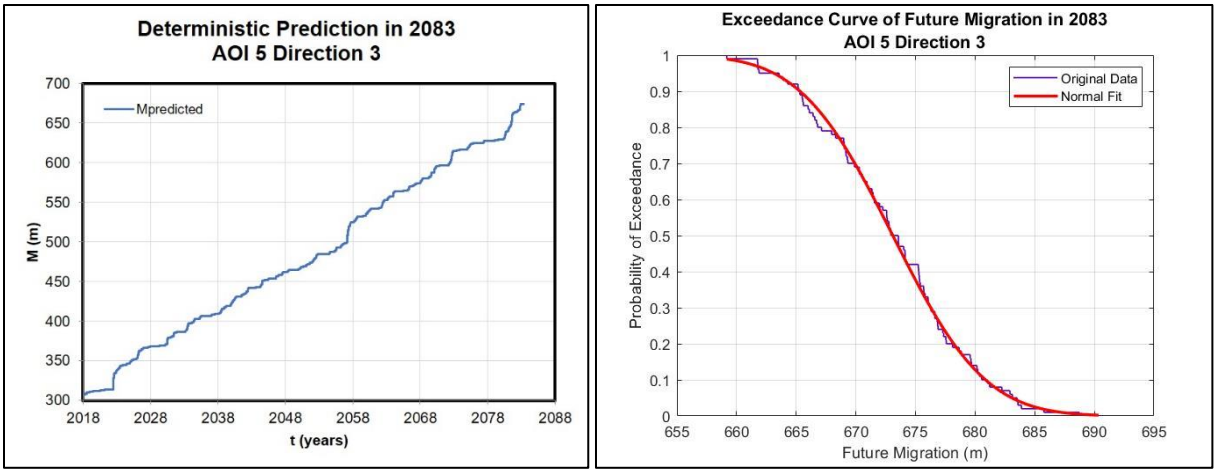

Figure 107. Future position of AOI 5 Direction 3 in 2083

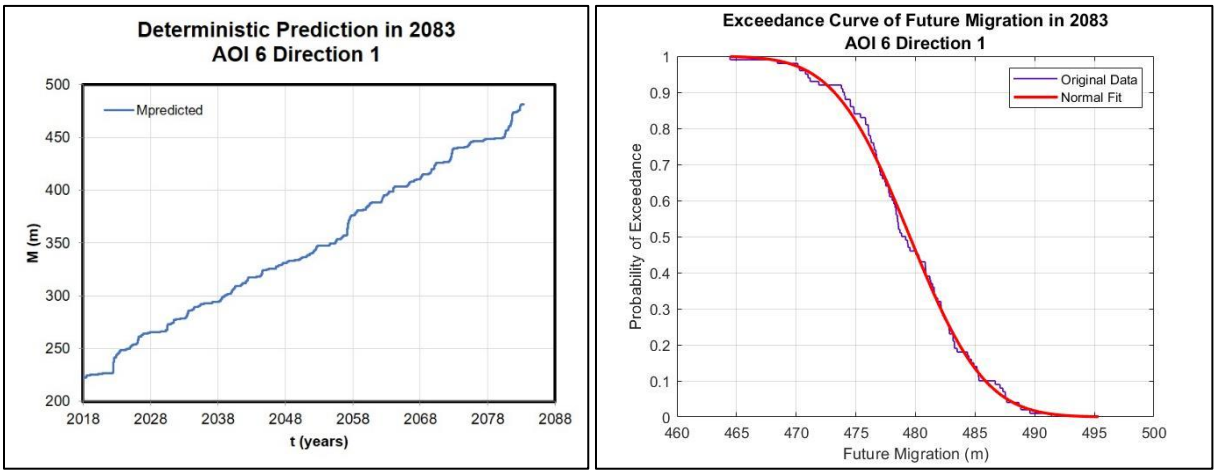

Figure 108. Future position of AOI 6 Direction 1 in 2083

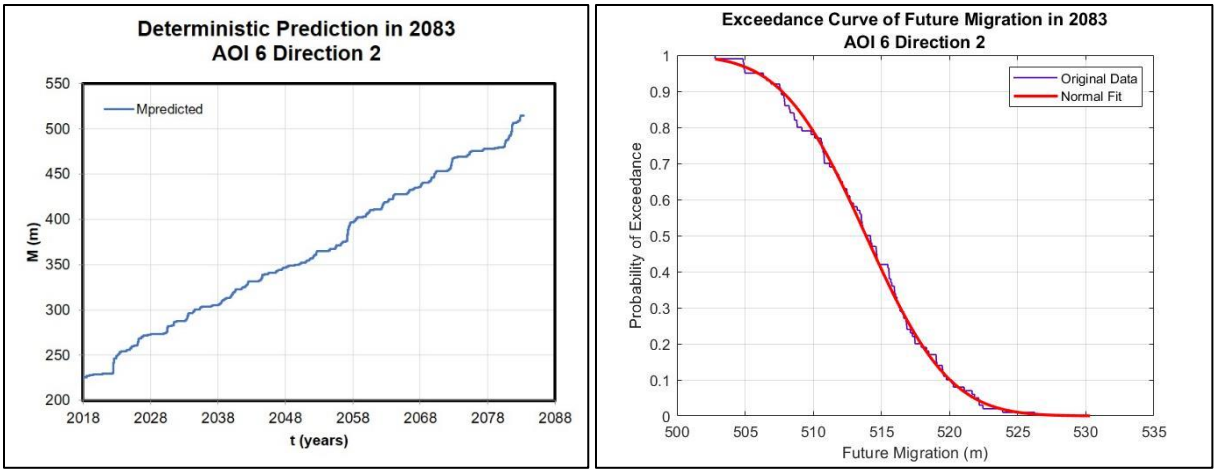

Figure 109. Future position of AOI 6 Direction 2 in 2083

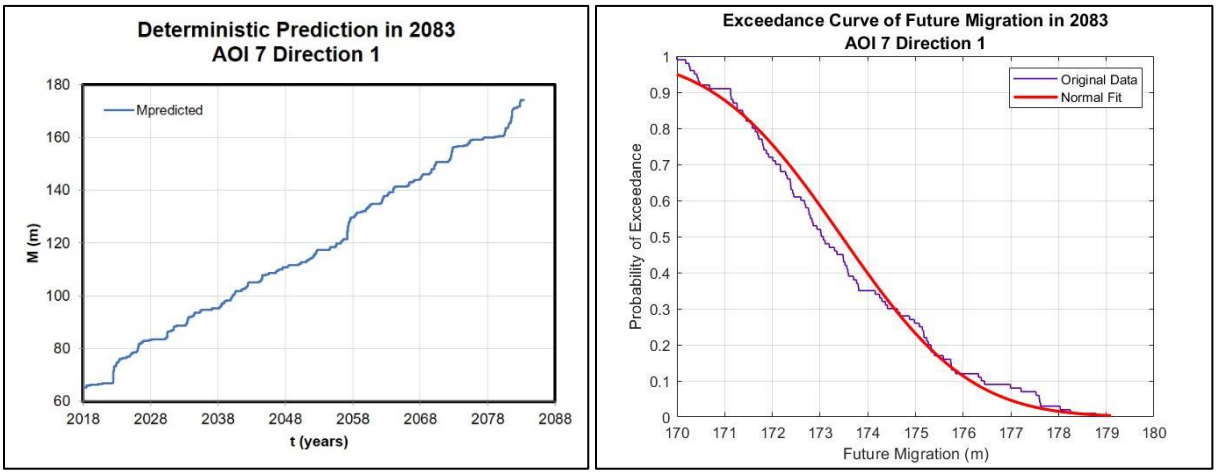

Figure 110. Future position of OAI 7 Direction 1 in 2083

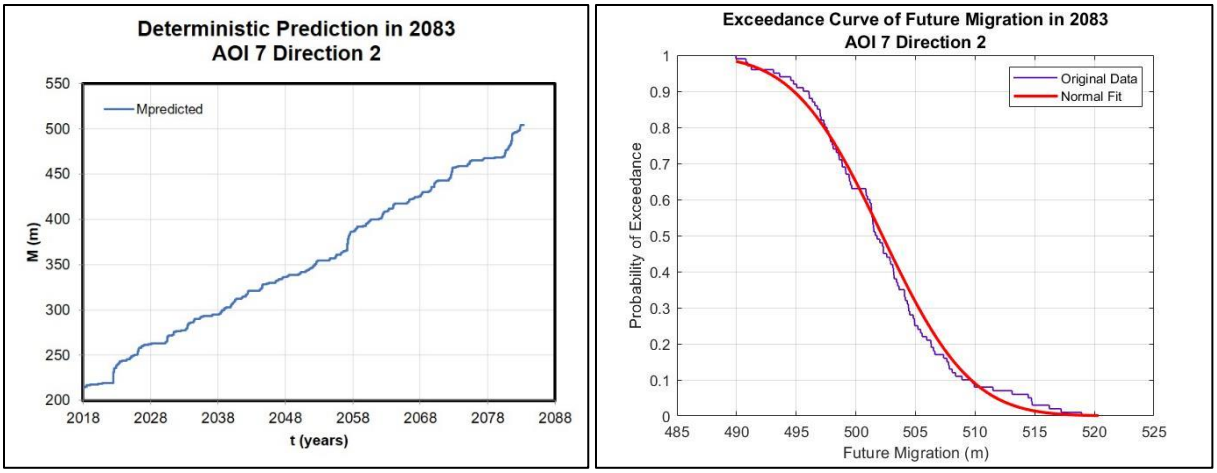

Figure 111. Future position of AOI 7 Direction 2 in 2083

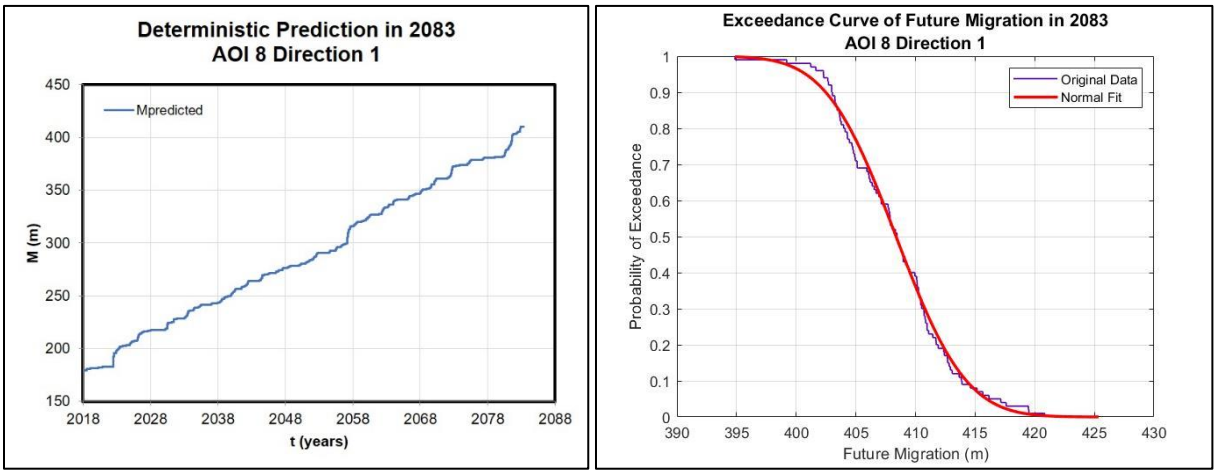

Figure 112. Future position of AOI 8 Direction 1 in 2083

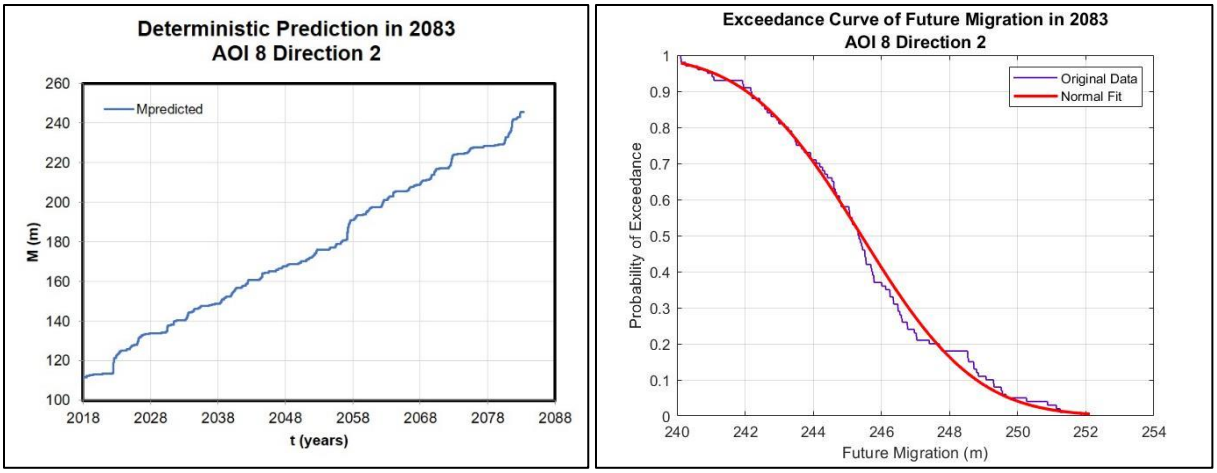

Figure 113. Future position of AOI 8 Direction 2 in 2083

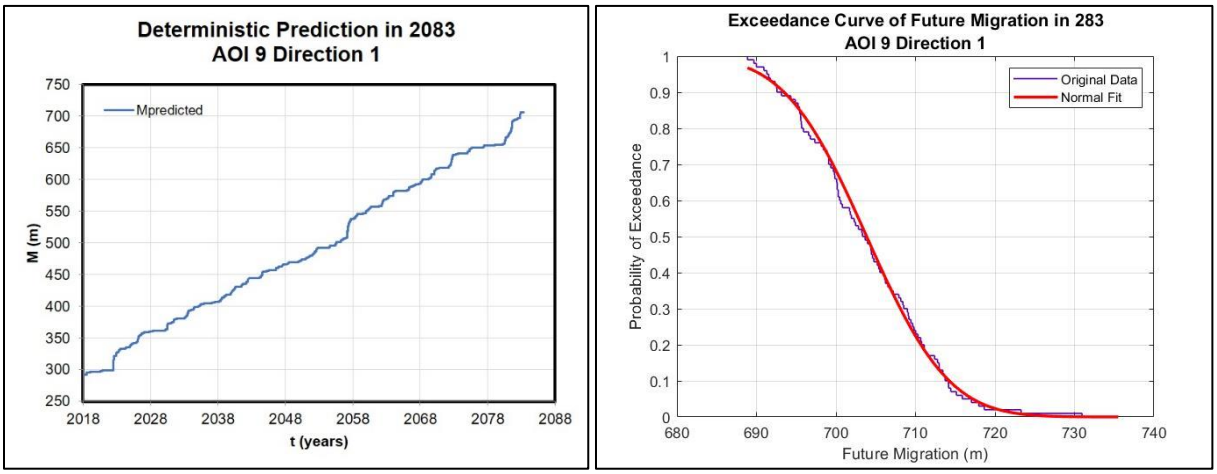

Figure 114. Future position of AOI 9 Direction 1 in 2083

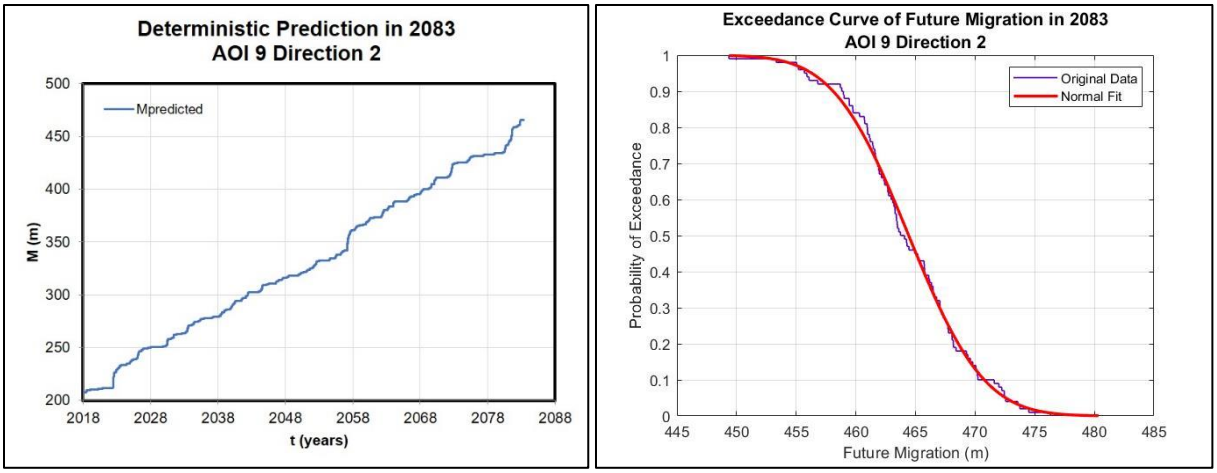

Figure 115. Future position of AOI 9 Direction 2 in 2083

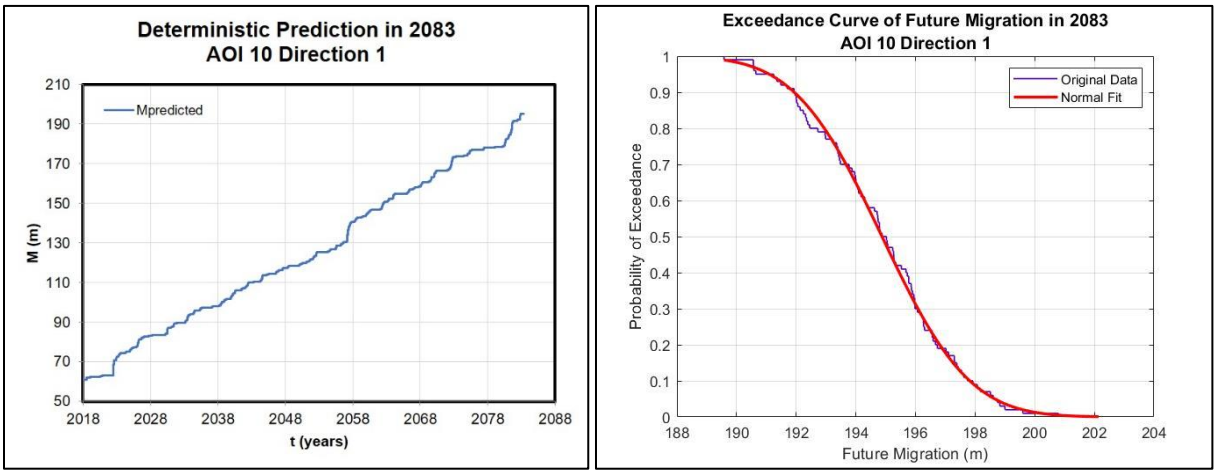

Figure 116. Future position of AOI 10 Direction 1 in 2083

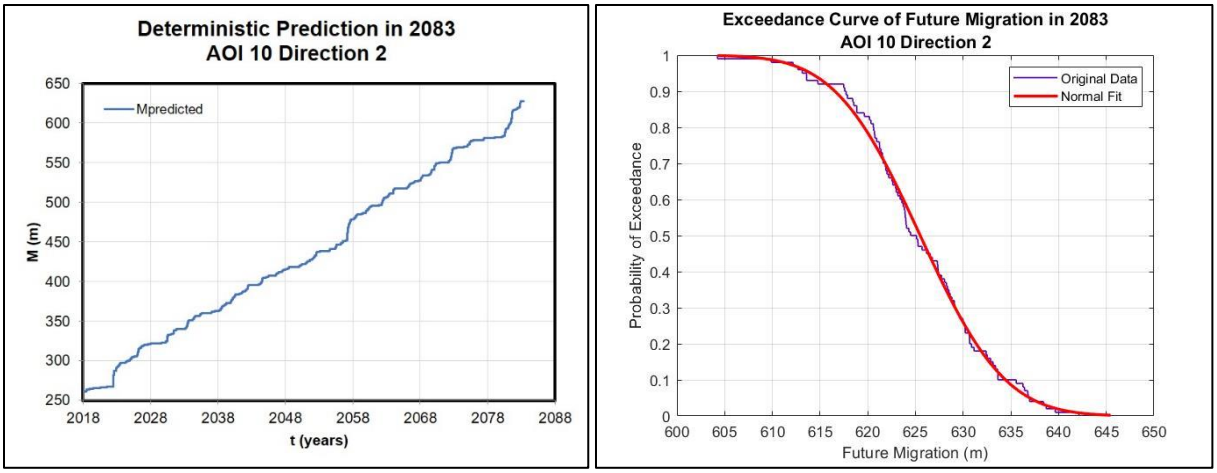

Figure 117. Future position of AOI 10 Direction 2 in 2083

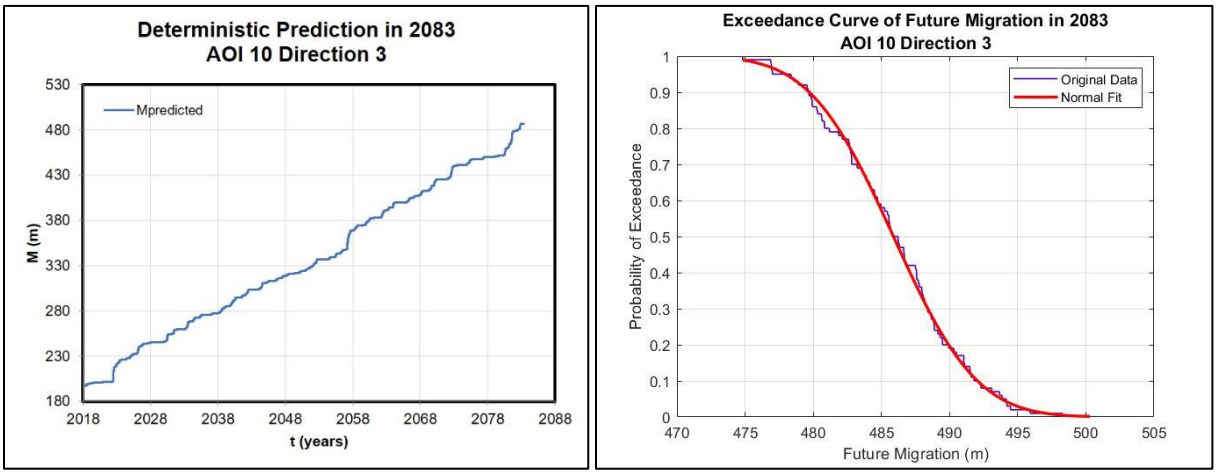

Figure 118. Future position of AOI 10 Direction 3 in 2083

5. CRITICAL ANALYSIS OF THE OMM

5.1. Optimum Prediction Direction

In a meandering river with ideal geometry, the optimum direction to measure the meander migration is a straight line from the center of curvature radius to bend apex for across-valley migration or a straight line from the center of curvature radius and perpendicular to river flow for down-valley migration. However, rivers in the nature do not always have an ideal geometry and can have multiple migration types in one meander. This condition is challenging to choose the best direction which can represent all of migration types.

In this study, the selection of prediction direction is primarily based on the migration type observed from sequential aerial photos. Meanders in the study area are dominantly by extension or across-valley migration type except meander in AOI 9. The first direction is from the center of curvature radius to bend apex. It is strongly recommended to take more than one direction for each meander. Ideally, two additional direction with certain angle from the first direction line is the better option. However, because the meanders are not perfectly symmetrical, the additional directions are drawn without specific angle but still represent the meander migration.

Each direction has different critical velocity (v_c) which represents the amount of migration at certain part of a meander. By having multiple direction lines, multiple predicted positions of the meander will be obtained and the drawing of outer riverbank line can be more reasonable and can illustrate its migration type(s). Result of pas river movement observation shows the location of meander node, the point which the migration is zero (Edwards & Smith, 2002). Although the OMM does not directly consider the migration types, the results both from deterministic and probabilistic

prediction show the meander node at the similar location. It presents that the OMM can give specific result according to the prediction direction.

Another issue with prediction direction is the OMM code assumes that the river always migrates forward along the time. However, results from observation method using aerial photos show that several meanders had retrograding migration(s) during the period. Retrogradation might happen because outer bend apex has more sedimentation than erosion. Sedimentation keeps go on if the river has low discharge in a long period. Also, the sediment can be more compacted and allow vegetation to exist thus the soil needs higher velocity to erode it. Therefore, the outer riverbank line will move backwards.

In the past, the effect of sedimentation rate is represented by river movement. However, for future prediction, the OMM assumes that river will move at the same critical velocity in the field obtained from past movement.

5.2. Future Hydrograph

Although the future flow hydrograph has identical distribution with the past flow hydrograph, time dependency is not considered during the generation of future hydrograph in this study because this study focuses on the sum migration distance during the period, not daily migration. Therefore, the predicted flow in a certain day is not affected by the flow in the previous day and it will result in a highly random future flow hydrograph. For example, in January 28, 2030, the predicted flow will reach the maximum discharge, it might have the minimum discharge in January 29, and then it can come back to the maximum discharge in January 30. In addition, the random sampling does not consider the seasonal cycle. The future flow hydrograph might have maximum discharge during summer and minimum discharge during winter. Therefore, the future hydrograph can be visually irrelevant with the past hydrograph (Figure 80).

However, the hydrograph is still credible to be used for prediction because it can give future migration with the similar pattern with deterministic prediction.

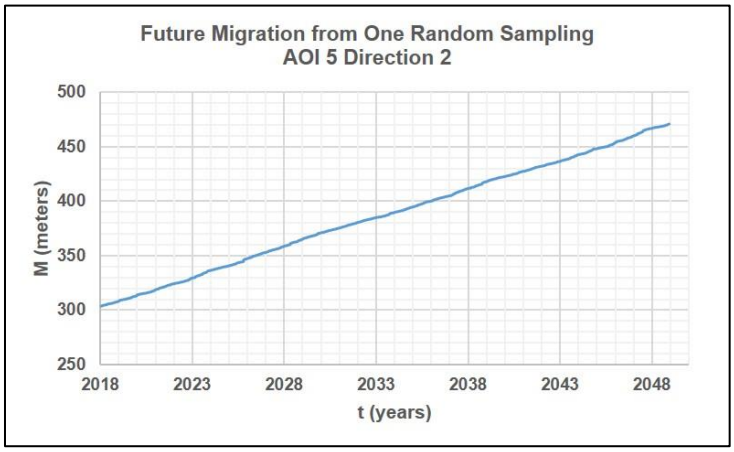

Figure 119. Future migration from one random sampling of probabilistic prediction

Using maximum yearly flow can result in more similar pattern of flow hydrograph and reduce the randomness of the predicted future flow because of the fewer number of data (Figure 99). However, as being explained in Section 4.3, the smaller amount of data will result in a rugged fitted curve of distribution (Figure 100). Table 27 shows the calculation of statistical parameters from original data and fitted distribution of maximum yearly flow by applying the same concept of lognormal and normal distribution. For confidence level of 99%, the confidence intervals of μ_Y and σ_Y for the fitted distribution are $\mu_Y \in (10.5011, 10.9323)$ and $\sigma_Y \in (0.5322, 0.8430)$. The error percentage of the standard deviation s_Q is 46.54% and the original data σ_Y are outside of the 99% confidence level of the fitted distribution. It shows that maximum yearly flow does not fit to lognormal distribution.

Table 28. Comparison of random sampling from original data dan fitted distribution of maximum yearly flow

Parameters	Original Data (cfs)	Fitted Distribution (cfs)	% Error
μ_Y	10.7712	10.7167	0.51
σ_Y	0.4890	0.6547	33.89
m_Q	53679	55884	4.11
s_Q	27901	40885	46.54

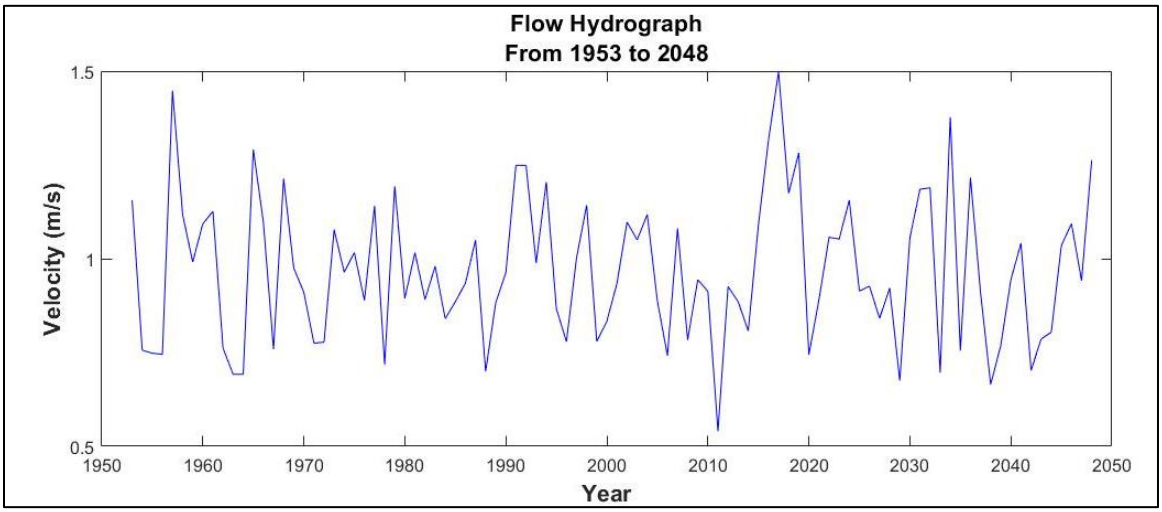

Figure 120. Past and predicted flow hydrograph using maximum yearly flow

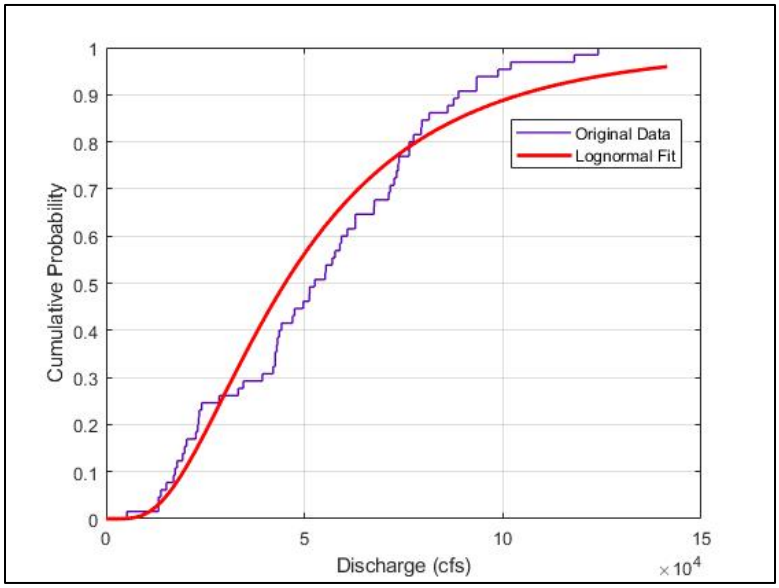

Figure 121. Cumulative density function (CDF) of original and fitted distribution of the past flow hydrograph using maximum yearly flow

In addition, maximum yearly flow cannot be applied for entire year. Kwak (2000) had similar problem in scour depth prediction. He obtained a whole hydrograph by transforming constant flow with the maximum velocity lasting the equivalent time (t_{eqv}). First, the equivalent time for each meander is calculated using Eq.13 by substituting time increment (Δt) with the equivalent time (t_{eqv}) and velocity with maximum velocity (v_{max}). In this study, the data set used for regression analysis is from the direction which has the lowest Ranking Index (RI) value of each meander. The calculation of equivalent time and selected parameters for regression analysis is shown by Table 27. In regression analysis, the variables used are t_{hydro}, t_{eqv}, and v_{max}-v_c. Variable α' and v_c are excluded because the product of α' and v_c is z_i with the equal value in all data sets.

Table 29. Equivalent time calculation for regression analysis

Location	Time period	ΔMi (m)	α' (x10^{-8})	t_{hydro} (years)	v_{max}-v_c (m/s)	v_{max} (m/s)	v_c (m/s)	t_e (s)	t_{eqv} (years)
AOI 3 Direction 1	1953-1968	7.45	4.09	15	0.750	1.45	0.70	5,896,618	0.19
	1953-1995	16.22	4.09	42	0.750	1.45	0.70	12,848,149	0.41
	1953-2002	13.24	4.09	49	0.750	1.45	0.70	10,481,807	0.33
	1953-2010	16.50	4.09	57	0.750	1.45	0.70	13,066,186	0.41
	1953-2014	15.95	4.09	61	0.750	1.45	0.70	12,633,319	0.40
	1953-2018	37.43	4.09	65	0.800	1.50	0.70	24,818,657	0.79
	1968-1995	8.78	4.09	27	0.550	1.25	0.70	15,130,050	0.48
	1968-2002	5.79	4.09	34	0.550	1.25	0.70	9,979,692	0.32
AOI 4 Direction 3	1953-1968	67.13	5.05	15	0.900	1.45	0.55	15,024,638	0.48
	1953-1995	66.92	5.05	42	0.900	1.45	0.55	14,977,637	0.47
	1953-2002	70.48	5.05	49	0.900	1.45	0.55	15,774,415	0.50
	1953-2010	81.48	5.05	57	0.900	1.45	0.55	18,236,370	0.58
	1953-2014	68.20	5.05	61	0.900	1.45	0.55	15,264,119	0.48
	1953-2018	53.53	5.05	65	0.950	1.50	0.55	10,030,781	0.32
	1968-1995	0.21	5.05	27	0.700	1.25	0.55	102,298	0.00
	1968-2002	3.35	5.05	34	0.700	1.25	0.55	1,631,894	0.05
AOI 5 Direction 3	1953-1968	7.45	6.32	15	1.010	1.45	0.44	517,584	0.02
	1953-1995	16.22	6.32	42	1.010	1.45	0.44	1,127,766	0.04
	1953-2002	13.24	6.32	49	1.010	1.45	0.44	920,056	0.03

Table 29. Continued

Location	Time period	ΔMi (m)	α' (x10^{-8})	t_{hydro} (years)	v_{max}- v_c (m/s)	v_{max} (m/s)	v_c (m/s)	t_e (s)	t_{eqv} (years)
AOI 5 Direction 3	1953-2010	16.50	6.32	57	1.010	1.45	0.44	1,146,904	0.04
	1953-2014	15.95	6.32	61	1.010	1.45	0.44	1,108,909	0.04
	1953-2018	37.43	6.32	65	1.060	1.50	0.44	2,178,495	0.07
	1968-1995	8.78	6.32	27	0.810	1.25	0.44	1,328,063	0.04
	1968-2002	5.79	6.32	34	0.810	1.25	0.44	875,982	0.03
AOI 6 Direction 1	1953-1968	89.71	5.91	15	0.980	1.45	0.47	8,811,173	0.28
	1953-1995	176.16	5.91	42	0.980	1.45	0.47	17,301,607	0.55
	1953-2002	168.48	5.91	49	0.980	1.45	0.47	16,547,114	0.52
	1953-2010	193.21	5.91	57	0.980	1.45	0.47	18,975,738	0.60
	1953-2014	199.64	5.91	61	0.980	1.45	0.47	19,607,666	0.62
	1953-2018	222.70	5.91	65	1.030	1.50	0.47	18,312,737	0.58
	1968-1995	86.45	5.91	27	0.780	1.25	0.47	18,479,481	0.59
AOI 7 Direction 2	1953-1968	124.84	6.04	15	0.990	1.45	0.46	10,954,520	0.35
	1953-1995	185.06	6.04	42	0.990	1.45	0.46	16,238,827	0.51
	1953-2002	175.75	6.04	49	0.990	1.45	0.46	15,422,013	0.49
	1953-2010	198.99	6.04	57	0.990	1.45	0.46	17,461,390	0.55
	1953-2014	188.35	6.04	61	0.990	1.45	0.46	16,527,281	0.52
	1953-2018	214.63	6.04	65	1.040	1.50	0.46	15,767,866	0.50
	1968-1995	60.22	6.04	27	0.790	1.25	0.46	11,501,327	0.36
	1968-2002	50.91	6.04	34	0.790	1.25	0.46	9,723,527	0.31
AOI 8 Direction 1	1953-1968	84.33	5.79	15	0.970	1.45	0.48	9,249,038	0.29
	1953-1995	154.08	5.79	42	0.970	1.45	0.48	16,897,948	0.54
	1953-2002	150.96	5.79	49	0.970	1.45	0.48	16,555,539	0.52
	1953-2010	175.79	5.79	57	0.970	1.45	0.48	19,278,823	0.61
	1953-2014	158.22	5.79	61	0.970	1.45	0.48	17,352,273	0.55
	1953-2018	179.11	5.79	65	1.020	1.50	0.48	16,446,277	0.52
	1968-1995	69.74	5.79	27	0.770	1.25	0.48	16,647,897	0.53
	1968-2002	66.62	5.79	34	0.770	1.25	0.48	15,902,642	0.50
AOI 9 Direction 2	1953-1968	117.79	5.91	15	0.980	1.45	0.47	11,568,782	0.37
	1953-1995	160.18	5.91	42	0.980	1.45	0.47	15,731,860	0.50
	1953-2002	166.01	5.91	49	0.980	1.45	0.47	16,304,829	0.52
	1953-2010	174.29	5.91	57	0.980	1.45	0.47	17,118,241	0.54
	1953-2014	153.52	5.91	61	0.980	1.45	0.47	15,078,218	0.48
	1953-2018	207.61	5.91	65	1.030	1.50	0.47	17,071,980	0.54
	1968-1995	42.39	5.91	27	0.780	1.25	0.47	9,060,963	0.29
	1968-2002	48.22	5.91	34	0.780	1.25	0.47	10,308,034	0.33

Table 29. Continued

Location	Time period	ΔMi (m)	α' (x10^{-8})	t_{hydro} (years)	v_{max}-v_c (m/s)	v_{max} (m/s)	v_c (m/s)	t_e (s)	t_{eqv} (years)
AOI 10 Direction 2	1953-1968	181.25	6.32	15	1.010	1.45	0.44	12,599,686	0.40
	1953-1995	231.08	6.32	42	1.010	1.45	0.44	16,063,562	0.51
	1953-2002	260.54	6.32	49	1.010	1.45	0.44	18,111,137	0.57
	1953-2010	273.75	6.32	57	1.010	1.45	0.44	19,029,712	0.60
	1953-2014	262.66	6.32	61	1.010	1.45	0.44	18,258,715	0.58
	1953-2018	261.02	6.32	65	1.060	1.50	0.44	15,191,563	0.48
	1968-1995	49.83	6.32	27	0.810	1.25	0.44	7,539,146	0.24
	1968-2002	79.28	6.32	34	0.810	1.25	0.44	11,995,706	0.38

The regression analysis results in the following equation

$$t_{eqv}(in\ years) = 0.046 \times (v_{max} - v_c)^{0.34}\left(t_{hydro}\right)^{0.51} \quad \text{(Eq. 21)}$$

The value of equivalent time substitutes time increment (Δt) during deterministic or probabilistic prediction using maximum annual flow. The calculation of equivalent time for one year in each meander location is shown by Table 29. By using maximum velocity from past flow of 1.5 m/s, the average of equivalent time for this study is 16.7 days. It means that the maximum yearly flow over 16.7 days will create the same amount of migration distance from mean daily flow over one year.

Table 30. Equivalent time calculation for prediction

Location	v_c (m/s)	v_{max}-v_c (m/s)	t_{eqv} (years)	t_{eqv} (days)	t_{eqv} (sec)
AOI 3 Dir 1	0.70	0.80	0.042639	15.6	1,344,668
AOI 3 Dir 2	0.68	0.82	0.042999	15.7	1,356,005
AOI 3 Dir 3	0.55	0.95	0.045205	16.5	1,425,576
AOI 4 Dir 1	0.66	0.84	0.043352	15.8	1,367,160
AOI 4 Dir 2	0.57	0.93	0.044879	16.4	1,415,300
AOI 4 Dir 3	0.55	0.95	0.045205	16.5	1,425,576
AOI 5 Dir 1	0.47	1.03	0.046465	17.0	1,465,309
AOI 5 Dir 2	0.44	1.06	0.046920	17.1	1,479,682

Table 30. Continued

Location	v_c (m/s)	v_{max}-v_c (m/s)	t_{eqv} (years)	t_{eqv} (days)	t_{eqv} (sec)
AOI 5 Dir 3	0.44	1.06	0.046920	17.1	1,479,682
AOI 6 Dir 1	0.47	1.03	0.046465	17.0	1,465,309
AOI 6 Dir 2	0.46	1.04	0.046618	17.0	1,470,130
AOI 7 Dir 1	0.55	0.95	0.045205	16.5	1,425,576
AOI 7 Dir 2	0.46	1.04	0.046618	17.0	1,470,130
AOI 8 Dir 1	0.48	1.02	0.046311	16.9	1,460,456
AOI 8 Dir 2	0.53	0.97	0.045526	16.6	1,435,710
AOI 9 Dir 1	0.43	1.07	0.047070	17.2	1,484,414
AOI 9 Dir 2	0.47	1.03	0.046465	17.0	1,465,309
AOI 10 Dir 1	0.53	0.97	0.045526	16.6	1,435,710
AOI 10 Dir 2	0.44	1.06	0.046920	17.1	1,479,682
AOI 10 Dir 3	0.46	1.04	0.046618	17.0	1,470,130

Prediction using maximum yearly flow is conducted by applying the same methods with the prediction except the time increment. By applying 16.7 days ≈ 17 days as the increment time, comparison of prediction using maximum yearly flow and mean daily is shown by Figure 101. In general, prediction using mean daily flow gives higher value than using maximum yearly flow. The biggest difference is from deterministic prediction while the smallest difference is from probabilistic prediction with exceedance probability of 1%.

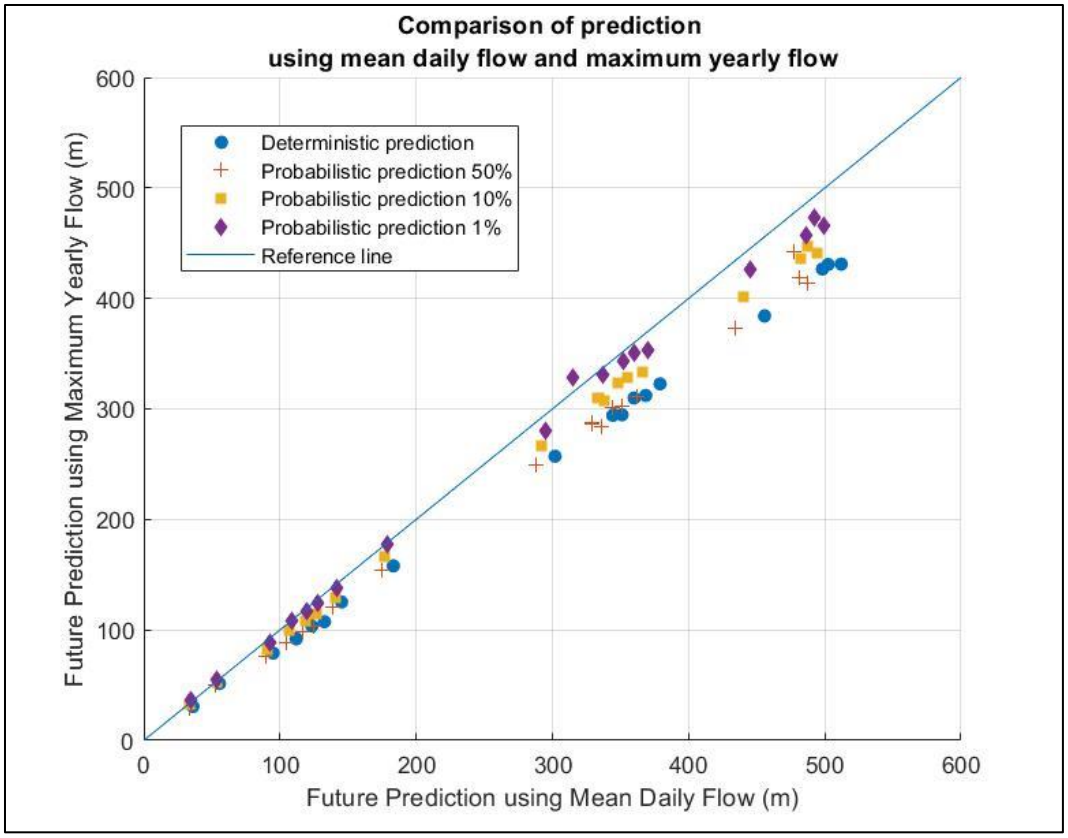

Figure 122. Comparison of prediction using mean daily flow and maximum yearly flow

5.3. Probability Density Function (PDF) of Meander Migration

The purpose of probabilistic prediction is to obtain various migration distance with certain probability. However, results from probabilistic prediction show that there is no significance difference in migration distance with exceedance probability of 50%, 10%, and 1% and the histogram also presents the narrow range from the minimum to maximum future migration. It might be because of the future flows are similar to each other which results in small error. It is also related to the prediction period. The longer prediction period will give the wider interval because the error is increasing.

Figure 102 shows the influence of prediction period in AOI 5 Direction 2. The current position in 2018 is 303.5 m away from its initial position. The predicted position in 2048 is from 466 m to 486 m which means that the meander is predicted to migrate 162.5 m to 182.5 m in the next 30 years or 5.4 – 6.1 m/year. By increasing the prediction period to 40 years, the future migration distance is 216 – 244 m (future position will be 522 – 550 m) or the interval is 28 m. Meanwhile, by reducing the prediction period to 20 years, the future migration distance is 108.5 – 126.5 m (future position will be 412 – 430 m) or the interval is 18 m.

If a wider interval of migration distance is necessary, the prediction period can be increased. However, prediction period is related to life design of infrastructure and sometimes in certain years. Consideration of flood discharge can be applied in probabilistic prediction to get more diverse value of future migration distance.

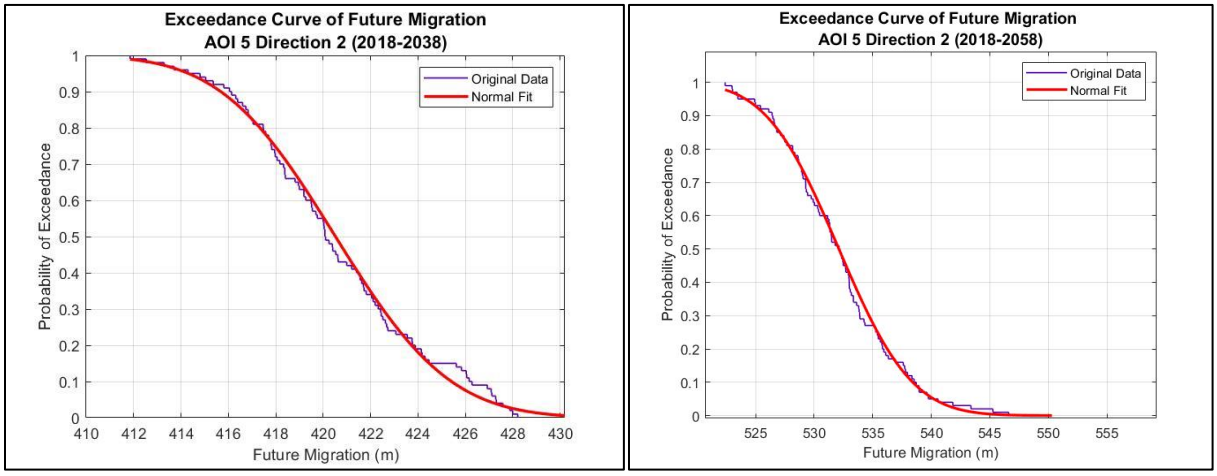

Figure 123. Future migration of AOI 5 Direction 2 probabilistic prediction for 20-year and 40-year prediction

5.4. Uncertainties Excluded in OMM

While probabilistic prediction is mainly used to consider any uncertainties of a problem, the OMM method only involves uncertainty in future flow hydrograph. For soil parameters, OMM assumes that the future soil is constant thus it uses the same critical velocity in the field (v_{cfield}), β, and α'. For river geometry, OMM also assumes that the future migration happens in the same way as the past migration occurred. Any disturbances which might appear such as vegetation and infrastructure are also excluded from OMM method for future prediction.

6. CONCLUSIONS AND RECOMMENDATIONS

6.1. Conclusions

River meander migration is a product of fluvial activities including erosion and deposition. It may cause problems if it is close to vital infrastructure and its migration rate is noticeable for design life of infrastructure. Various studies have been conducted to analyze meander migration prediction by using different methods which can be classified into three categories: time sequences map and extrapolation, empirical methods, and analytical methods. However, most of them do not integrate all general components of meander: geometry, flow, and soil.

The Observation Method for Meander (OMM) is a prediction method which is developed by accommodating those components. River geometry is represented by past river movement from aerial photos or map observation, river flow is represented by discharge data from United States Geological Survey, and soil properties are represented by erosion function parameters obtained from erosion tests. This method results critical velocity in the field and soil parameters to create calibrated and observed migration versus time plot. For future prediction, the previous OMM used deterministic analysis by duplicating past flow and results in a single precise predicted migration.

Eight meanders in Brazos River near City of Sugar Land were selected for this study. The prediction was conducted for a 30-year period. Deterministic prediction was carried out by using the same method of the previous OMM. Probabilistic prediction was carried out by generating 100 equally possible future flows from statistical parameters of the past flow and them applying them to predict future migration. Each future migration will have certain probability of exceedance.

Compared to the previous study, the calibration step in this study results in higher Ranking Index (RI) value averaging 0.5 because there might be migration rate changes in the past and this issue cannot be considered by the OMM.

The further analyses result in some issues about the OMM. Although there is no specific method to choose the best prediction direction line, drawing more than one lines for each meander can give a more reasonable prediction. Future flow prediction without time-dependent analysis will result a highly random daily hydrograph. However, it is not a fundamental concern because the OMM focuses on the total migration during the prediction period instead of daily migration. Maximum yearly flow can be used by applying equivalent time but it requires additional steps to analyze. In addition, the prediction period influence the interval between minimum and maximum future migration.

6.2. Recommendations

This study has improved the previous OMM method by including probabilistic prediction. It can provide the simple and quick way to predict meander migration in a single MATLAB code which can be modified as needed. The following are recommended concerns for further research to improve the result of the OMM.

1. The current OMM only uses past flow data without considering additional parameters such as rainfall and evapotranspiration. It should be improved to provide a better and more reasonable solution for future flow prediction.
2. The Erosion Function Apparatus (EFA) tests should be conducted on soil samples at each meander to improve the accuracy in calibration step.
3. The current OMM only assumes constant erosion and does not consider sedimentation rate in the future which can cause any changes in migration rate and retrogradation movement.

4. If there is a flood during past flow, it is recommended to use prediction period with the same length as past flow to have similar statistical properties between deterministic and probabilistic future flow.

REFERENCES

Briaud, J.L., Chen, H. C., Park, S., (2001). Predicting meander migration: evaluation of some existing techniques. *Federal Highway Agency Report No. FHWA/TX-02/2105-1*. College Station, TX: Texas Transportation Institute.

Briaud, J. L., Brandimarte, L., Wang, J., & D'Odorico, P. (2007). Probability of scour depth exceedance owing to hydrologic uncertainty. *Georisk, 1*(2), 77-88.

Briaud, J.L., Chen, H. C., Chang, K. A., Chung, Y. A., Park, N., Wang, W., & Yeh, P. H. (2007). Establish guidance for soil properties-based prediction of meander migration rate. *Federal Highway Agency Report No. FHWA/TX-07/0-4378-1*. College Station, TX: Texas Transportation Institute.

Briaud, J. L. (2013). *Geotechnical engineering: unsaturated and saturated soils*. Hoboken, NJ: John Wiley & Sons

Briaud, J. L. & Montalvo-Bartolomei, A. M. (2017). Meander migration: the observation method. *Canadian Geotechnical Journal, 54*(8), 1104-1117.

Brice, J. C. (1982). Stream channel stability assessment. *Federal Highway Administration Report No. FHWA/RD-82/021*. Washington, DC: US Department of Transportation.

Edwards, B. F. & Smith, D. H. (2002). River meandering dynamics. *Physical Review E, 65*(4), 046303.

Google Earth V7.3.2.5776. (2018). *Brazos River, Sugarland, Texas*. 29º33’24.44”N, 95º39’46.10”W, elevation 27 m, eye altitude 14.80 km. Google.

Hooke, J. M. (1980). Magnitude and distribution of rates of river bank erosion. *Earth Surface Processes, 5*(2), 143-157.

Kwak, K. (2000). *Prediction of scour depth versus time for bridge piers in cohesive soils in the case of multi-flood and multi-layer soil systems*. Ph. D. Dissertation. Zachry Department of Civil Engineering, Texas A&M University, College Station.

Lagasse, P.F., Spitz, W. J., Zevenbergen, L. W., & Zachmann, D. W. (2004). Handbook for predicting stream meander migration. *National Cooperative Highway Research Program Report 533*. Washington, DC: Transportation Research Board.

Montalvo-Bartolomei, A. M. (2014). *Observation method to predict meander migration and vertical degradation of rivers*. M. Sc. Thesis. Zachry Department of Civil Engineering, Texas A&M University, College Station.

Mood, A. M. , Graybill, F. A., & Boes, D. C. (1974). *Introduction to the theory of statistics 3rd*. Singapore: Mc.Graw-Hill Book Company.

Nanson, G. C. & Hickin, E. J., (1983). Channel migration and incision on the Beatton River. *Journal of Hydraulic Engineering, 109*(3), 327-337.

Odgaard, A. J. (1987). Streambank erosion along two rivers in Iowa. *Water Resources Research, 23*(7), 1225-1236.

APPENDIX

OBSERVATION METHOD FOR MEANDER (OMM) MATLAB CODE

```
close all
clear all
clc

disp('TAMU OMM for Meander Prediction');
disp(' ');
disp(' ');

%A. Calibration Step%
%1. Load USGS Database from Excel "USGSdatabase.xlsx"
Input1 = readtable ('USGSdatabase.xlsx');
t = Input1 {:,2};
Q = Input1 {:,3};
%2. Velocity from flow
HECQ=[206000 164000 147000 103000 68667 51500 34333 25750 17167 8583 4000 200
0]';
HECV=[6.77 5.91 5.54 4.34 3.47 3.07 2.75 2.6 2.44 2.07 1.66 0.61 0.61]';
Velocity=interp1(HECQ, HECV, Q);
v=Velocity/3.28;
%3. Input other parameters
B = input ('Enter the beta component: ');
zdotc = input ('Enter the erosion rate at critical velocity: ');
deltat = input ('Enter the increments of time (delta t): ');
number = input ('Enter the number of observations: ');

disp(' ');

for i=1:number
    i
    t0(i,1)=input('Enter the year of observation: ');
    M0(i,1)=input('Enter the position of the river: ');
end

tomo=[t0,M0];

vmin=min(v);
vmin=round(vmin/.01)*.01;
vmax=max(v);
vmax=round(vmax/.01)*.01;

vec=[vmin:.01:vmax];

lt=length(t);
Ma=zeros(lt,1);
M=zeros(lt,1);

for i=1:length(vec)
a=zdotc/vec(i);
    for j=1:length(t)
        if (v(j)/vec(i))>1
```

```
            M(j)=a*((v(j)/vec(i))^B)*vec(i)*deltat;
        else
            M(j)=0;
        end

        Ma(1)=M(1);
    end

    for j=2:length(t)
        Ma(j)=Ma(j-1)+M(j);
    end

td(1,:)=[t(1),Ma(1)];

for k=1:(length(t0)-1);
    td(k+1,:)=[t((t0(k+1)*365-t0(1)*365)+1),Ma((t0(k+1)*365-t0(1)*365)+1)];
end

    Mcp=[td(:,2)];
    Mco=[tomo(:,2)];

for kk=1:(length(t0)-1);

    Mcpp(kk,1)=Mcp(kk+1,1);
    Mcoo(kk,1)=Mco(kk+1,1);
end

average=abs(mean(log(Mcpp./Mcoo)));
standard=std(log(Mcpp./Mcoo));

RI=standard+average;
results(i,:)=[vec(i),RI,standard,average];

end

[minnum,minindex]=min(results(:,2));
[row, col]=ind2sub(size(results(:,2)), minindex);

Vc=results(row,1);
RI=results(row,2);

for j=1:length(t)
a=zdotc/Vc;
        if (v(j)/Vc)>1
            M(j)=a*((v(j)/Vc)^B)*Vc*deltat;
        else
            M(j)=0;
        end
    Ma(1)=M(1);
end

for j=2:length(t);
    Ma(j)=Ma(j-1)+M(j);
end
```

```
for k=1:(length(t0)-1);
    td(k+1,:)=[t((t0(k+1)*365-t0(1)*365)+1),Ma((t0(k+1)*365-t0(1)*365)+1)];
end

Mcp=[td(:,2)];
Mco=[tomo(:,2)];

for kk=1:(length(t0)-1);
    Mcpp(kk,1)=Mcp(kk+1,1);
    Mcoo(kk,1)=Mco(kk+1,1);
end

%%Figures%%

disp(' ');
disp('Critical velocity (m/s) is');
Vc
disp(' ');
disp('Alpha prime is');
a
disp(' ');
disp('Ranking Index is');
RI

figure(1)
plot(t,Ma,'linewidth',.5);
grid on;

title({'Calibrated and Observed Migration','AOI Direction
'},'fontweight','bold');
xlabel('t(years)','fontweight','bold');
ylabel('M(meters)','fontweight','bold');

hold on
scatter(t0,M0);

figure(2)
x=[0:.01:100];
x=x';
xx=(x/Vc);
for i=1:length(x)
    if xx(i)<1
        xx(i)=0;
    else
        xx(i)=xx(i);
    end
end

yy=a.*(xx.^B);
loglog(xx,yy)

xlabel('V/Vc','fontweight','bold');
ylabel('zdotc/Vc','fontweight','bold');
title('Dimensionless EFA curve from predicted critical
velocity','fontweight','bold');
```

```
figure(3)

plot (t,v)
xlabel('Time (days)','fontweight','bold');
ylabel('Velocity (m/s)','fontweight','bold');
title('Velocity vs Time','fontweight','bold');

hold on
plot(t,Vc,'r')

figure(4)

scatter(Mcp,Mco,'k');

title('Brazos River','fontweight','bold');
xlabel('Mc(m)','fontweight','bold');
ylabel('Mo(m)','fontweight','bold');
grid on;

title('Observed vs Calibrated','fontweight','bold');

hold on

Mmax=max(Mcpp);
if max(Mcoo)>Mmax
    Mmax=max(Mcoo);
end

Mmax=round(Mmax/10)*10;
xxx=[0,Mmax];
yyy=[0,Mmax];
plot(xxx,yyy,'k');

%B. Deterministic Prediction Steps%
%1. Input flow from past hydrograph
DetFutHyd=Input1{12509:23786,3};
t1 = datetime(2018,2,15,'Format', 'MM/dd/yyy');
t2 = datetime(2048,12,31,'Format', 'MM/dd/yyy');
FutureTime=[t1:t2];

%2. Velocity from flow
HECQ=[206000 164000 147000 103000 68667 51500 34333 25750 17167 8583 4000 200
0]';
HECV=[6.77 5.91 5.54 4.34 3.47 3.07 2.75 2.6 2.44 2.07 1.66 0.61 0.61]';
DetFutVel=interp1(HECQ, HECV, DetFutHyd);
DetFutVelSI=DetFutVel/3.28;

%3. Input other parameters
beta=B;
vcfield=Vc;
deltatime=deltat;
alphaprime=zdotc/vcfield;
Mt=M0(end,:);
```

```
for i=1: length(FutureTime)
    year(i)=t(end,:)+i/365
end

period=year;
Mdp=zeros(length(FutureTime),1);
Mdpday=zeros(length(FutureTime),1);

for j=1:length(period)
    if (DetFutVelSI(j)/vcfield)>1

Mdpday(j)=alphaprime*((DetFutVelSI(j)/vcfield)^beta)*vcfield*deltatime;
    else
        Mdpday(j)=0;
    end

    Mdp(1)=Mt;
end

for j=2:length(period)
    Mdp(j)=Mdp(j-1)+Mdpday(j)
end

%4. Figures
figure
plot(FutureTime,Mdp,'linewidth',1.5);
grid on;
title ({'Deterministic Prediction 2018-2048','AOI
Direction'},'fontweight','bold')
xlabel ('t(years)','fontweight','bold')
ylabel ('M(meters)','fontweight','bold')

%C. Probabilistic Prediction Steps%
%1. Distribution of Past Flow
%%Creating and fitting the probability density function pdf
figure
hold on;
LegHandles = []; LegText = {};

% --- Plot data originally in dataset "Original Data"
[CdfF,CdfX] = ecdf(Q,'Function','cdf');  % compute empirical cdf
BinInfo.rule = 1;
[~,BinEdge] = internal.stats.histbins(Q,[],[],BinInfo,CdfF,CdfX);
[BinHeight,BinCenter] = ecdfhist(CdfF,CdfX,'edges',BinEdge);
hLine = bar(BinCenter,BinHeight,'hist');
set(hLine,'FaceColor','none','EdgeColor',[0.333333 0 0.666667],...
    'LineStyle','-', 'LineWidth',1);
title('Density of the Past Flow', 'fontweight','bold','fontsize',14);
xlabel('Discharge (cfs)');
ylabel('Density')
LegHandles(end+1) = hLine;
LegText{end+1} = 'Original Data';

%--- Create grid where function will be computed
XLim = get(gca,'XLim');
```

```
XLim = XLim + [-1 1] * 0.01 * diff(XLim);
XGrid = linspace(0,XLim(2),100);

%--- Create fit "Lognormal Fit"
%%%Fit this distribution to get parameter values
pd1 = fitdist(Q, 'lognormal');
YPlot = pdf(pd1,XGrid);
hLine = plot(XGrid,YPlot,'Color',[1 0 0],...
    'LineStyle','-', 'LineWidth',2,...
    'Marker','none', 'MarkerSize',6);
LegHandles(end+1) = hLine;
LegText{end+1} = 'Lognormal Fit';

%--- Adjust figure
box on;
grid on;
hold off;

%--- Create legend from accumulated handles and labels
hLegend = legend(LegHandles,LegText,'Orientation', 'vertical', 'FontSize', 9,
'Location', 'northeast');
set(hLegend,'Interpreter','none');

%%Creating and fitting the cumulative density function pdf
figure
hold on;
LegHandles = []; LegText = {};

% --- Plot data originally in dataset "Original Data"
hLine = stairs(CdfX,CdfF,'Color',[0.333333 0 0.666667],'LineStyle','-',
'LineWidth',1);
title('Cummulative Probability of the Past Flow',
'fontweight','bold','fontsize',14)
xlabel('Discharge (cfs)');
ylabel('Cumulative Probability')
LegHandles(end+1) = hLine;
LegText{end+1} = 'Original Data';

%--- Create fit "Lognormal Fit"
YPlot = cdf(pd1,XGrid);
hLine = plot(XGrid,YPlot,'Color',[1 0 0],...
    'LineStyle','-', 'LineWidth',2,...
    'Marker','none', 'MarkerSize',6);
LegHandles(end+1) = hLine;
LegText{end+1} = 'Lognormal Fit';

%--- Adjust figure
box on;
grid on;
hold off;

%--- Create legend from accumulated handles and labels
hLegend = legend(LegHandles,LegText,'Orientation', 'vertical', 'FontSize', 9,
'Location', 'northeast');
set(hLegend,'Interpreter','none');
```

```
%---The 99% confidence of mu and sigma for the fitted lognormal distribution
[parmhat,parmci] = lognfit(Q,0.01);
[M,V]= lognstat(parmhat(1),parmhat(2));
FittedMean=M;
FittedStd=sqrt(V);

%Computing the actual average and the standard deviation of the flow data
ActualAvgQ = mean(Q);
ActualStdQ =std(Q);
ActualAvgV = mean(Velocity);
ActualStdV =std(Velocity);
ActualAvgVSI = ActualAvgV/3.28;
ActualStdVSI =ActualStdV/3.28;
%Computing the actual average and standard deviation of Y=lnQ, based on the
the actual average and the standard deviation of the flow data and using
lognormal equations
ActualAvgY = log(ActualAvgQ^2/sqrt(ActualAvgQ^2+ActualStdQ^2));
ActualStdY =sqrt(log((ActualStdQ/ActualAvgQ)^2+1));

%2. Creating Future Flow
num = length(FutureTime);
RandFlow = zeros(num,100); %matrix containing 100 vectors of future discharge
RandUniValue=zeros(num,1); %matrix containing 100 vectors of random uniform
values

for i=1:100
    %%Generate random values from uniform distribution
    RandUniValue= rand(num,1);
    for j=1:num
    %%Compare to the eCDF, and draw samples from the eCDF
    [m,n] = min(abs(RandUniValue(j)-CdfF));
    RandFlow(j,i) = CdfX(n);
    end
end

%3. Distribution of Future Flow
%Mean, Std and eCDF of 1 randomly generated sample for validation
RandSamplemean=mean(RandFlow(:,1));
RandSamplestd=std(RandFlow(:,1));

[CdfF2,CdfX2] = ecdf(RandFlow(:,1));
figure
plot(CdfX,CdfF,'linewidth',2)
set(gca,'fontsize',12)
title({'Cummulative Probability','Past Flow and Future Flow'},
'fontweight','bold','fontsize',16)
xlabel('Discharge (cfs)','fontweight','bold','fontsize',16)
ylabel('Cumulative Probability','fontweight','bold','fontsize',16)
hold on
plot(CdfX2,CdfF2,'linewidth',2)
legend('Original Data', 'Random Sample')

%Future velocity from HEC-RAS Interpolation
ProbFutVel=interp1(HECQ, HECV, RandFlow);
```

```
ProbFutVelSI=ProbFutVel/3.28;

%4. Plotting Past and One Random Sampling Future Flow
%%Creating the total time string array
TotalTime = strings(35064,1);
TotalTime(1:23786)=datetime(Input1{:,1},'Format','MM/dd/yyy');
TotalTime(23787:35064)=datetime(FutureTime, 'Format','MM/dd/yyy');
TotalTime1=datetime(TotalTime, 'Format','MM/dd/yyy');

%%Creating the total flow array (past flow and 1 sample of the future flow)
TotalFlow=zeros(35064,1);
TotalFlow(1:23786)=v;
TotalFlow(23787:35064):ProbFutVelSI(:,50);

%%Plot the Hydrograph from 1953 to 2048
figure
plot(TotalTime1, TotalFlow,'b');
set(gca,'fontsize;,12);
title({'Flow Hydrograph','from 1953 to
20148'},'fontweight','bold','fontsize',14);
xlabel('Year','fontweight','bold','fontsize',12);
ylabel('Velocity (m/s)','fontweight','bold','fontsize',12))


%5. Meander Migration Calculation
%Input other parameters
beta=B;
vcfield=Vc;
deltatime=deltat;
alphaprime=zdotc/vcfield;
Mt=M0(end,:);

for i=1: length(FutureTime)
    year(i)=t(end,:)+i/365
end

period=year;
Mpp=zeros(length(FutureTime),1);
Mppday=zeros(length(FutureTime),1);

for j=1:length(FutureTime)
    for k=1:100
    if (ProbFutVelSI(j,k)/vcfield)>1

Mppday(j,k)=alphaprime*((ProbFutVelSI(j,k)/vcfield)^beta)*vcfield*deltatime;
    else
        Mppday(j,k)=0;
    end

    Mpp(1,k)=Mt+Mppday(1,k);
    end
end

for j=2:length(FutureTime)
    for k=1:100
```

```
    Mpp(j,k)= Mpp((j-1),k)+Mppday(j,k);
    end
end

%68. Distribution of Meander Migration
ProbFutMigration = transpose(Mpp(end,:));
ProbFutMigrationMean = mean(ProbFutMigration);
ProbFutMigrationStd = std(ProbFutMigration);

%%Creating and fitting the probability density function pdf
figure
hold on;
LegHandles = []; LegText = {};

% --- Plot data originally in dataset "Original Data"
[CdfF,CdfX] = ecdf(ProbFutMigration,'Function','cdf');  % compute empirical
cdf
BinInfo.rule = 1;
[~,BinEdge] =
internal.stats.histbins(ProbFutMigration,[],[],BinInfo,CdfF,CdfX);
[BinHeight,BinCenter] = ecdfhist(CdfF,CdfX,'edges',BinEdge);
hLine = bar(BinCenter,BinHeight,'hist');
set(hLine,'FaceColor','none','EdgeColor',[0.333333 0 0.666667],...
    'LineStyle','-', 'LineWidth',1);
title ({'PDF of Future Migration','AOI
Direction'},'fontweight','bold','fontsize',12)
xlabel('Future Migration (m)');
ylabel('Density')
LegHandles(end+1) = hLine;
LegText{end+1} = 'Original Data';

%--- Create grid where function will be computed
XLim = get(gca,'XLim');
XLim = XLim + [-1 1] * 0.01 * diff(XLim);
XGrid = linspace(min(ProbFutMigration),XLim(2),max(ProbFutMigration));

%--- Create fit "Normal Fit"
%%%Fit this distribution to get parameter values
pd1 = fitdist(ProbFutMigration, 'normal');
YPlot = pdf(pd1,XGrid);
hLine = plot(XGrid,YPlot,'Color',[1 0 0],...
    'LineStyle','-', 'LineWidth',2,...
    'Marker','none', 'MarkerSize',6);
LegHandles(end+1) = hLine;
LegText{end+1} = 'Normal Fit';

%--- Adjust figure
box on;
grid on;
hold off;

%--- Create legend from accumulated handles and labels
hLegend = legend(LegHandles,LegText,'Orientation', 'vertical', 'FontSize', 9,
'Location', 'northeast');
set(hLegend,'Interpreter','none');
```

```
%%Creating and fitting the cumulative density function pdf
figure
hold on;
LegHandles = []; LegText = {};

% --- Plot data originally in dataset "Original Data"
hLine = stairs(CdfX,CdfF,'Color',[0.333333 0 0.666667],'LineStyle','-',
'LineWidth',1);
title ({'CDF of Future Migration','AOI
Direction'},'fontweight','bold','fontsize',12)
xlabel('Future Migration (m)');
ylabel('Cumulative Probability')
LegHandles(end+1) = hLine;
LegText{end+1} = 'Original Data';

%--- Create fit "Lognormal Fit"
YPlot = cdf(pd1,XGrid);
hLine = plot(XGrid,YPlot,'Color',[1 0 0],...
    'LineStyle','-', 'LineWidth',2,...
    'Marker','none', 'MarkerSize',6);
LegHandles(end+1) = hLine;
LegText{end+1} = 'Normal Fit';

%--- Adjust figure
box on;
grid on;
hold off;

%--- Create legend from accumulated handles and labels
hLegend = legend(LegHandles,LegText,'Orientation', 'vertical', 'FontSize', 9,
'Location', 'northeast');
set(hLegend,'Interpreter','none');

% Plot Exceedance Curve
figure
hold on;
LegHandles = []; LegText = {};

% --- Plot data originally in dataset "Original Data"
[eCdfF,eCdfX] = ecdf(ProbFutMigration,'Function','survivor');  % compute
empirical cdf
BinInfo.rule = 1;
[~,BinEdge] =
internal.stats.histbins(ProbFutMigration,[],[],BinInfo,eCdfF,eCdfX);
[BinHeight,BinCenter] = ecdfhist(eCdfF,eCdfX,'edges',BinEdge);
hLine = bar(BinCenter,BinHeight,'hist');
set(hLine,'FaceColor','none','EdgeColor',[0.333333 0 0.666667],...
    'LineStyle','-', 'LineWidth',1);
title ({'PDF of Future Migration','AOI
Direction'},'fontweight','bold','fontsize',12)
xlabel('Future Migration (m)');
ylabel('Density')
LegHandles(end+1) = hLine;
LegText{end+1} = 'Original Data';
```

```
%--- Create grid where function will be computed
XLim = get(gca,'XLim');
XLim = XLim + [-1 1] * 0.01 * diff(XLim);
XGrid = linspace(min(ProbFutMigration),XLim(2),max(ProbFutMigration));

%--- Create fit "Normal Fit"
%%%Fit this distribution to get parameter values
pd1 = fitdist(ProbFutMigration, 'Normal');
YPlot = pdf(pd1,XGrid);
hLine = plot(XGrid,YPlot,'Color',[1 0 0],...
    'LineStyle','-', 'LineWidth',2,...
    'Marker','none', 'MarkerSize',6);
LegHandles(end+1) = hLine;
LegText{end+1} = 'Normal Fit';

%--- Adjust figure
box on;
grid on;
hold off;

%--- Create legend from accumulated handles and labels
hLegend = legend(LegHandles,LegText,'Orientation', 'vertical', 'FontSize', 9,
'Location', 'northeast');
set(hLegend,'Interpreter','none');

%%Creating and fitting the survivor function pdf
figure
hold on;
LegHandles = []; LegText = {};

% --- Plot data originally in dataset "Original Data"
hLine = stairs(eCdfX,eCdfF,'Color',[0.333333 0 0.666667],'LineStyle','-',
'LineWidth',1);
title ({'Exceedance Curve of Future Migration','AOI
Direction'},'fontweight','bold','fontsize',12)
xlabel('Future Migration (m)');
ylabel('Probability of Exceedance')
LegHandles(end+1) = hLine;
LegText{end+1} = 'Original Data';

%--- Create fit "Normal Fit"
YPlot = 1-cdf(pd1,XGrid);
hLine = plot(XGrid,YPlot,'Color',[1 0 0],...
    'LineStyle','-', 'LineWidth',2,...
    'Marker','none', 'MarkerSize',6);
LegHandles(end+1) = hLine;
LegText{end+1} = 'Normal Fit';

%--- Adjust figure
box on;
grid on;
hold off;

%--- Create legend from accumulated handles and labels
```

```
hLegend = legend(LegHandles,LegText,'Orientation', 'vertical', 'FontSize', 9,
'Location', 'northeast');
set(hLegend,'Interpreter','none');
```

GUIDELINE FOR OMM CODE

1. Have a spreadsheet file of flow hydrograph containing time and flow discharge column.
2. Open the code in MATLAB.
3. Adjust some parts according to the condition and necessity, such as:
    - name of the spreadsheet file (line 11)
    - HEC-RAS interpolation to convert the flow into velocity (line 15 – 16)

```
 9     %A. Calibration Step%
10     %1. Load USGS Database from Excel "USGSdatabase.xlsx"
11 -   Input1 = readtable ('USGSdatabase.xlsx');
12 -   t = Input1 {:,2};
13 -   Q = Input1 {:,3};
14     %2. Velocity from flow
15 -   HECQ=[206000 164000 147000 103000 68667 51500 34333 25750 17167 8583 4000 200 (
16 -   HECV=[6.77 5.91 5.54 4.34 3.47 3.07 2.75 2.6 2.44 2.07 1.66 0.61 0.61]';
17 -   Velocity=interp1(HECQ, HECV, Q);
18 -   v=Velocity/3.28;
```

    - future flow for deterministic prediction (line 14)
    - future time for deterministic prediction and probabilistic (line 195 – 196)

```
192      %B. Deterministic Prediction Steps%
193      %1. Input flow from past hydrograph
194 -    DetFutHyd=Input1{2091:23786,3};
195 -    t1 = datetime(2018,2,15,'Format', 'MM/dd/yyy');
196 -    t2 = datetime(2048,12,31,'Format', 'MM/dd/yyy');
197 -    FutureTime=[t1:t2];
```

    - number of random sampling (line 334)

```
332      %2. Creating Future Flow
333 -    num = length(FutureTime);
334 -    RandFlow = zeros(num,100); %matrix containing 100 vectors of future discharge
```

4. Run the program.
5. Enter the value of β exponent, erosion rate at critical velocity ($\dot{z}_c$), increments of time or Δtime (86400 if using average daily flow), and total number of observations.
6. Enter the year of the first observation.
7. Enter the position of the river at the year (0 for the first year).
8. Repeat the step 5 and 6 until reaching the total number of observations.

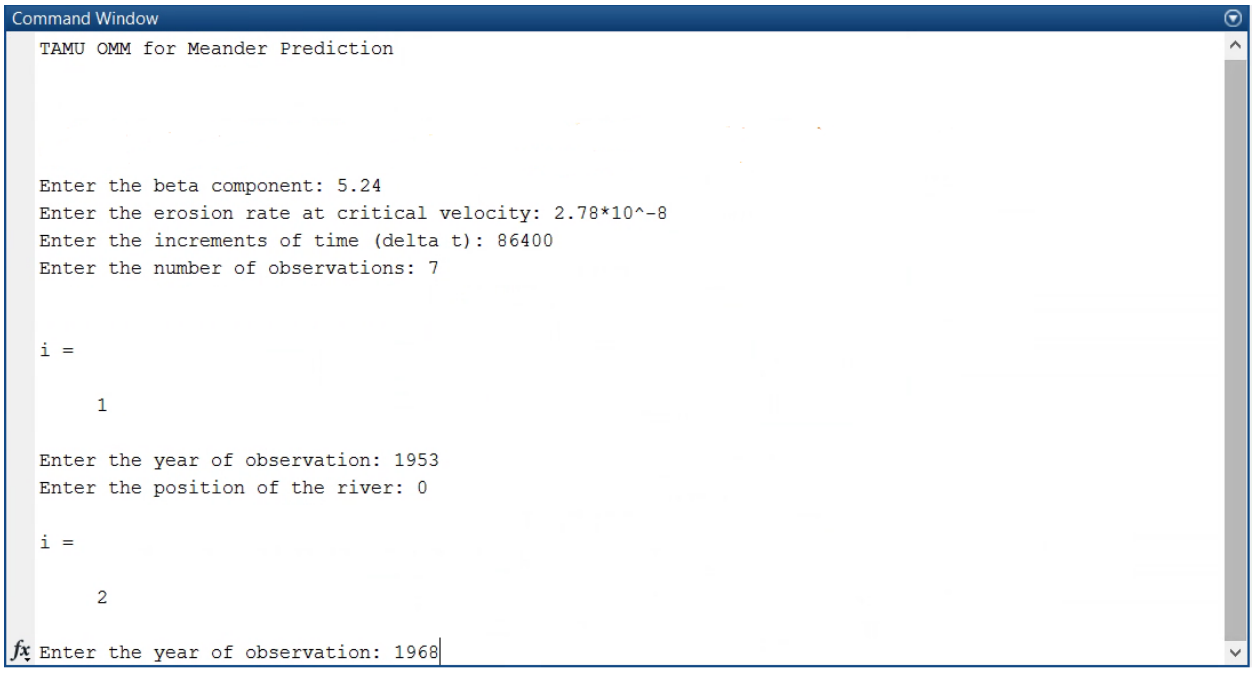

9. The program will calculate critical velocity (v_c) and α' with the lowest Ranking Index (RI) value.

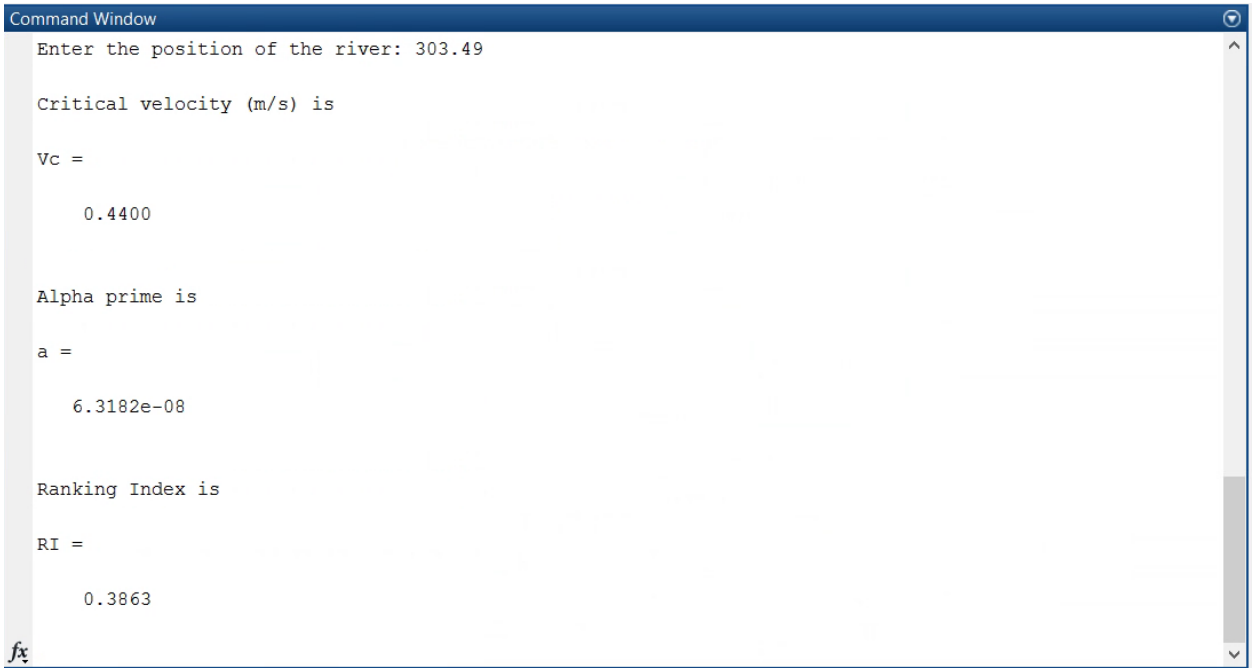

10. The program will continue to run until obtaining the result.
11. Result:
    - Calibrated and observed migration
    - Dimensionless EFA curve from predicted critical velocity
    - Velocity vs time hydrograph
    - Observed vs calibrated migration

- Deterministic prediction
- Density past flow
- Cumulative probability of the past flow
- Cumulative probability of the past and future flow
- Flow hydrograph of past and future flow
- PDF of future migration
- CDF of future migration
- PDF of exceedance curve
- Exceedance curve

WORKFLOW OF THE OMM CODE

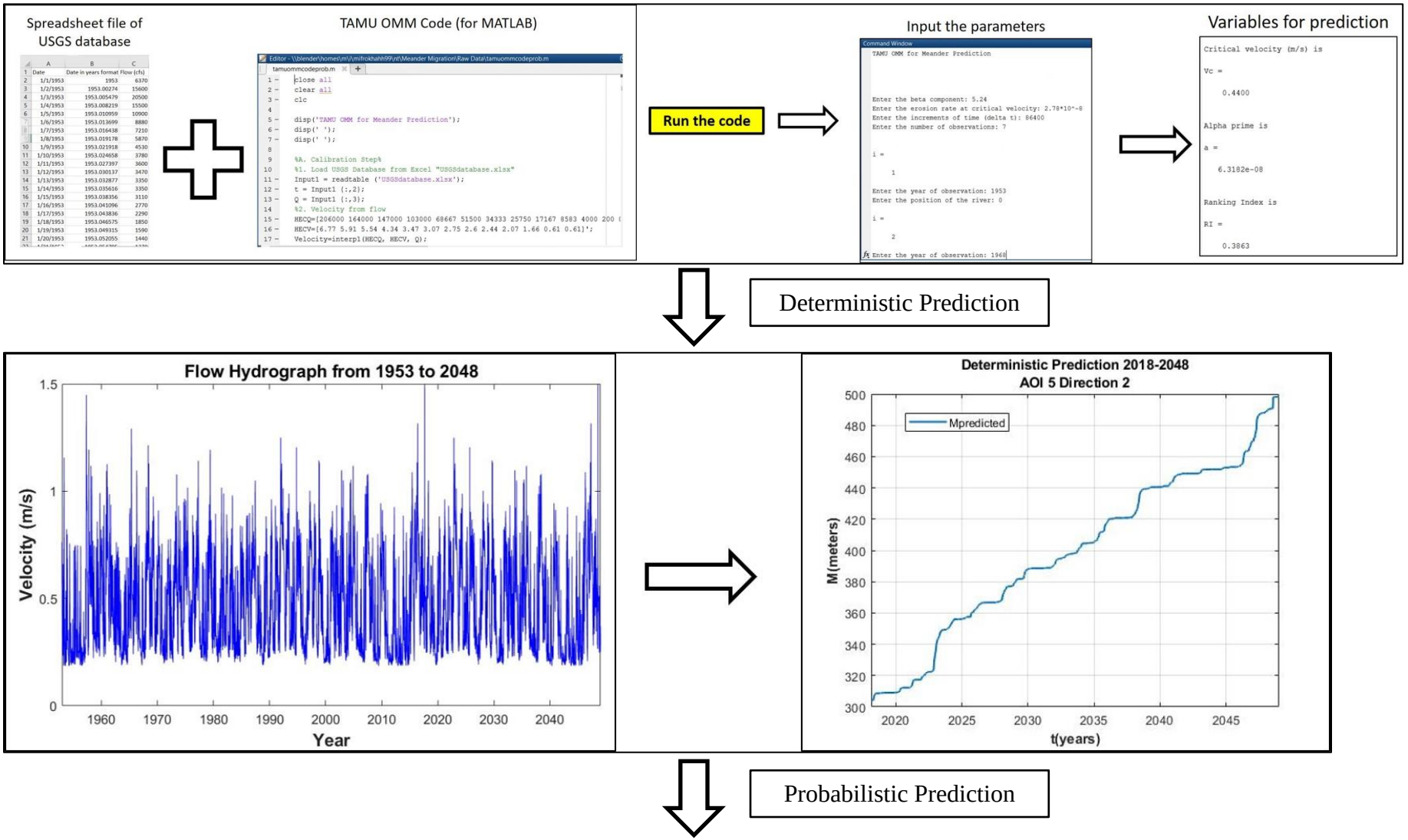

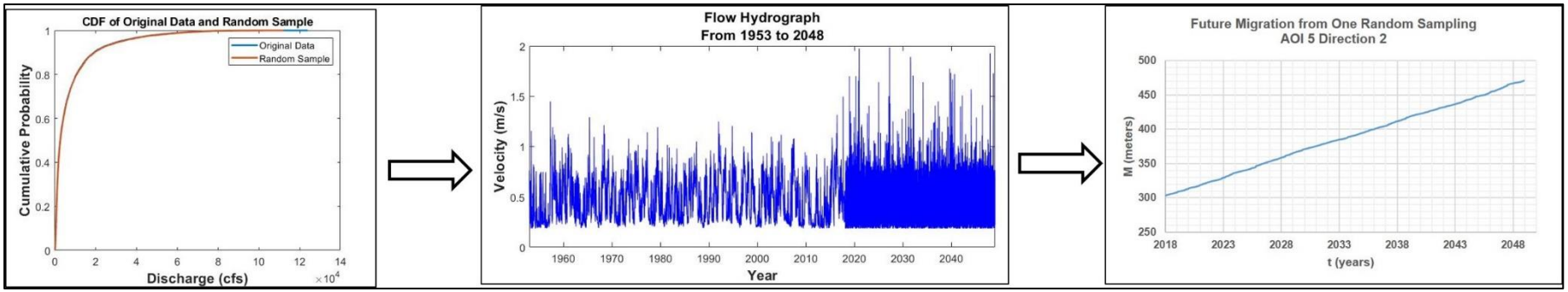
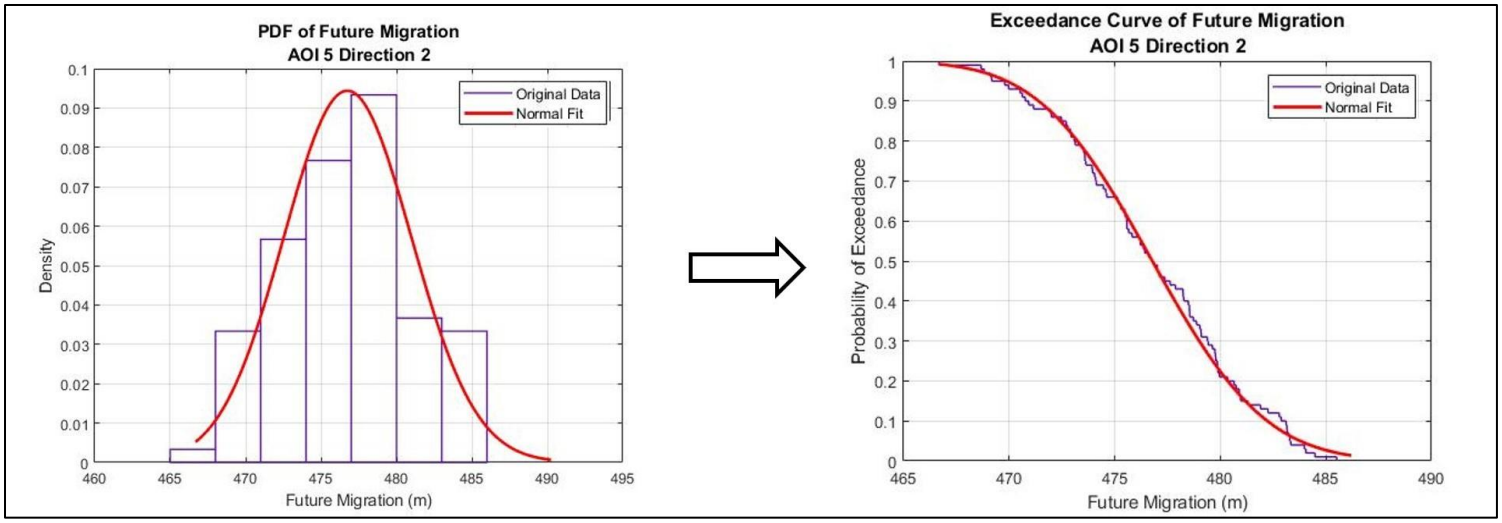
The code will automatically repeat *x* times